WRINKLING IN MULTILAYER DECORATIVE LAMINATES

THERMALLY INDUCED WRINKLING IN MULTILAYER DECORATIVE LAMINATES AND A METHOD TO MINIMIZE

By ROHAN NOEL PUKADYIL, B. ENG

A Thesis

Submitted to School of Graduate Studies

In Partial Fulfillment of the Requirements

For the Degree

Master Of Applied Sciences

McMaster University

MASTER OF APPLIED SCIENCES (2013) **McMaster University**

(Chemical Engineering) **Hamilton, Ontario**

TITLE: **Thermally Induced Wrinkling In Multilayer Decorative Laminates And A Method To Minimize**

AUTHOR: **Rohan Noel Pukadyil**

B. Eng. (McMaster University)

SUPERVISOR: **Dr. Michael R. Thompson**

NUMBER OF PAGES: xx, 133

ABSTRACT

Multilayer polymer decorative films are showing a growing presence in the automotive industry, substituting conventional paint applications while maintaining similar aesthetic appeal. However for certain film constructions that have distinct layer properties, the polymer film laminates have shown to form wrinkles on application of heat during thermoforming. In this study, attempts were made to identify the factors influencing wrinkling and to predict the variation in the wrinkle parameters under changing forming conditions using existing theoretical models. A new modified thermoforming technique is proposed for producing thermoformed parts without wrinkles and thereby achieving a Class A finished surface.

The thermally induced wrinkling phenomena observed in a multilayered automotive-grade polymer film (film-black-out, FBO) affixed on to substrate laminates with polypropylene (PP) substrate as well as an optically clear grade polycarbonate (PC) substrate was studied. To investigate occurrence of wrinkling in practical industrial applications, a new device (*thermoformer simulator)* was designed to mimic the actual thermoforming conditions. Processing parameters such as temperature and heating rate were found to show a strong correlation to wrinkle amplitude, wavelength and growth rate. Four distinct heating rates in the forming temperature range of 130°C to 180 °C were chosen for the study. On comparison of two polymer substrates (PP, PC) with very different thermo-mechanical properties to the film (FBO), it was observed that the modulus ratio of substrate to film dictated the compliancy of the wrinkle and

conformation of the substrate to wrinkle undulations. In FBO/PP laminates, with increasing temperatures, wrinkles in three defined states were observed. Whereas, in FBO/PC laminates, irrespective of the thickness of the substrate used, wrinkles in only one state was observed in the temperature range of study. PC substrate, been optically clear, enabled an extra advantage to observe the damage caused to base layer of FBO film due to wrinkling. Localized yielding and/or thinning of the black pigmented base layer of FBO film at wrinkle undulations was observed which further affirmed the need to prevent wrinkling for long term stability in practical use.

As the wrinkling was primarily seen only when there is a distinct mismatch in thermal behaviour between the component layers of the multilayered laminate to overcome the wrinkling, a conventional thermoforming method may not be effective. In this study, a new processing technique has been proposed that could be adapted to remove or minimize wrinkling. This technique involves a multi-stage operation which includes heating and biaxial stretching prior to the forming step and thus referred to as *stretch-assisted thermoforming (STF)* in this work. For a temperature range of 130°C to 180°C, a minimum of 6% to 8% biaxial strain applied while heating the laminate during the heating stage of thermoforming operations was required to relieve the thermally-induced compressive stresses and avoid wrinkling. Two different operation modes following different strain paths were studied for creating thermoformed specimen viz. *Isothermal* and *Dynamic STF*. In the former method, the multilayered laminate was heated until a stable temperature was reached and then biaxially stretched to remove the wrinkles prior to forming step. In the latter method, simultaneous heating and stretching was done which

completely prevented the formation of wrinkles. The specimens by Dynamic STF most closely resembled the pristine appearance of the original film based on color & gloss measurements, surface finish, and peel strength and was found to be very effective in retaining the Class A finished surface in the finished product.

ACKNOWLEDGEMENTS

This thesis work would not have been possible without the help of so many individuals in so many ways. I can confidently say that this thesis is a product of fortuitous encounters with people who have changed the course of my academic career. First and foremost, I would like to express my sincere gratitude to my professor, supervisor and mentor, Dr. Michael .R. Thompson, for giving me the opportunity to work on this project as well as his continued patience, expert guidance and flexibility during the period of this work. Dr. Thompson has always been supportive in the innovative approaches implemented in this work and has ensured that adequate resources are available at my disposal to get the work done. Under his supervision and guidance, I also had the opportunity to work in other industrial projects through which I was able to hone my problem solving and troubleshooting skills. These broad experiences have helped me develop the cross-disciplinary knowledge and confidence to work in any industry.

A very special thanks to Dr. David Potter who introduced me to the exciting field of polymers and research. During my undergraduate years I had the privilege of working in his laboratory part-time and developed key research skills that paved the way for the following years to come. He was an excellent guide and professor who identified my interest in polymers and encouraged me to do Masters with Dr. Thompson. Dr. Tayyab Hameed, a then PhD student under Dr. Potter was a great support and help in formative years of my research and was influential in successful completion of my undergraduate independent thesis. In terms of exceptional professors, I must mention Dr. Shipping Zhu whose knowledge, teaching methods and dedication to polymers will reverberate in me for the years to come. I also had the opportunity to be selected as a teaching assistant for his popular undergraduate course for which I am most grateful.

A very special thanks goes to Paul Gatt and Dan Wright for their continual help in building new equipments and fixtures for the experiments. They have been instrumental in bringing my ideas to fruition and always provided expert design suggestions and

modifications without which I would not have been able to complete this work. I would also like to appreciate the training, guidance and support from Elizabeth Takacs, Mike Bruhis, Maneesh Khanna with the MMRI/CAPPA-D facilities, as well as Chris Butcher and Glynis de Silveira with BIMR facilities. I thank Dr. Mukesh K. Jain and Dr. Stephen Veldhuis for giving me access to their MMRI lab facilities. I extend my gratitude to Doris Stevanovic for providing me training and access to Clean room laboratory.

I extend my warm gratitude to Dr. Prasath Balamurugan who has been a great mentor, colleague, friend and advisor who is always open to discussions anytime of the day and providing me with guidance throughout the work. His motivation and encouragement has led me to be able to complete this work. I will always cherish the vibrant & compelling discussions during our coffee breaks and late evening experimental works where some of the most excellent ideas were born. An everlasting friendship that cannot be forgotten.

I would also like to extend my gratefulness to Kent Nielsen and Frank Brandys for their technical advice and timely supply of materials. I appreciate the financial support extended from NSERC, OCE, 3M Canada and McMaster University for the duration of this work. I would also like to thank the Chemical Engineering Department at McMaster University in particular Kathy Goodram, Lynn Falkiner, and Cathie Roberts for their constant help & guidance during the work. And Nanci Cole, you are always a delight to talk to!

Lastly and most importantly, I would like to extend my greatest gratitude to my loving family, especially my parents, Sonia and Noel Pukadyil, and my younger sibling Rahul for their unconditional support, encouragement and confidence in my abilities and providing with timely guidance. I also thank my caring Aunts, Uncles and cousins for their emotional support and having a warm meal & bed ready for me whenever I took a break from research work or during holidays. And Finally, Rima Pandya, your unwavering faith in me and support through the smooth and turbulent times has worked wonders! I thank you for always been by my side and believing in me.

TABLE OF CONTENTS

INDEX OF FIGURES

NOMENCLATURE

E_f , E_s = Modulus of the film and substrate, respectively (MPa)

$\overline{E_f}$, $\overline{E_s}$ = Biaxial modulus of the film and substrate, respectively (MPa)

T = Temperature (°C)

h, H = thickness of the film and substrate respectively (μm)

υ_f, υ_s, = Poisson ratio of the film and substrate

$\Delta\alpha$ = difference in the thermal expansion of the film and substrate

σ_o , σ_c = Compressive stress and critical compressive stress for wrinkling (MPa)

ε_o , ε_c = Compressive strain and critical compressive strain for wrinkling (MPa)

λ = Wavelength of wrinkles (μm)

A = Amplitude of wrinkles (μm)

K = Wave number of the wrinkles

t = Time for wrinkling (s)

Ψ = amplification factor for the modulus ratio

σ_{co}, $\sigma_{c\infty}$ = critical compressive stress in the glassy at $t=0$ and rubbery state $t=\infty$ (MPa)

A_{e0} , $A_{e\infty}$ = Equilibrium amplitude in the glassy at $t=0$ and rubbery state $t=\infty$ (μm)

λ_o, λ_∞ = Equilibrium wavelength in the glassy at $t=0$ and rubbery state $t=\infty$ (μm)

a = growth rate(s^{-1})

γ_{22} = out-of-plane displacement component of wrinkle

$\mu(t)$, μ_o, μ_R= Relaxation modulus, glassy state and rubbery state relaxation modulus(MPa)

HS = Heating Source

BUC = Biaxial blowing unit with clamp

TS = Thermoforming simulator

IB, DB = Isothermal bulging and Dynamic bulging, respectively.

STF = Stretch assisted Thermoforming

DOI = Distinctness of image

CHAPTER 1 INTRODUCTION

Over the past several decades, there has been a growing collective conscience for environment change which is becoming overwhelmingly difficult to ignore. To the automotive industry, apart from the current laws, policies and regulations tightening up around emissions control and rising fossil fuel cost; there is an ever increasing demand from consumers for higher levels of product differentiation and product reliability while expecting lower prices. Lean and sustainable approaches are being increasingly implemented in every step of the design, part production and assembly. Apart from the intensive research and development into innovative engine designs for efficient fuel consumption as well as transitioning to new sources of power i.e. fuel cells, electric, solar etc, there is also growing interest in rethinking the materials used in building cars. Here, plastics and polymer composites are attempting to fill this criteria with their high material strength to weight ratio, ease of formability, superior corrosion and aging resistance, smaller unit operation floor space requirements, etc. The overall roll-out-cost, weight reduction and resultant fuel savings are quite attractive to the automotive industry and OEMs, with newer cars being increasingly made with higher contents of plastics. Figure 1-1 is reproduced from A.T. Kearney analysis on the projected trends regarding use of plastics in automotives [1].

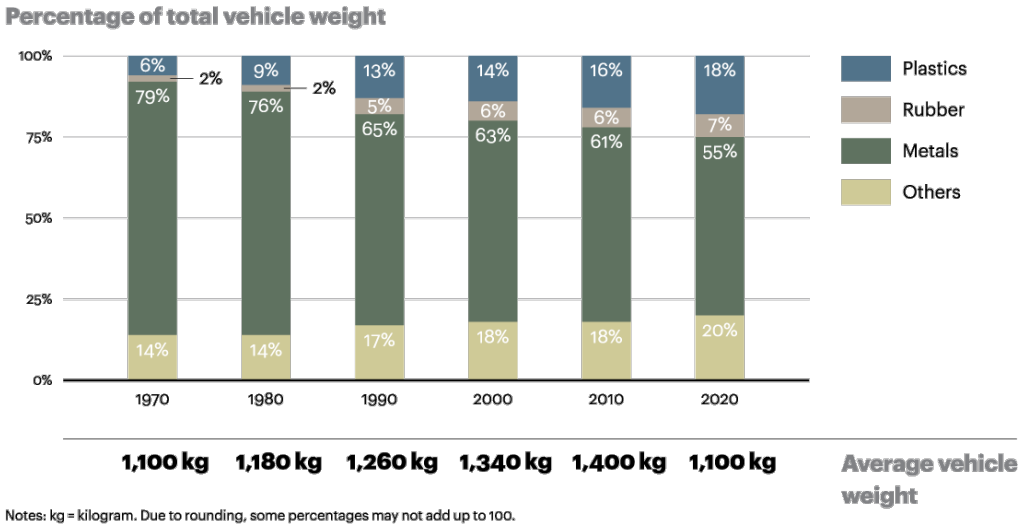

Figure 1-1: Projection of increasing % weight of plastics in an average car by 2020. Reproduced from [1]

While the plastics use described above pertains to the structural components of a vehicle, coatings and specifically paints have long been important examples of polymer use in vehicles. Paints have their environmental stigma as they emit volatile organic compounds (VOC) during curing and can account for as high as 50% of the unit cost of an individual part on a vehicle and so there is growing interest to replace them with more benign methods to color and protect. In addition, paint application and paint assembly lines represent the most expensive step in automobile production, requiring large floor space and have the capacity to generate over 1500 tons of VOCs/year [2]. Here, polymer decorative films are envisioned for replacement of exterior and interior paint application. These films can also reproduce other aesthetically desired surface-appearance that may have physical resemblance to metallic chrome, brushed metallic (See Figure 1-3(c)), carbon fiber, wood gravure, and leathered textures, often seen in luxury and sports cars

[3][4][5][6]. The ability to fine tune the construction of the polymer decorative film layers has helped achieve "luxury" appearance at a much cheaper cost to the consumers. The usage of decorative films can bring about substantial cost savings in the form of lower initial investment costs and lower piece price costs as well as VOC reductions of 98% compared to electro-spray painting and chroming [3].

1.1.How It's Made

Multilayered polymer decorative films are not limited to the automotive industry, with applications seen in other sectors including aerospace, electronics, construction, and medical [7]. In the automotive sector, decorative films are developed in various manners based on its place of use in a vehicle and intended features. To replace conventional paint application (electrophoretic coating), these decorative films have be designed to provide a long list of important physical properties such as: high gloss, hardness, distinctness-of-image (DOI), abrasion resistance[8], weatherability (UV resistance)[9], impact strength, thermal stability, gasoline and acid resistance, cleanability, adhesion to the substrate, resistance to water and humidity exposure and opacity of the coating[10][11]

Currently, in the market there are several different variations of automotive decorative films. However, the most typical top-down architecture of a decorative film consists of cap or clearcoat layer (i.e. outer layer exposed to the environment), a decorative or color layer, and an adhesive layer (i.e. layer contacting the autopart in question) as shown in Figure 1-2 [11] [12][13].

Figure 1-2: Typical construction seen in a automotive-grade multilayer decorative film

The **clearcoat** or cap layer is essentially an optically clear, high gloss layer typically made of a supplier's proprietary blend of acrylic, polyesters, fluoropolymers or polyurethanes [12] [13]. The chemical make-up of this layer provides the necessary weathering, UV protection [14] and other physical characteristics such as scratch and mar resistance. The **decorative/color layer** of the decorative film has seen lot of recent developments with earlier inventions from paint coats applied to carrier layers to more recent dry paint transfer [2][4], vapor deposition [15], vacuum sputtering deposition for metallic colors [6]. More recent inventions have developed glossy colored film (coined molded-in color film) by co-extrusion which are reportedly less expensive than dry paint films and have better applicability to deep drawn parts like bumper fascias [3]**.** The **adhesive layer,** typically an acrylic-based pressure sensitive adhesive (PSA), is the final layer in the decorative film construction [12]. In some inventions decorative films with a heat reactive adhesive are also available. Current inventions have also taken advantage of using structured PSA that have repetitive spaced passageways [16]. These structured or micro-patterned PSA layer with intended passageways are designed to enable repositionability of the film as well as provide relief ports to any entrapped air between

the film and substrate that usually occurs during the lamination stage and may even hinder bonding [3] [16].

1.2.Method Of Application

The application of automotive polymer decorative films onto metal substrates or any flat surfaces is relatively easy. In such applications, decorative films with pressure sensitive adhesives are usually employed. For a metal substrate the surface is initially cleaned with an alcohol based solvent and then wiped with a thin layer of adhesive primer to improve bonding. The polymer decorative film is then applied onto the surface with the application of pressure. Common applications by this method have been to the window surround and b-pillar of a car [3]. For application to more complex 3D parts using automotive grade plastic substrates such as acrylonitrile butadiene styrene (ABS), thermoplastic polyolefin (TPO), or polycarbonate (PC), *in-mold decoration* (IMD) process is a newly envisioned approach [17].

1.3.In-Mold Decoration Process

In-mold decorating (IMD) is a process for decorating plastic parts or components during the molding process [18][19][20]. A specific IMD process known as *insert film injection* starts with the decorative film laminated to a very thin substrate that is deep-drawn into the mold shape by vacuum thermoforming [2]. The molded decorative pre-form is then transferred into the mold of an injection molding machine and molten plastic

is injected behind it, creating a thicker part. Initially, IMD processes were limited to modestly sized and relatively flat parts for interior and exterior applications like door panels. With progressing years, the technology has progressed in its ability to mold complex 3D shapes such as the front and rear-end bumper fascias, roofs, hoods, as well as the instrumentation console of automobiles (See Figure 1-3(a)) [2][5]**.** IMD processes boast lower scrap rates, an ability to mold and decorate in one location, and improved recyclability of finished parts.

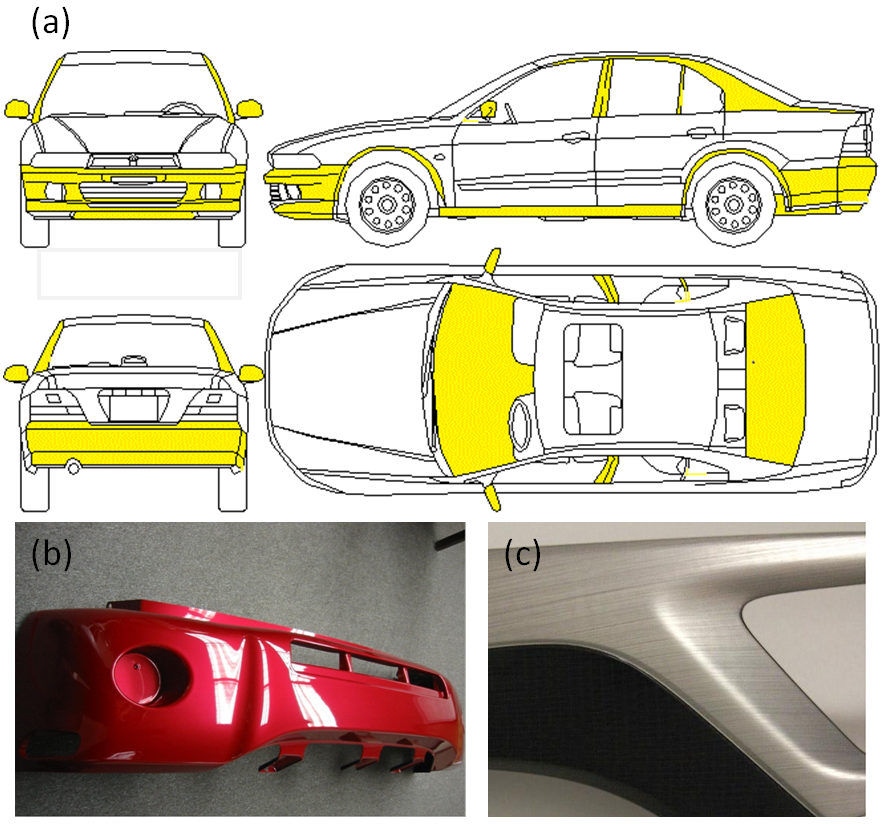

Figure 1-3: (a) Typical schematic of automotive framework with highlighted regions employing decorative film application (b) An automotive rear-end fascia prepared by Thick sheet forming (TSF) (c) Decorative film with decorative layer resembling brushed stainless steel quality. Reproduced from [5] ,[6].

Conventionally injection molding machines are well designed for manufacturing high numbers of small, high-precision parts with excellent control over thickness and dimension. However, when extending the boundaries of application to large complex shapes, factors such as capital and operating cost, mold cost, part production time, and energy requirements can increase the part cost substantially. In addition, issues such as dimensional stability and shrinkage become more concerning and pronounced when molding large single piece fascia parts[2][21]. Thus, thermoforming has seen to be a more viable method for forming of multilayered laminates. Thermoforming boasts faster part production rate, comparatively lower energy requirements (as the substrate is not completely melted), lower capital investment and the ability to still form large fascia parts [17][5]. Exclusively using thermoforming for IMD is termed by the automotive industry as 'thick sheet forming' (TSF) [17]. In this process, the decorative film laminate is heated to above its glass transition temperature till the laminate is more soft and pliable but does not flow. The laminate is then draped over a male mold by applying vacuum or by applying air pressure to force the laminate against a female mold. Once the part is cooled down, the mask film is peeled off (See Figure 1-3(b)).

1.4.Motivation Of Work

Thermoforming of decorative multilayered polymer laminates can lead to possible undesirable defects especially when dealing with materials having huge variation in thermo-mechanical properties between the individual component layers. The response of such materials to applied heat can induce undesirable outcomes such as buckling that

could manifest as blistering [22], or delamination [23], or even wrinkling [24]. This would limit the range of materials that could be selected to form multilayered laminates for automotive as well as in aerospace, electronic and medical applications. To push the boundaries of multilayered film design for newer, physically demanding applications, an understanding of the so-called undesirable phenomena have to be closely investigated. A remedial method is to leave the mask layer of decorative film laminates during the thermoforming step [13]. This does alleviate some issues to a certain extent as it compensates for mismatched thermal properties. However, use of such a layer hinders the complexity of shape formed [5]. Also, removal of the mask layer after thermoforming still may result in the same distortions when stresses are inadequately relieved or could induce other surface distortions that could lower the gloss and DOI. In some rare cases, the mask film could strongly bond with the clear-coat layer of the decorative film laminate and damage the surface lowering the aesthetic value[4][25]. So use of mask should not be considered as a reasonable solution for routine manufacturing practices.

1.5.Objectives

In this work, we focus on a commercially available multilayered automotive-grade film blacked-out (FBO) decorative film laminate that was seen to wrinkle on application of heat during thermoforming. Wrinkling has been generally understood as a stress driven instability similar to buckling of an elastic column under compression. For a solid film bonded to a substrate; however, the instability is constrained. Under compression, the film may buckle and delaminate from the substrate [26] [24].

Alternatively, the film and the substrate stay bonded and deform concurrently to form wrinkles [27].

The specific objectives of the study are:

- To identify the critical conditions and variation in the material properties that cause spontaneous wrinkling in multilayered polymer laminate systems
- To study the influence of processing parameters such as temperature, heating rate on the wrinkle formation during processing
- To investigate the progress in wrinkle evolution with the change in the expansion and relaxation behaviour of the constituent layers of the materials under the action of temperature and heating rate
- To study the effect of laminate systems with substrates of distinctly different stiffness (PP and PC) on the wrinkle patterns generated and their state of compliancy to the wrinkle patterns
- To check the applicability of existing mathematical models those describe the wrinkled systems with the experimentally obtained wrinkle morphological parameters
- To quantify the damage caused due to thermal wrinkling on the base layer of the decorative film
- To identify a method to effectively overcome the problem of wrinkling in multilayered systems by adapting a new technique and thereby achieving a class A surface finish.

CHAPTER 2 LITERATURE REVIEW

2.1.Introduction

Wrinkling is an age-old phenomena which can manifest in our daily lives as wave patterns at the sea surfaces, sand dunes, ruptures of paint from a wall, skin of a shriveled apple, or even aging human skin[28]. Although buckling and wrinkling instabilities has historically been viewed as a mechanism for structural failure[29][30][31][32], pioneering work in the late 1990s [33][34] showed that this behavior can be controlled in micro- and nanoscale systems to generate interesting structures with well defined geometries and dimensions. The periodic nature of wrinkles/buckles has recently led to the development of interesting applications such as to assemble complex wrinkle patterns [34][35][36][37][38][39], to fabricate novel electronic devices, [40][41]diffraction gratings, [42]and micro lens arrays, [43][44]to tune surface wetting [45] and adhesion,[46]and to switch photonic [47] and phononic properties [48], as well as measuring the mechanical properties of ultrathin films [49].

2.2.Wrinkling In Film/Substrate Systems

Wrinkling is related to compressive stresses increasing in the elastic top layer of thin multi-layered systems as it resists the tensile expansion in neighboring layers. Once a critical limit for the mismatched strain is reached, the structure buckles to relieve the strain energy which in turn causes delamination or wrinkling depending on the bond

strength between layers and the compliancy of the substrate. Thin films tend to delaminate while buckling on hard substrates as the energy release rate often exceeds the interface fracture toughness [26][50][51]. However, thin films that experience buckling on a compliant substrate will more often wrinkle along with localized deformation of the substrate [52][53] forming non-linear distortion patterns.

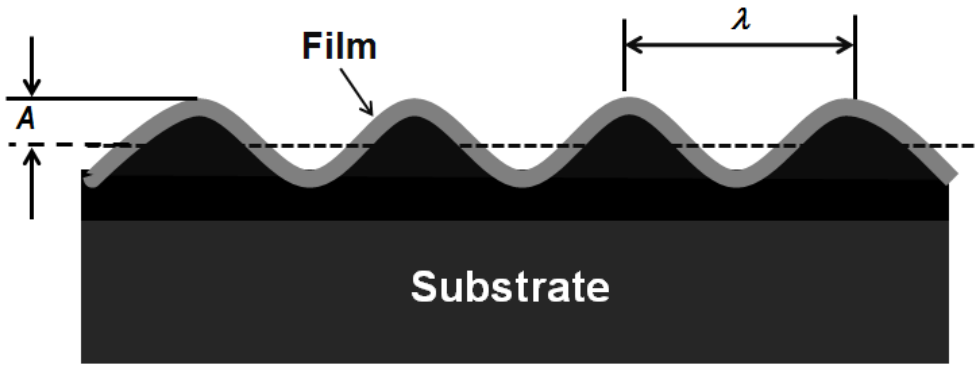

Figure 2-1: Schematic of the wrinkling in a multilayered film /substrate laminate

Wrinkling and it's condition for growth and evolution are greatly influenced by nature of the substrate. If the substrate is elastic, a critical compressive stress has to be achieved for the film to wrinkle and a stable wavelength is derived by minimizing the total elastic energy within itself and the substrate[54][55][56]. If the substrate is viscous, wrinkling behaves as a kinetic process since the viscous substrate does not store elastic energy and a compressed film is always unstable energetically[57][58] [56]. If the substrate is viscoelastic, both energetics and kinetics play important roles and wrinkling kinetics varies at different stress levels in the film[55] [56] [59]. In the following sections, different types of film/substrate systems are discussed in detail. In all these

cases the film is typically considered elastic in nature and substrate is relatively compliant unless mentioned otherwise.

2.3.Models For Wrinkling

The earlier theoretical models for wrinkling were derived from a generalization of classical Euler buckling for a compressed column, flat plate, or shells [30][31][32][60][61]. More recent models have also adapted nonlinear von Karman plate theory and Reynolds lubrication theory [58] to improve the predictability of these models for systems involving viscous substrates. The underlying mechanism of wrinkling has generally come to be understood as a stress driven instability when a material system experiences both equilibrium and non-equilibrium states [62]. In systems where a thin film is bonded to a compliant/rigid substrate, wrinkles are manifested due to localized buckling by *compressive stresses* acting on the film. These compressive stresses could be generated by a number of ways: i) a thermal expansion mismatch between constituent layers[63], ii) external stresses acting on substrate/film causing elastic mismatch/recovery, iii) by differential swelling/shrinkage between the constituent layers during solvent absorption [64] [65]. To minimize these compressive stresses acting on the layers, out-of plane deformations manifesting as delamination, blisters or wrinkles arise.

Distinct from the above works, wrinkling observed in thin free-standing layers *under in-plane tension* was better explained by "**tension-field theory**" which was first introduced by Wagner [66]and followed by Steigmann's work [67] adapted for the

analysis of wrinkling in isotropic elastic membranes. The premise of this theory is applicable only to elastic membranes where bending stiffness can be neglected. Essentially, this is a two-dimensional non-linear theory which regards wrinkling to be infinitesimally close and where stress fields were *not allowed to be compressive* [68]. This theory describes wrinkles typically seen in thin elastic sheets under uniaxial tension as shown in Figure 2-2.

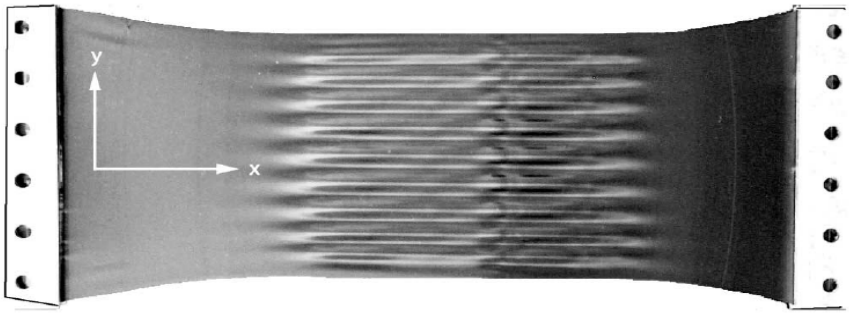

Figure 2-2: Wrinkles in a polyethylene sheet of length~25 cm, width ~10 cm and thickness ~0.01 cm under uniaxial tensile strain (10%). Reproduced from[28].

Wrinkling here is assumed to take place in the direction perpendicular to the lines of uniaxial tension [68]. A major setback of this method was the out-of plane deformations could not be accurately determined. A scaling analysis of the wavelength and amplitude of wrinkles produced under in-plane tension that complemented the tension field theory was presented by Cerda et al. [28]. However the tension field theory is not directly applicable to the systems where no external mechanical force (tension) acting on the system is the primary cause for wrinkling. In the film/substrate system studied in this work, wrinkling occurred spontaneously by virtue of the compressive

stresses generated due to differential thermal expansion between the layers. Hence the models which consider the relative expansion/relaxation between the constituent layers with the changing processing parameters such as temperature and heating rate etc., were fitted to describe the wrinkle evolution process.

2.3.1. Elastic Film/Elastic Substrate

As discussed earlier, in an elastic film/elastic substrate laminate where the substrate is relatively compliant, wrinkling is dictated by energetics and the selected wavelength and amplitude is based on an energy minimization method. Considering an elastic film/elastic substrate system where wrinkling is caused due to mismatch in thermal expansion between them, the biaxial compressive residual stress (σ_o) and mismatched thermal strain (ε_o) acting on the laminate are given by:

$$\sigma_0 = \frac{12E_f \Delta\alpha\Delta T}{1-\upsilon_f} \tag{2-1}$$

$$\varepsilon_0 = \Delta\alpha\Delta T \tag{2-2}$$

where $\Delta\alpha$ is the difference between the thermal expansion of the film and the substrate, ΔT is the temperature difference, E_f is the film modulus and υ_f is the Poisson ratio of the film. For very small strains it is energetically more favourable to buckle globally or bend instead of wrinkling. The extent of compression the film can undergo really depends on the elasticity as well as the stiffness of the film and substrate. Beyond a point, the film

deforms elastically to relax the compressive stresses which manifests as wrinkles. The critical strain (ε_c) beyond which wrinkling occurs is defined by[26]

$$\varepsilon_c = -\frac{1}{4}\left(\frac{3\bar{E}_s}{\bar{E}_f}\right)^{2/3} \tag{2-3}$$

where $\bar{E}_s = E_s/(1-v_s)$ and $\bar{E}_f = E_f/(1-v_f)$ are the biaxial moduli of the substrate and film respectively. The elastic energy stored in the compressed film will decrease as the buckling amplitude increases the wrinkle. However, an opposing force, bending energy increases as the amplitude grows. The total strain energy in the system is the summation of membrane and bending energy in the thin film and the strain energy in the substrate. And by minimizing the total energy with respect to amplitude (A) and wavelength (λ), the following selected wavelength and amplitude result:

$$\lambda = 2\pi h\left(\frac{3\bar{E}_f}{\bar{E}_s}\right)^{\frac{1}{3}} \tag{2-4}$$

$$A = h\sqrt{\frac{\varepsilon_0}{\varepsilon_c} - 1} \tag{2-5}$$

The sinusoidal wrinkle can be represented as $w = Acoskx$ where k is the wavenumber defined as $2\pi/\lambda$. Here h is the film thickness. The magnitude of both amplitude and wavelength is decided by the stiffness of the film and substrate. For a stiff film, long wavelength are favoured when buckled because it costs less energy than buckling into a rather short wavelength. On the other hand, the soft substrate favors shorter wavelength. When combined, there is an optimum wavelength that minimises the total free energy. When combined, the buckling yields a value somewhere between these large and small wavelengths. From the above equations, it is clear that both amplitude and wavelength

linearly change with the thickness of the film. The amplitude is shown to increase with applied strain. However, the wavelength is shown to change with the film/substrate modulus ratio and is independent of the applied strain which would seem contradictory to basic understanding of a sinusoidal wave. The above equations are based on small deformation approximations and linear stress-strain behaviour; they are applicable to strains less than 5% [54][63]. At larger strains, experimentally measured wavelength were shown to decrease with increasing applied strain and amplitude could not be accurately predicted. Thus for strain larger than ~5%, wavelength and amplitudes equations were modeled as neo-Hookean using the 2nd Piola-Kirchoff stress formulation proposed by Jiang et al. [54][63] as follows:-

$$\lambda = \frac{\lambda_0}{(1+\varepsilon_0)(1+\xi)^{1/3}} \tag{2-6}$$

$$A = \frac{A_0}{\sqrt{1+\varepsilon_0}(1+\xi)^{1/3}} \tag{2-7}$$

$$\text{where, } \xi = \frac{5}{32}\varepsilon_0(1+\varepsilon_0) \tag{2-8}$$

Here, λ_0 and A_0 are wavelength and amplitude, respectively for the small-strain case given by equations (2-4) and (2-5). The above equations are based on simple accordion bellow mechanics and ξ accounts for the large deformations and non-linear constitutive model for the substrate.

Groenewold[59] re-derived the original wrinkling theory following the energy minimizing approach however incorporating Poisson's ratio of the film and the substrate shown below:

$$\lambda = 2\pi h\left(\frac{E_f}{E_s}\frac{(1+\upsilon_s)(3-4\upsilon_s)}{12(1-\upsilon_m)(1-\upsilon_f^2)}\right)^{1/3} \tag{2-9}$$

$$A = \sqrt{\varepsilon_0}\left(\frac{2}{k}\right) \tag{2-10}$$

Huang[56] proposed both equilibrium and energetic analysis to predict the stability condition for both wrinkle amplitude and wavelength with elastic film/elastic substrate systems. Unlike the original wrinkling theory given by Allen[29] and Groenewold[59], the influence of substrate thickness, Poisson's ratio, stiffness ratio of substrate and film, and shear tractions are considered in Huang theoretical model. The equilibrium and energetic analysis differ only on the boundary conditions applied to derive the model. Equations based on the equilibrium state are reported and the author directed readers to Huang's paper for equations pertaining to energetics analysis.

$$A_e = \frac{2\sqrt{(1-v_f^2)}}{k}\left[-\frac{\sigma_0}{E_f} - \frac{(kh)^2}{12(1-v_f^2)} - \frac{2\mu}{\gamma_{22}E_f kh}\right]^{1/2} \tag{2-11}$$

where, the dimensionless coefficient

$$\gamma_{22} = \frac{1+\kappa}{4}\frac{\kappa sinh(2kH)-2kH}{\kappa cosh^2(kH)+(kH)^2+(\frac{1-\kappa}{2})^2} \tag{2-12}$$

here, μ is the shear modulus of the substrate and, $\kappa = 3 - 4v$. Note that the influence of substrate thickness (H) is captured through the coefficient γ_{22} shown above. The effect of substrate thickness diminishes if H/λ >1 and the dimensionless coefficient depends only on the Poisson's ratio of the substrate , γ_{22} = 2(1-v).

The selected wave number ($k=2\pi/\lambda$) that minimizes the total strain energy is shown as follows:

i) For a thick substrate ($H/h \rightarrow \infty$):

$$k = \frac{1}{h}\left[\frac{6(1-v_f)^2\mu}{(1-v_s)E_f}\right]^{1/3} \tag{2-13}$$

ii) For a thin substrate ($H/h \rightarrow 1$):

$$k = \frac{1}{h}\left[\frac{24\left(1-v_f^2\right)(1-v_s)}{(1-2v_s)}\frac{\mu}{E_f}\frac{h}{H}\right]^{1/4} \tag{2-14}$$

and to determine the corresponding wrinkle amplitude for the selected wavenumber, substitute (2-13) and (2-14) into (2-11). The wavelength is shown to be dependent on the moduli, Poisson's ratios, and thickness of both substrate and film, and is independent of the compressive stress acting on the film.

The three competitive terms inside the bracket of Equation (2-11) determine the stability of the film to wrinkle. The first term promotes wrinkling to relax the in-plane compression, the second term favours large wavelength due to the flexural rigidity of the film and the third term favours small wavelength due to elastic constraint of the substrate. The film will not wrinkle if the last two terms are greater in magnitude than the first term. Huang [56] defined the minimum critical stress for film to wrinkle as follows:

$$\sigma_c = -E_f\left[\frac{9}{16\left(1-v_f^2\right)(1-v_s)^2}\right]^{1/3}\left(\frac{\mu}{E_f}\right)^{2/3} \tag{2-15}$$

for case where, ($H/h \rightarrow \infty$)

and $\sigma_c = E_f \left[\frac{2(1-v_s)}{3\left(1-v_f^2\right)(1-2v_s)} \frac{\mu}{E_f} \frac{h}{H}\right]^{1/2}$ (2-16)

for case where, $(H/h \rightarrow 1)$.

From the above equations, the critical stress to wrinkle is shown to be directly related to the stiffness ratio (μ/E_f) of the substrate and film, and to the thickness ratio (H/h). When the thickness ratio is greater than 10, the substrate thickness has minimal influence on the critical condition and can therefore be neglected. Conversely, for thinner substrate a fixed boundary condition has been assumed at the bottom surface of the substrate. Alternatively, if the bottom of the substrate is free of tractions, the effect of substrate thickness would be the opposite. Unfortunately, Huang [56]paper did not show any equations pertaining to this case.

Work done by Cerda et al. [28]shows a particularly interesting development to wrinkling theory and proposed a general theory that could describe wrinkling in virtually any geometry and not limited to only flat sheets. The summarized findings are shown below

$$\lambda \sim \left(\frac{B}{K}\right)^{1/4} \quad (2\text{-}17)$$

$$A \sim \lambda \left(\frac{\Delta}{w}\right)^{1/2} \quad (2\text{-}18)$$

here B is the bending stiffness of the film $B = E_f h/[12\left(1-v_f^2\right)]$, K is stiffness of the effective elastic foundation (substrate) and (Δ/w) is the imposed compressive strain. Depending on the given system, K and Δ will vary accordingly. The authors discussed

scaling laws for wavelength (λ) and amplitude (A) from several case studies [28]. For a flat sheet, equation (2-17) would reduce to a form similar to equation (2-4).

2.3.2. Elastic Film/Viscoelastic Substrate

Unlike an elastic substrate where energetics dictate wrinkling or a viscous substrate where viscous flow controls the kinetics of wrinkling, a viscoelastic system has a profound effect on both energetics and kinetics.

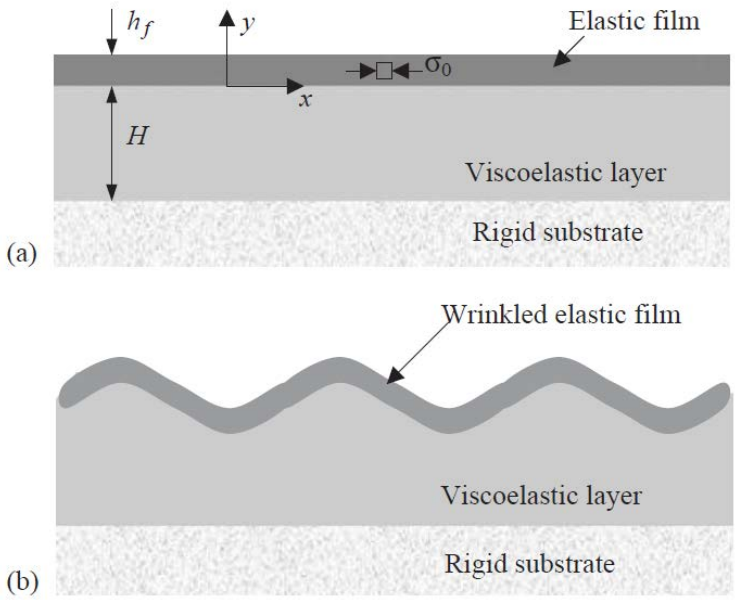

Figure 2-3: Schematic of model structure (a) reference state (b) wrinkled state. Reproduced from[56]

Huang et al. [57][56][69]studied wrinkling of a compressed elastic film bonded onto a viscoelastic substrate which was in turn set on a rigid substrate. The schematic representation is reproduced in Figure 2-3. The film is under biaxial compressive stress and the substrate conformed to the wrinkle maintaining complete interface contact. The elastic film is modelled by von Karman plate theory. The top surface of the film is

traction free and the bonded surface to the substrate is subjected to both normal and shear tractions. To simplify the model, in-plane displacement and shear tractions have been ignored. The substrate was considered to be isotropic and linearly viscoelastic. The substrate is assumed to have normal and shear tractions at the top surface (bonded to film) and a fixed boundary at the bottom surface. The relaxation moduli of the substrate is considered since unlike an elastic substrate, for a viscoelastic substrate its relaxation modulus $\mu(t)$ is a function of time with defined boundaries given as its glassy modulus $\mu(0)=\mu_0$ and rubbery modulus $\mu(\infty)=\mu_\infty$. For a given viscoelastic substrate experimental measurements of relaxation modulus $\mu(t)$ can be fitted to a micromechanical model (see Figure 2-4) consisting of an array of spring-dashpot analogs in parallel and can be described as

$$\mu(t) = \mu_\infty + \sum_i \mu_i \exp(-p_i t) \tag{2-19}$$

here, $p_i=\mu_i/\eta_i$ is the relaxation parameter of one branch. η is viscosity of the given branch.

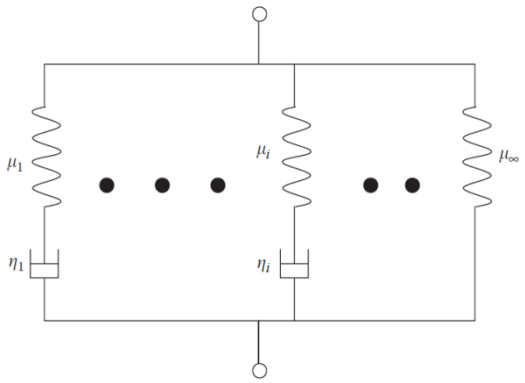

Figure 2-4: Mechanical model of viscoelastic substrate

By fitting the experimental data to the model form shown in equation (2-19), the glass modulus and rubbery modulus can be estimated. The critical condition for wrinkling is based on the governing state of the substrate- glassy or rubbery:

At time, *t=0+*, glassy state prevails, and critical stress (σ_{c0}) can be defined using equation (2-15) for thick substrate ($H/h \rightarrow \infty$) can be adapted as follows:

$$\sigma_{c0} = -E_f \left[\frac{9}{16\left(1-v_f^2\right)(1-v_s)^2}\right]^{1/3} \left(\frac{\mu_0}{E_f}\right)^{2/3} \quad (2\text{-}20)$$

At time, $t=\infty$, rubbery state prevails and the critical stress ($\sigma_{c\infty}$) :

$$\sigma_{c\infty} = -E_f \left[\frac{9}{16\left(1-v_f^2\right)(1-v_s)^2}\right]^{1/3} \left(\frac{\mu_\infty}{E_f}\right)^{2/3} \quad (2\text{-}21)$$

Similarly, for thin substrates where ($H/h \rightarrow 1$), equation (2-16) can be adapted as shown above.

Three cases can be observed when comparing the magnitude of compressive stress in the film (σ_0) to its critical stresses, (σ_{c0}) & ($\sigma_{c\infty}$) which are summarized as follows:

I. $|\boldsymbol{\sigma_0}| < |\boldsymbol{\sigma_{c\infty}}|$ **(small stress):-** The flat film is stable at both rubbery and glassy states, and wrinkling does not occur.

II. $|\boldsymbol{\sigma_0}| > |\boldsymbol{\sigma_{c0}}|$ **(large stresses):-** Film wrinkles immediately at the glassy state and further growth is dependent on softening of substrate as it transitions from glassy to rubbery state. The wrinkle wavelength transitions from λ_0 to λ_∞. The selected wavelength (for thick substrates) can be described in the glassy state (based on equation (2-13)):

$$\lambda_0 = 2\pi h \left[\frac{(1-v_s)}{6(1-v_f^2)}\frac{E_f}{\mu_0}\right]^{1/3} \quad (2\text{-}22)$$

And at the rubbery state:

$$\lambda_\infty = 2\pi h \left[\frac{(1-v_s)}{6(1-v_f^2)}\frac{E_f}{\mu_\infty}\right]^{1/3} \quad (2\text{-}23)$$

For large compressive stresses, the film immediately wrinkles to its equilibrium state at the glassy state.

For the case of a *thick substrate* $(H/h \to \infty)$, the corresponding equilibrium amplitude can be defined from equation (2-22) through the relation ($\lambda_0=2\pi/k_0$) in equation (2-11), to give:

$$A_0 = h\sqrt{\frac{\sigma_0}{\sigma_{c0}} - 1} \quad (2\text{-}24)$$

The wrinkle growth here is a function of time and amplitude can be defined as follows:

$$A(t) = A_0 + A_0 \frac{\mu_0-\mu_\infty}{\alpha' E_f-\mu_\infty}\left[exp\left(\frac{\alpha' E_f-\mu_\infty}{\mu_0-\alpha E_f}p_1 t\right) - 1\right] \quad (2\text{-}25)$$

here, α' is defined as:

$$\alpha' = \alpha - \frac{3\gamma_{22}k_0^3 h A_0^2}{8(1-v_f^2)} \quad (2\text{-}26)$$

and

$$\alpha = \frac{\gamma_{22}(v_s k_0 H)}{24\left(1-v_f^2\right)k_0 h}\left[-k_0^4 h^4 - \frac{12(1-v_f^2)\sigma_0}{E_f}k_0^2 h^2\right] \quad (2\text{-}27)$$

where the dimensionless coefficient γ_{22} is given by equation (2-12).

At the limit of a thick substrate, where the $\gamma_{22} = 2(1-\nu)$

$$\alpha' = \frac{\mu_0}{E_f}\left(4 - 3\frac{\sigma_0}{\sigma_{c0}}\right) \quad (2\text{-}28)$$

Note: The above equations are based on a mechanical model that fitted well (equation (19)) for the relaxation modulus of the substrate, with one dashpot and one spring to give $\mu(t) = \mu_\infty + \mu_1 \exp(-p_1 t)$ and $\mu_0 = \mu_\infty + \mu_1$. For systems in which relaxation modulus is described by combination of several springs and dashpots in series and parallel, specific equations were derived and presented by Huang et al[56].

For a viscoelastic substrate, depending on the stress level, three characteristic wrinkle growth behaviour can be defined based on equation (26): - $\alpha' > \mu_\infty/E_f$, the growth is accelerating, $\alpha' < \mu_\infty/E_f$, the growth is decelerating, $\alpha' = \mu_\infty/E_f$, linear growth.

III. $|\boldsymbol{\sigma}_{c\infty}| < |\boldsymbol{\sigma}_0| < |\boldsymbol{\sigma}_{c0}|$ **(intermediate stresses):** Flat film is energetically stable at the glassy state but unstable at the rubbery state. In this case, the growth of the wrinkle depends on the viscoelastic behaviour of the substrate and is described by kinetics analysis. A linear perturbation analysis is conducted.

The wrinkle amplitude (for viscoelastic substrate with 1 dashpot and 1 spring) as a function of time is shown as:

$$A(t) = A_o \exp[\beta p_1 t] \quad (2\text{-}29)$$

and $\beta = \frac{\alpha E_f - \mu_\infty}{\mu_0 - \alpha E_f}$

The above linear perturbation analysis is only valid for initial stage of wrinkling. And to describe the wavelength and amplitude growth at the rubbery limit would require non-linear analysis[56]. Figure 2-5 summaries the wrinkling kinetics spanning the glassy

modulus of the substrate for a elastic film/viscoelastic substrate, assuming a constant ratio between the rubbery and glassy modulus.

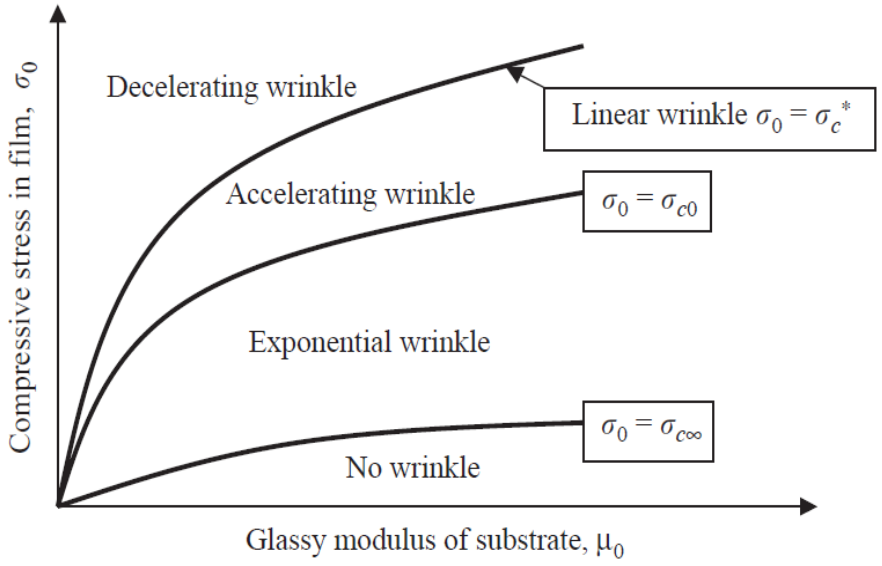

Figure 2-5: Schematic map of wrinkling kinetics snapping the glassy modulus thick substrate for a elastic film/viscoelastic substrate. Reproduced from[56].

Studies conducted by Yoo et al. [47] examined the morphological changes in wrinkling seen for a metal film bonded onto a polymer substrate which was in turn bonded to rigid surface. Here the compressive stress for wrinkling was generated due to mismatch in thermal expansion between the layers. They identified interesting morphological behaviours around the glass transition of the polymer (polystyrene) where it transitioned from elastic to viscoelastic to viscous. Yoo et al. [70] reported influence by factors such as temperature, polymer film thickness, heating condition and time, molecular weight of the polymer and cross-linking level of the polymer. The work presented five wrinkling regimes that were defined by the thermo-mechanical behaviour of the polymer.

2.3.3. Elastic Film/Viscous Substrate

Many researchers have observed that the viscous substrate relieves the compressive stresses in the film causing wrinkling, by being "compliant" to the wrinkles formed by viscous flow of the substrate. Experiments conducted by Hobart et al. [71] showed evidence of slower buckling of semiconductor film during annealing when bonded to a low viscosity glass compliant layer. Sridhar et al.[72]examined elastic film on viscous glass layer which was in turn placed on a rigid surface and studied the kinetics of buckling, however assumed shear traction along the interface to be negligible and ignored displacement parallel to the interface. Such simplifications cannot be justified when the thickness of the viscous layer is small. Huang et al. [73] also considered elastic film on viscous substrate and developed theoretical models and stability conditions for the wrinkling process[73]. Here, the elastic film was modeled with the non-linear thin plate theory subjected to in-plane and out-of plane loads and the viscous flow of the substrate was described by Reynold's lubrication theory [74]. Wrinkling in such systems is understood to be a compromise between the elastic energy of film as a driving force and viscous flow of substrate as a kinetic process. Since the viscous substrate does not store elastic energy, a compressed film on top is always energetically unstable. The viscous flow in the substrate controls the kinetics of wrinkle growth, selecting a fastest growing wavelength[69].

Based on Huang et al. [56][73] models, Equation (2-11) for equilibrium wrinkle amplitude can be used for a viscous substrate by setting $\mu=0$ in the equation. The

amplitude growth as a function of time from equation (2-29) can be used as a limiting case for a substrate with constant viscosity η, the relaxation modulus is a delta function, μ(t)= ηδ(t) and equation (2-29) reduces to

$$A(t) = A_0 \exp\left[\frac{\alpha E_f}{\eta} t\right] \quad (2\text{-}30)$$

Overall, if the wavelengths are too short, the bending costs too much elastic energy, and the wrinkles decay. If the wavelengths are too long, the viscous flow takes too much time for the shape to noticeably change. The wrinkles have infinitely many unstable equilibrium configurations. The longer the wavelength, the lower the elastic energy. However, these unstable wrinkles are kinetically constrained not linear in behaviour. The elastic film may spend a long time in the neighborhood of one equilibrium configuration before evolving further into a longer wave to lower the elastic energy. The real wrinkle amplitude is not uncontrolled growth even though linear perturbation analysis suggests otherwise and thus the available models fail here[72]. The linear analysis is valid for shorter time scales; however, non-linear analysis is required to model the wrinkling behaviour at larger time scales. The driving force for wrinkle amplitude growth is elastic energy stored in the compressed film and this will decrease as the buckling amplitude increases and at longer time scales, a equilibrium amplitude would develop. As for the wrinkle wavelength, during wrinkling, the dominating wavelength is the wavelength that grows the fastest[72]. However, as amplitude saturates at later times, the wavelength growth would be very slow and depend on the viscous flow the substrate for an elastic film on a viscous substrate.

CHAPTER 3 EXPERIMENTAL

3.1.Materials

An automotive-grade *blackout* decorative film (FBO) was supplied by 3M Canada (London, ON), made from a dual-layered polymer construction and a pressure-sensitive adhesive. The dual layers consisted of an optically-clear amorphous polyethylene terephthalate (PET) layer of 20μm thickness overlaid on top of a 80μm thickness carbon black-pigmented base layer of polyethylene-polypropylene copolymer (PE-PP). The adhesive layer bonded to the underside of the base layer consisted of an acrylic pressure-sensitive adhesive (PSA) of 50μm thickness. Two different polymer substrates of varying thickness were employed for the study, namely polypropylene (3M Canada) and polycarbonate (Lexan 8010, Sabic Innovative Plastics; Pittsfield, MA, USA). This work mainly focused upon the black polypropylene (PP) substrate which was a 500 μm thick sheet coated with a micro-layer of maleic anhydride grafted (MAH) copolymer of polypropylene and polyethylene (PP-co-PE-g-MAH) onto one surface to ensure adequate bonding with the PSA of the film; polypropylenes are common polymers in automotive part manufacturing. Optically clear polycarbonate (PC) sheets were used to allow observation of the adhesive interface during wrinkling but it also allowed examination of another viscoelastic substrate, having a different stiffness compared to the PP for influencing wrinkling behavior. Two different thicknesses (125 μm and 508 μm) of PC sheets were examined. An acrylate based adhesive primer (Adhesion Promoter 4298UV,

provided by 3M Canada) was sprayed onto the PC substrate before adhering the FBO film to ensure adequate interfacial bonding.

3.2.Film Lamination

The decorative film was laminated onto the PP and PC substrates using a HL-100 hot roll laminator (Chemsultants International; Cincinnati, OH) equipped with a top metal roller and a lower rubber roller. The holding line pressure on the top roller of the laminator and the compression ratio (total laminate thickness/nip gap opening) were kept constant as P = 483 kPa and CR = 1.3, respectively for all laminates prepared. These lamination conditions were identified through a series of tests (not presented in this paper) as optimal settings. Lamination was done at 23°C using a roller speed of 1 RPM, requiring two passes through the laminator to ensure uniform adhesion; each laminate was placed on a flat surface for 72 hours to cure before characterization and testing.

3.3.Wrinkling And Biaxial Stretching Equipment

The wrinkling during heating and biaxial stretching of the multilayered laminates was studied in detail using a custom designed bench-top thermoforming simulator equipment (TSE), shown in Figure 3-1. It was designed and fabricated to best mimic the transient conditions in a thermoformer during the heating stage while allowing quantitative monitoring of the system. The simulator consists of two key parts, (1) a radiant heating element enclosed in a metal shrouding (HS) that can be moved vertically

and horizontally above the laminate sample surface, and (2) a blowing unit used for mounting and biaxially stretching the heated sample (BUC). The setup was a modified form of a bulge testing device, an established testing technique used for biaxial tensile testing of thin films. A brief overview of bulge testing with governing principles, equations, design consideration and limitations are mentioned in the following section.

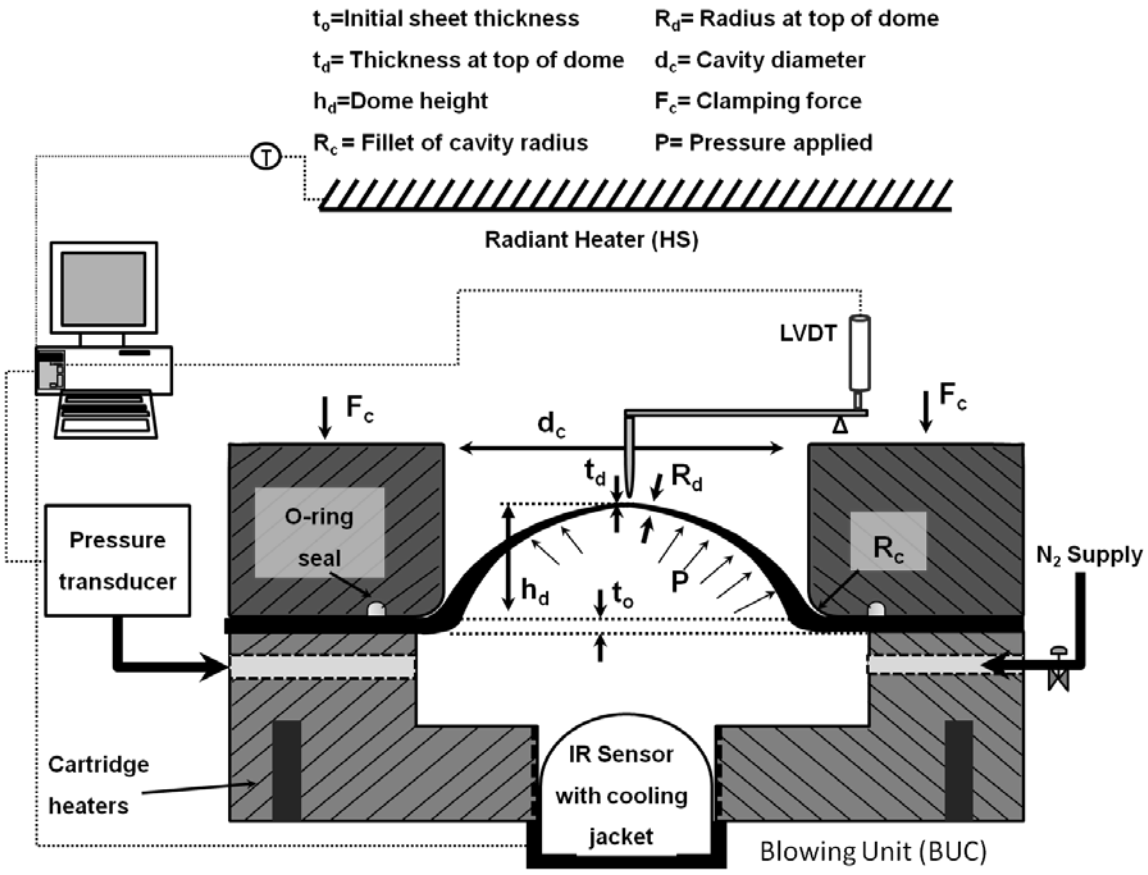

Figure 3-1: Thermoforming Simulator Equipment designed with Biaxial- stretching unit

The BUC consisted of a cylindrical aluminium block with outer diameter of 15 cm and inner bore of 7 cm (h_d). The bore hole when enclosed on its top end by a clamped sample had a volume of 220 cm^3. The block temperature was maintained at an

initial temperature of 100ºC by a set of 8-cartridge heaters (0.965 cm x 7.62 cm; 200W, 120V) drilled and installed into the walls of the block, to minimize heat loss from the sample during testing. Under normal operations, the bore was pressurized with nitrogen (N_2) gas regulated by a needle valve. The selected pressures applied under the samples, between 3-17 kPa, were monitored by a pressure transducer affixed through the wall of the BUC. To maintain a sealed volume below the sample as well as maintain uniform clamping stresses around its periphery, a metal ring clamp securely tightened down on a sample that had been positioned atop of a 100mm diameter O-ring (PTFE) seated within a grooved channel in the cylindrical block. The metal ring clamp also had curvature radius (R_c) of 6.35 x 10^{-3}m so as to minimize bending forces, reduce friction and possible necking arising due to compressive forces acting on the clamp edges. The bulge height was measured from a fulcrum attached to a LVDT (Linear variable differential transducer) placed on top of the sample; the LVDT could not be directly used to contact the inflated sample due to its small contact area causing damage to the polymer as well as the high environmental temperature that would affect its accuracy. The fulcrum was made from copper wire which experiences a thermal expansion of less than 1.05×10^{-6} cm/cm-K for the exposed fulcrum leg length of 6.35cm which experienced temperatures from 23°C to 180°C; this expansion was considered negligible compared to the displacements being studied. The deflection and pressure data were recorded using a custom developed data logging system that could be monitored by a Lab View (National Instruments) interface.

The radiant heating source (HS) consists of heating rod of 60 cm long (dia 5 mm, 200W, 120V), controlled by a PID controller coupled with a K-type thermocouple. The heating rod is bent and affixed into a square stainless steel casing so as to cover an area of 120cm ^{2} .The actual sample temperature was measured by a non-contact infrared (IR) sensor (Type K T/C OS 136-1-K, 0-400F, Omega Engineering Inc. Quebec, Canada) mounted underneath in the bore at a distance of 76 mm and was thermally shielded from the heated wall of the BUC by a cooling jacket.

The whole setup (HS and BUC) was enclosed in a large chamber with acrylic windows to isolate it from convective drafts in the room and to minimize heat losses to the environment. The ambient temperature inside the enclosure stabilized at 65 ± 5ºC for all experiments. The HS temperature, BUC temperature, sample temperature, ambient temperature was all monitored and logged to the same data logging interface.

3.4.Biaxial Stretching By Bulge Test Rig

Biaxial stretching of the film and or laminate samples was carried out using the BUC unit of the Thermoforming simulator equipment (TSE) by increasing N_2 pressure supplied to bulge the sample. This methodology is well established one and was widely used for biaxial testing of thin metal sheets and is being adapted for polymer films as well. It is the preferred method of testing for thin films and in such cases bending stresses near the clamp region can be neglected by selecting a larger aperture diameter[75][76]. The bulge pressure for deforming the sample can be achieved by supplying gas, fluids, or even low viscosity polymer-based lubricants [75][76]**.** A typical bulge tester set-up

indicating the important dimensions and test variables is depicted in Figure 3-1. For bulge tester with larger aperture diameter, membrane theory ~~is~~ can be used to compute stress, strain and pressures. Based on membrane theory, the pressure applied (P) for a given specimen of thickness (t) can be related to the principle stresses (σ_1, σ_2) on the surface of the specimen through the following relation, where R_1 and R_2 are radii of the bulged dome for its two principle axes, which are perpendicular to each other:

$$\frac{\sigma_1}{R_1} + \frac{\sigma_2}{R_2} = \frac{P}{t} \tag{3-1}$$

For an equi-biaxial case, where the bulge is a perfect hemisphere, $R_1=R_2= R_d$ and $\sigma_1= \sigma_2= \sigma$. The equation is further simplified to

$$\sigma = \frac{PR_d}{2t_d} \tag{3-2}$$

where t_d is the thickness of the sample at the top of the dome (pole). The dome radius (R_d) can be defined as

$$R_d = \frac{\left[\left(d_c/2\right) + R_c\right]^2 + h_d{}^2 - 2R_c h_d}{2h_d} \tag{3-3}$$

based on bulge height (h_d) and the curvature of the top clamp (R_c). With the known initial thickness of the sample (t_o),the thickness at the pole after bulging can be estimated

$$\text{as } t_d = t_o \left(\frac{1}{1+\left(\frac{2h_d}{d_c}\right)^2} \right)^{2-n} \quad (3\text{-}4)$$

and the strain at the bulged dome's pole can be estimated as follows:

$$\varepsilon = 2\ln\left[1+\left(\frac{h_d}{(d_c/2)}\right)^2\right] \quad (3\text{-}5)$$

Slota et al [77] stated that a die aperture of at least one hundred times the thickness of the sheet is required to neglect bending stresses. Especially for determining reliable strain fields this is important, because under practical conditions the localized variation in the strain may cause a thickness reduction along the dome surface during bending. Hence with a large aperture opening diameter of 70mm which is 128 times and 115 times the thickness of the FBO/PP and FBO/PC laminates respectively, was safer to neglect that bending influences.

The validity of the above equations is based on a circular dome assumption for purely equibiaxial deformation. There is a need to verify if the inflated/bulged height and thereby the strain at pole estimated using the above mentioned equations are still an approximate estimation of the actual strains experienced by the deformed specimen. The validation was done by bulging a laminate to a known height and comparing the strain at the pole estimated using the above equations (Eq.3-5) and cross validating the same

sample with an offline optical 3D strain analysis system ARGUS. This system has a strain accuracy of 0.1% with range of 0.5 to 300% strains. It provides the 3D coordinates of the specimen's surface and the forming changes (major and minor strains).

For this study, a FBO/PP laminate system was used. Evenly spaced dots (using a dot stencil with 3mm grid, dot diameter of 1mm) were marked on the surface of the laminate samples by spray paint (Tremclad high heat enamel; Rust-Oleum Corp., Concord, ON). The sample was initially heated to 140°C and allowed to equilibrate for 10 minutes before deforming. A bulge height of 13.5 mm was selected, as beyond this inflation height, the laminate samples were observed to neck and fail. Once the laminate reached the desired deformation, the heat source was removed, pressure was relieved and the deformed sample was allowed to cool to room temperature. The strain at the pole based on equation was estimated to be **11.22%**. The 3D non-contact strain mapping system, ARGUS, was then used to record the displacement of the dots from their original position. From the displacement data, the strain was estimated at the pole. The strain mapping recorded from the ARGUS system is shown in Figure 3-2.

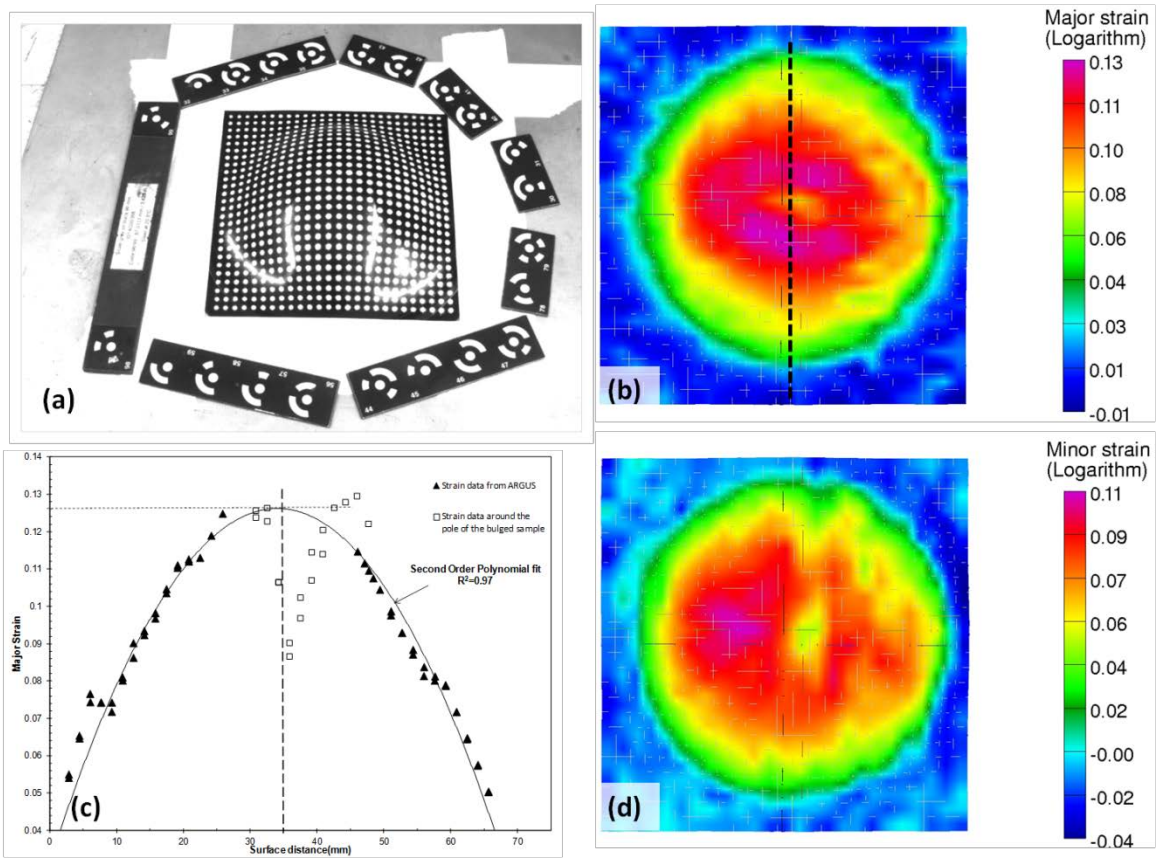

Figure 3-2: Analysis done using non contact 3D optical strain mapping system. (a) Real image of deformed FBO/PP laminate with displaced dots. Black strip used optically tracking position coordinates (b) Major Strain distribution in the FBO/PP (c)Plot of the major strain points across diameter of the sample with a polynomial fit. (d) Minor Strain distribution in the FBO/PP laminate

The strain at pole was estimated to be **~12.6%.** It should be noted that this value was estimated based on the polynomial fitting by neglecting the strain points from the pole (marked as □) and using the strain data points from edges (marked as▲). In reality, some amount of relaxation of the material occurs once it is allowed to cool down and relieve the stresses acting on its surface. As this technique is an offline optical stain analysis system, achieving the actual strain at its fully inflated height was not possible. Also from Figure 3-2 (b), it was observed that the maximum strain experienced by the sample was noticed in a ring just around the pole of the dome. It should be noted that

during bulging, the strain at the pole would be more equi-biaxial in nature whereas in the other regions would be more non-equi-biaxial. Thus the rupture in the sample occurred in the regions where there is a transition from equi-bixial to non-equibiaxial, i.e., in the circular region located immediate next to pole. For this study, it was concluded that the equations based off membrane theory were adequately valid and applicable to the laminate systems, though this analysis allowed us to take into account the limitations and capability of the measurements in this work.

3.5. Thermoforming

A conventional vacuum thermoformer (Model BV C-Class 61 cm x 122 cm, Bel-O-Vac Inc., USA) was retrofitted with a bellow that created a sealed environment underneath a clamped sample, which could be pressurized with gas yet allow the vacuum box assembly to move up and down freely, as shown in Figure 3-3. Nitrogen gas was supplied into the bellow at a regulated flow rate. The normal metal clamp of the thermoformer was modified with a silicone rubber seal to minimize gas leakage around the laminate sample during heating. The top clamp has a circular aperture of 30 cm which exposes the effective laminate area for forming. To ensure all samples had replicable inflation height, a metallic wire (shown in Figure 3-3) held in tension between two adjustable rods is set in place above the sample. The length of the wire runs along the diameter of the bulge. The oven consisted of three radiant heating panels located 20 cm above the sample.

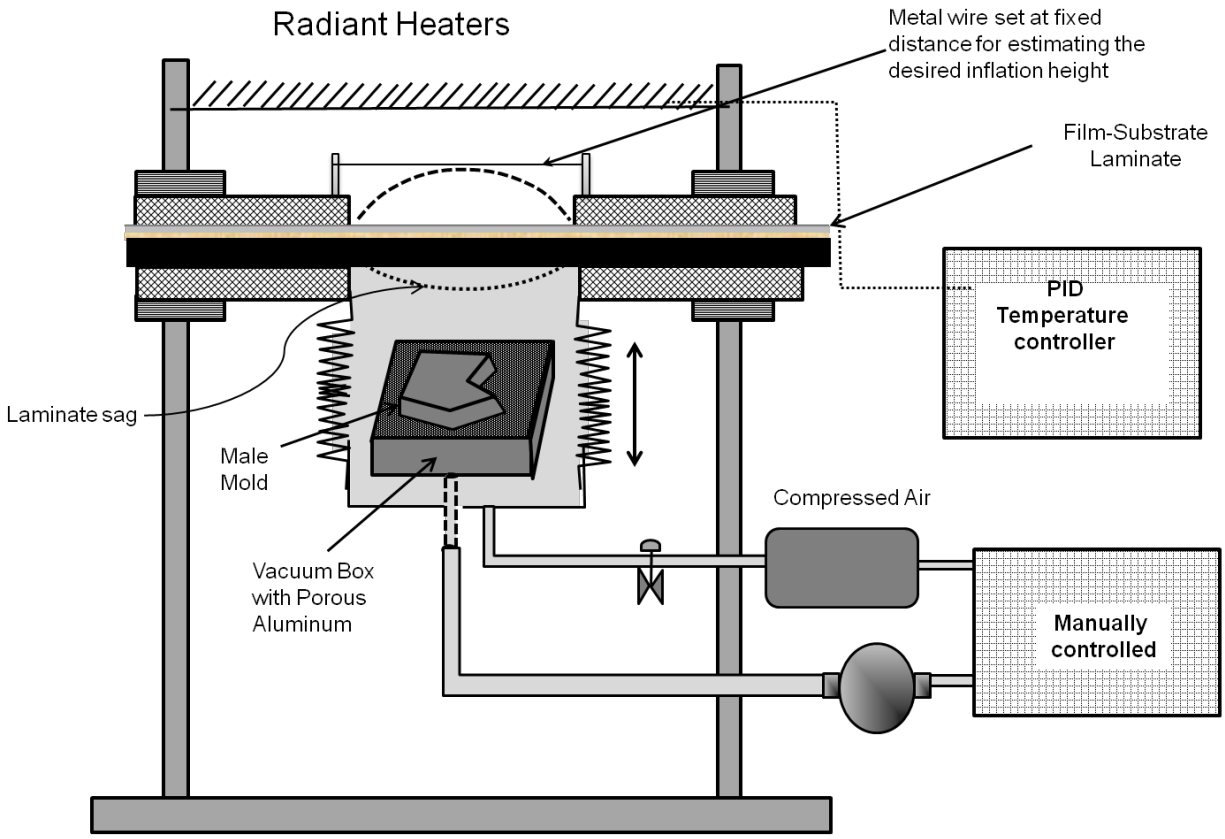

Figure 3-3: Modified Thermoformer-Stretch assisted thermoformer (STF)

Three processing conditions were tested in this study. *Normal (Conventional) thermoforming* operations involved a heating stage whereby the temperature of a laminated sheet held in the clamp increased until sagging was noticed, taking approximately 5 minutes. The heaters were set to 300 ºC, which is measured using a hand-held infrared pyrometer so as to achieve a sample temperature of ~160ºC. The vacuum box was then raised from beneath for the forming step where the softened sample was drawn over a male mold under vacuum. A complex mold shape with featured regions of high strain along its edges but also a large flat region where no stretching occurs, is shown in Figure 3-3. The mold design had various draw angles and features to

encompass a range of draw capability typically seen in industrial applications for such materials. A detailed mold design is shown in the Appendix A

Stretch-assisted thermoforming (STF) operations were accomplished by two methods for this study, as a two-step process and as a dynamic one-step process. For *Isothermal STF*, the sample was heated and allowed to sag just as done in the conventional procedure but then included an intermediate inflation step under a fixed N_2 pressure before the forming step. In this procedure, the wrinkles were allowed to form during heating, and an attempt was made to eliminate them by bulging. For the *dynamic STF* method, bulging and heating of the sample was carried out simultaneously until the sample reached the required softened state. This method prevented the formation wrinkles during heating as the compressive stress induced during heating was continuously relieved by the stretching force due to bulging. The forming step for both STF operations was identical to that described for the normal thermoforming operation, namely that the vacuum box and mold rose up within the bellow and vacuum drew the softened laminate into shape.

3.6. Characterization

3.6.1. Dynamic Mechanical Analysis

The variation in material stiffness with respect to temperature was obtained by dynamic mechanical analysis (DMA) for the film and substrates using a Model 2980 dynamic mechanical analyzer (V1.7B; TA instruments, USA). The test was conducted

on rectangular specimens of 30mm x 5mm by mounting them in a film tension clamp with a pretension force of 0.01N. The dynamic storage modulus (G''), loss modulus (G') and tanδ were recorded over a temperature range of 20-180ºC. For determining the modulus of FBO, PP, and PC specimens with increasing temperature, the test conditions (frequency, amplitude) had to be varied for different temperature ranges by holding a fixed temperature ramp of 3ºC/min. For measurements at temperature ranges of 25-100ºC, testing was conducted with (frequency, amplitude) set to (1Hz, 15μm). And at temperature ranges of 100-180 ºC, testing was conducted with (frequency, amplitude) set at (10Hz, 200μm) for FBO and PP whereas (10Hz, 25μm) for PC. As material softens at elevated temperatures, low frequency signals would get easily damped by the material and thus stress transfer through the specimen would be very minimal. Hence a higher frequency and amplitude is required to detect stiffness of a material at elevated temperatures. Figure 3-4 shows the dynamic moduli (G', G'', tanδ) for FBO, PP, PC specimens over temperature range of 20-180ºC**.** The stress relaxation modulus was measured by DMA using similar rectangular specimens at a constant strain of 1% at isothermal conditions for different temperatures ranging from 100 ºC to 180 ºC. Each iso-strain test lasted 25 minutes.

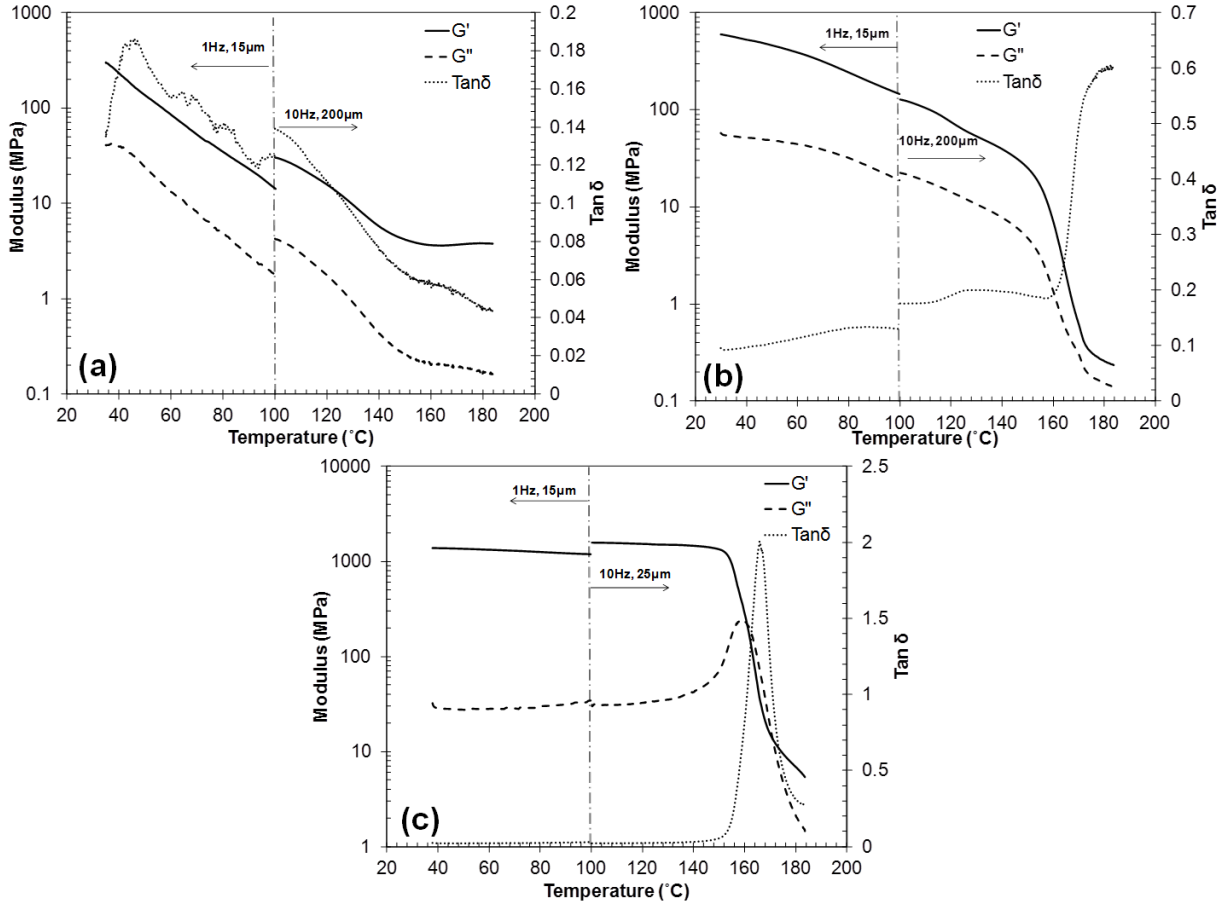

Figure 3-4: Dynamic Moduli (G',G", tanδ) for (a) FBO film (b) PP substrate (c) PC substrate. Temperature range of 20-180°C measured at heating ramp of 3°C/min. The frequency & amplitude for applicable temperature ranges are shown.

3.6.2. Differential Scanning Calorimetry

The thermal transitions of the constituent layers were determined for a heating rate of 10^{o}C/min from -40^{o}C to 200^{o}C, using Q200 differential scanning calorimeter (DSC) from TA Instruments (USA). The modulating feature was used with ±1^{o}C/60s oscillations for the specific case to resolve the glass transition of the PET layer in the multilayered decorative film construction. Figure 3-5(a) shows a DSC thermogram of the first heating cycle for FBO, PP, PC specimens over temperature range of 20^{o}C to 180^{o}C.

The concerned temperature transition points are marked for each curve. These transitions are glass transition temperatures (Tg) and melting temperatures (T_m) of the component layers for the given material. Similar observations were seen when the first derivative of tanδ with respect to temperature were taken for FBO film, PP and PC susbtrates **(see** Figure 3-5: b, c, &d). This is done to resolve the transition points and determine the peak temperatures corresponding to the above mentioned transitions. The transition points seen in both DSC thermogram and first derivative tanδ curves were comparable.

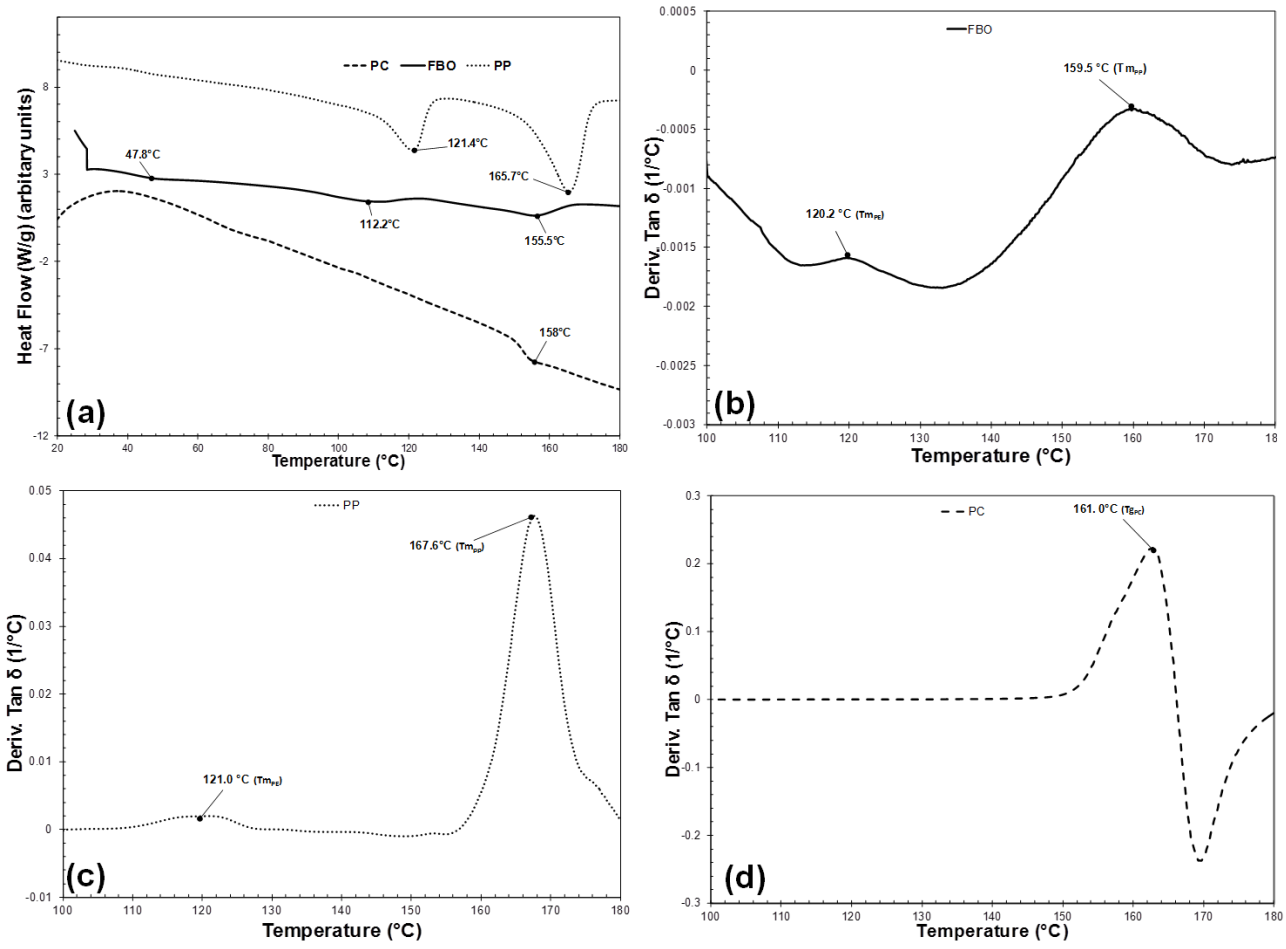

Figure 3-5:Comparison between DSC thermogram and first derivative of tanδ curves w.r.t temperature. (a)DSC Thermogram of first heating cycle of FBO film, PP & PC substrate for a temperature range of 20-180°C; Derivate of tanδ w.r.t temperature (100-180°C) for (a) FBO film, (b) PPsubstrate,(c) PC substrate.

3.6.3. Coefficient Of Linear Thermal Expansion

The coefficient of linear thermal expansion for the film and substrates was determined using the digital image correlation (DIC) technique [78][79]. Film and the substrate strips of width 6 mm and length 13 cm were individually placed in a specially designed mounting stage where one end of the strip sample was gripped by a fixed clamp and the other end was attached to a freely movable clamp supported on low friction bearings. The whole setup was placed inside a convective oven with a high temperature resistant quartz window. In order to avoid bending or deflection of the sample during heating a small load of 0.1 N was applied to the movable clamp. Figure 3-6 shows a sketch of the thermal expansion setup. Randomly placed dots were marked on the surfaces of the samples by spray paint (Tremclad high heat enamel; Rust-Oleum Corp., Concord, ON). Thermal strain data was calculated by the displacement of the dots while the sample was heated at 10°C increments going from 25^{o}C to 200^{o}C with 5 minutes hold at each temperature condition to allow the sample to reach a thermal equilibrium. A non-contact strain mapping system, ARAMIS (V6.0, GOM mbH, Braunschweig, Germany) equipped with a camera was used to record the displacement of dots from their original position in real-time. From the displacement data, the strain was estimated and subsequently thermal expansion values were determined.

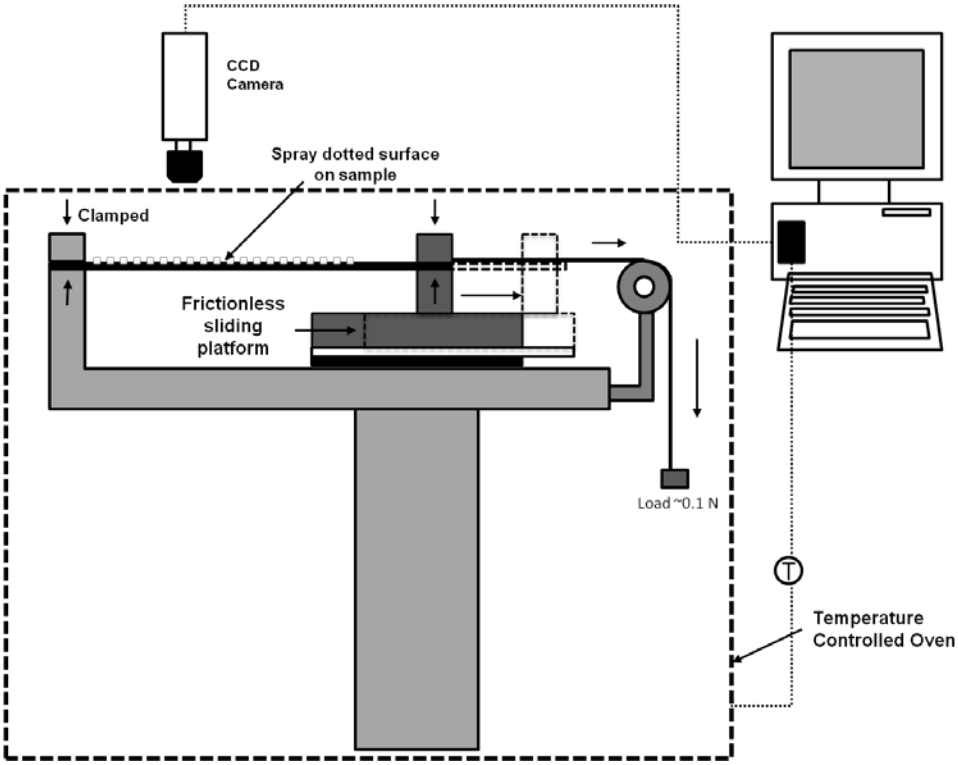

Figure 3-6: Linear Thermal Expansion equipment with DIC technique

The thermal strain produced for FBO, PP and PC specimens with increasing temperature is shown in Figure 3-7. The coefficient of linear thermal expansion (CLTE) denoted by α is determined by taking the slope of the linear region of thermal strain data points (~100°C to 160°C).

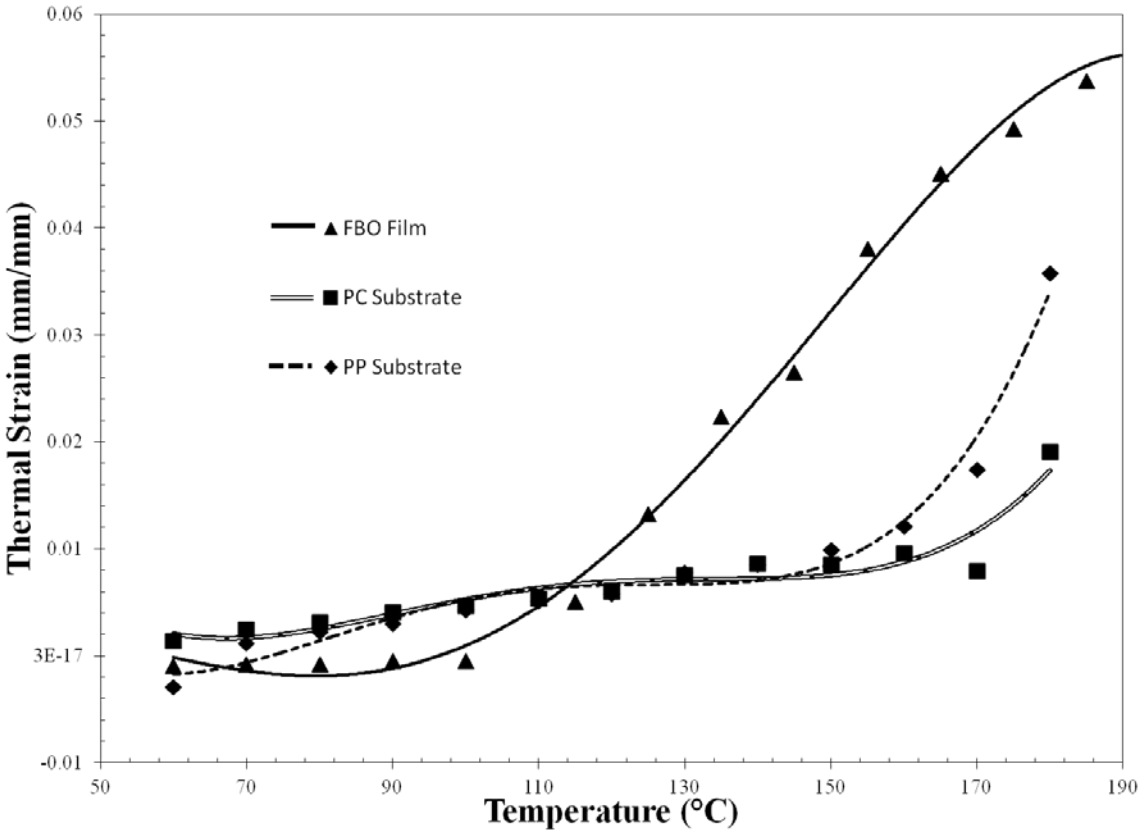

Figure 3-7: Thermal Strain estimated by DIC technique plotted against temperature to determining the coefficient of linear thermal expansion for FBO, PP, and PC specimens.

3.6.4. Profilometry

The descriptive wrinkle parameters, amplitude and wavelength, were measured for samples using a 2-D surface profilometer (KLA-Tencor Alpha-Step 200) equipped with a standard stylus of 12.5 micron radius. The stylus rides smoothly over the wrinkled samples along the x direction and a 2-D image was generated automatically after the scan. Measurements with resolution up to 5 nanometers can be obtained from the profilometer.

3.6.5. Film Light Transmission

In order to quantify the damage caused to the samples due to thermal wrinkling, light transmission through laminate samples was measured. The FBO/PC samples were clamped between two light-guides of diameter 70mm with a spectrometer-grade reflective coating in their inner lining. A variable intensity light source was placed on the end of one guide and a handheld digital microscope (Aven Inc. MI, USA) connected to the computer on the end of the other guide. The images were recorded after calibrating the light source intensity with a standard light meter to an intensity of 1050 lux. A laminated FBO/PC sample that was never heated or strained was taken as the reference. All images for the wrinkled FBO/PC samples were then converted to 8-bit gray scale images and a corresponding mean gray value was determined using a java-based image processing software (ImageJ, v1.43m). The values ranged between 0-255 with 0 corresponding to completely black sample and 255 to white sample. The reference mean gray value was deducted from each sample for a given intensity level to give the net change in mean gray value. This value is an indirect estimate of the extent of damage to layers of FBO. Figure 3-8 shows the setup. The plots and detailed discussions are given in the following chapter.

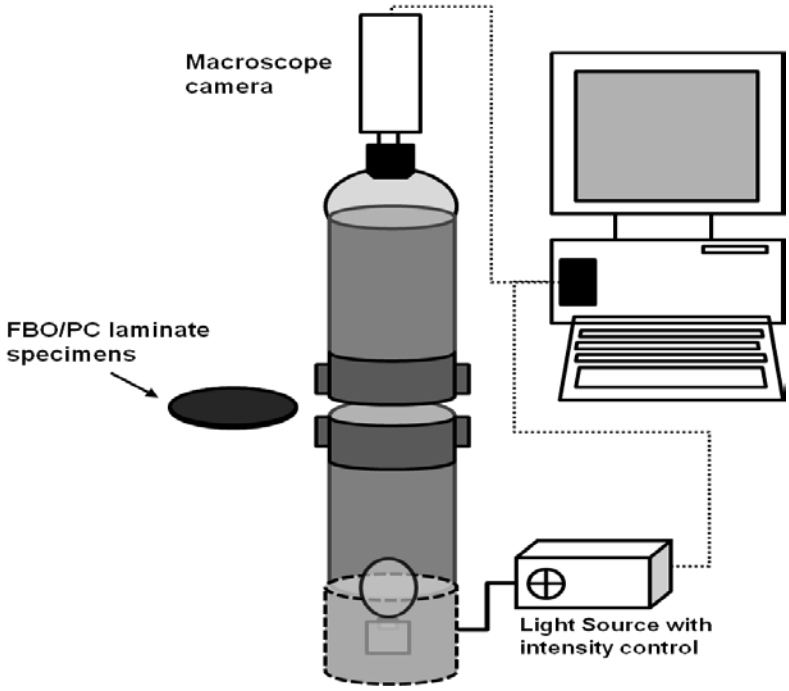

Figure 3-8: Sketch of the Light Intensity measurement setup

3.7.Experimental Design

The study on wrinkling phenomena was conducted using two distinct substrates PP and PC, laminated onto FBO film. For FBO-PP laminates, samples at five distinct temperatures ranging from 135-180 °C and at four distinct heating rates were studied. For FBO-PC laminates, two different thicknesses of PC substrates were studied. Samples at five distinct temperatures and two distinct heating rates were studied for each thickness of PC. For each wrinkled samples, 50 sets of distinct amplitude and corresponding wavelengths were measured by employing the AlphaStep profilometer. The median of this data set was taken as the representative amplitude and wavelength of the wrinkled laminate sample for a given temperature and heating rate.

For biaxial stretching via *Isothermal* and *Dynamic* forming, inflation pressures ranging from 3- 17 kPa was used. For isothermal forming, four distinct temperatures (130-180 °C) were used, attained by altering the HS temperature. For both methods of stretching, the samples were initially allowed to equilibrate in the clamped state for 10 minutes before the HS source was swung in to heat the sample. For isothermal forming, the sample was allowed to heat and equilibrate to the set point temperature for another 5 minutes before biaxial stretching step by application of predetermined inflation pressure. For dynamic forming, the samples were biaxially stretched and heating simultaneously. Deflection and pressure reading was measured to be used for populating the stress-strain curves.

CHAPTER 4 RESULTS AND DISCUSSION

4.1. Wrinkling Behaviour in Multilayer Polymer Film/Substrate Laminates

Wrinkling of FBO film laminated on two different substrates viz., Polypropylene (PP) and Polycarbonate (PC) with varying thicknesses when subjected to heating under the radiant heater in the thermoformer, has been reported in the present investigation. The influence of parameters such as temperature (T) and the rate of heating (R) of the sample have been our special focus as they were the primary variables that could cause thermal wrinkling. Wrinkling behaviour was studied using the specially designed thermoformer simulator (with BUC and HS units), as described in Chapter 4, Figure 3-1. Both the parameters T and R were varied by varying the radiant heat source temperature (T_s), so as to mimic the practical conditions in the conventional thermoformer. The other factors which could influence the heating rate of the sample are the radiant heating source material and its emissivity, sample emissivity and absorption, distance between radiant heating source and sample surface, sample thickness and ambient air temperature. In the present study, as we tried to mimic the practical thermoforming conditions, the radiant heat source temperature was the only variable that was altered to achieve different heating rates while the other factors were kept constant. It should be noted that in a multilayered laminate system, each and every constituent layer might get heated at a different rate based on their thermal conductivity and their infrared absorption ability at

that temperature. However, since we are using thin films, the differences in heating rate between the layers were assumed to be infinitesimally small.

4.2. Influence of Temperature on Modulus, Expansion and Relaxation Behaviour

In order to study the wrinkling behaviour under dynamic variation of the temperature, change in the material properties such as the dynamic modulus, thermal expansion values and their relaxation properties have been experimentally determined. The corresponding variation in the compressive buckling strain and the critical conditions causing buckling were modelled in the following sections. Refer to Chapter 4, Figure 3-7 for the thermal expansion curves of FBO film, PP and PC substrates.

The changes in the modulus of the film (E_f), and the substrate (E_s) with increasing temperature (T) for the FBO/PP system are shown in Figure 4-1. The modulus of the PP substrate decreased almost exponentially from 47 MPa at 135ºC to a very low value of 0.25 MPa at 180ºC, whereas the film modulus decreased gradually from a value of 6.4 MPa (at 135ºC) to 3.8 MPa (at 180ºC). This range of temperatures was most important to this work, since no wrinkles occurred below and the substrate was unusable above.

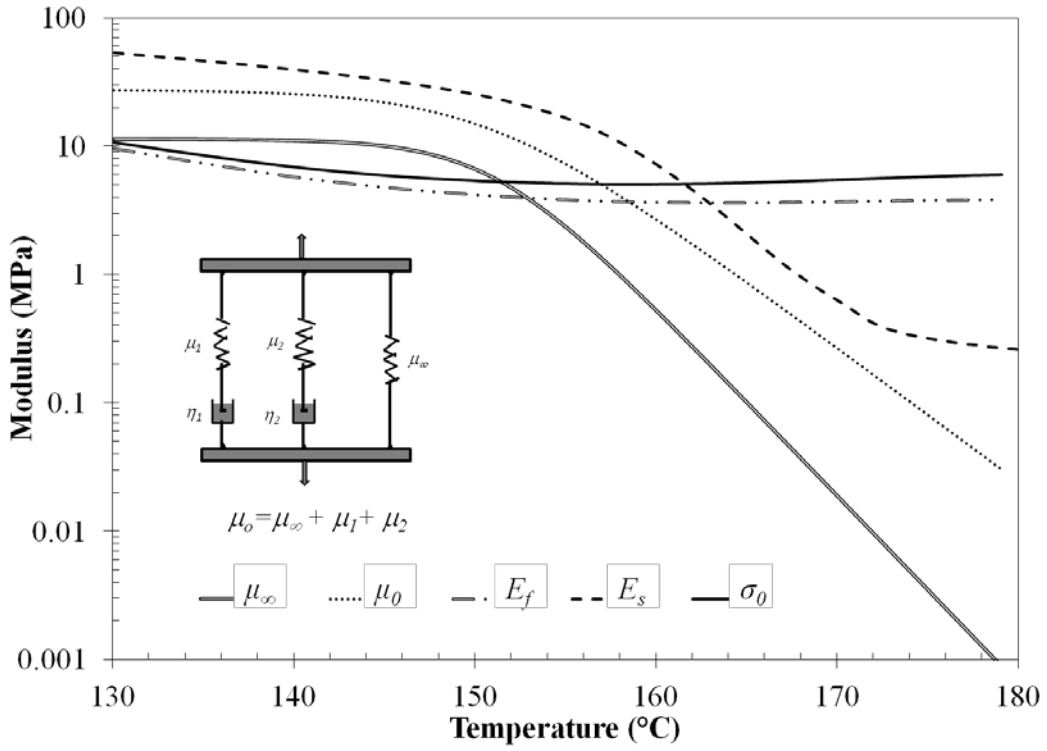

Figure 4-1: Change in the modulus with temperature: (i) E_f is the FBO Film modulus, (ii) E_s is the PP substrate modulus and (iii) μ_0 & μ_∞ are the relaxation modulus of the PP in the glassy and rubbery state, and (iv) σ_0 is the thermally induced compressive stress on the film

The value of E_s was substantially higher than E_f until reaching 162ºC, indicating the dominance of substrate elasticity over the film at lower temperatures. On the other hand, for T >162ºC, the behaviour was vice versa i.e., the value of E_s dropped below the value of E_f implying that now the elastic properties of the film were more dominant in the laminate. The drop in moduli between 130°C to 180°C corresponds to the melting of the PE and PP crystalline segments confirmed from DSC data (See Chapter 4, Figure 3-5**).** The onset of wrinkling at around 135°C was seen due to the softening of PE segments in the film and substrate. At this temperature, there was a transition from elastic behaviour to more viscoelastic behaviour in the component layers. At around 150°C and above, the

softening of PP segments began and the material lost most of its strength (moduli) behaving like a viscous material.

The experimental viscoelastic relaxation modulus of the substrate $\mu(t)$ obtained over a temperature range of 135ºC to 180ºC was used to estimate the glassy (μ_o) and the rubbery state modulus (μ_∞) by identifying a suitable theoretical model that could fit the data. The PP relaxation modulus data included in Figure 4-1 obeyed a standard linear mechanical model with three parallel branches, i.e., a branch with only one spring connected in a parallel manner to two other branches each consisting of a spring and dashpot in series. The model can be mathematically expressed by reducing Eqn (4-1) to the form of Eqn (4-2):

$$\mu(t) = \mu_\infty + \mu_i \sum\nolimits_i \exp(-p_i t) \tag{4-1}$$

and $\mu_0 = \mu_\infty + \mu_{i=1-n}$

$$\mu(t) = \mu_\infty + \mu_1 \exp(-p_1 t) + \mu_2 \exp(-p_2 t) \tag{4-2}$$

where $\mu_0 = \mu_\infty + \mu_1 + \mu_2$ is the glass modulus, μ_∞ is the rubbery modulus and μ_1, μ_2 are the modulus values of the springs in the two parallel branches respectively. The fitted coefficients are shown in Appendix B. The relaxation modulus values of the glassy state μ_o and the rubbery state μ_∞ obtained from the experimental shear modulus data showed an identical trend over a temperature range of 135-180 ºC. Both the value of μ_o and μ_∞ remained almost constant up to 150ºC and showed an exponential decrease beyond

150ºC. This drop corresponded to the viscous-like behaviour of the substrate as PP segments began to soften.

During heating, compressive stresses arise due to the mismatch in thermal expansion which is stored in the form of elastic energy within the film. To relieve this thermally induced stress in the film, out-of-plane deformation such as wrinkling occurs. Due to the stiffness of the layers, this tendency of out-of-plane deformation is prevented at lower temperatures (below 130°C) by storing the elastic energy within the film layers. However with increasing temperature, the material losses its elastic strength, due to softening of PE and PP segments in the base layer of FBO film, and its capability to store the compressive stresses in form of elastic energy depreciates, resulting in the manifestation of out-of plane deformations in the form of wrinkles. The formation of wrinkles will also be influenced by the reducing stiffness of the substrate with temperature. The compliancy and conformation of the substrate to wrinkle pattern in these two temperature ranges will be discussed in followings sections.

The modulus data for the FBO/PC system is presented in Figure 4-2. In this case, the elastic modulus of the PC substrate remained substantially higher than the film throughout the temperature range studied.

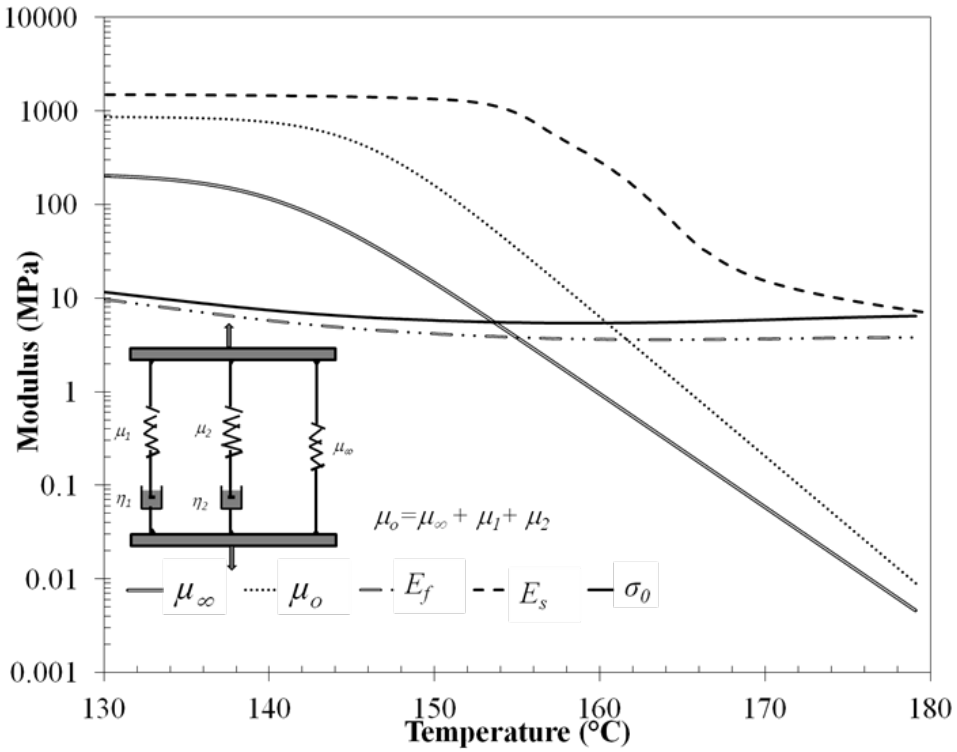

Figure 4-2: Change in the modulus with temperature: (i) Ef is the FBO Film modulus, (ii) Es is the PC substrate modulus and (iii) μ_0 & μ_∞ are the relaxation modulus of the PC in the glassy and rubbery state (iv)σ_0 is the thermally induced compressive stress on the film.

The glassy state (μ_o) and the rubbery state (μ_∞) relaxation moduli for the PC substrate shown in Figure 4-2 were obtained by fitting a standard linear model with 4 parallel branches using the mathematical form of Eqn (4-3):

$$\mu(t) = \mu_\infty + \mu_1 \exp(-p_1 t) + \mu_2 \exp(-p_2 t) \qquad (4\text{-}3)$$

where μ_∞ is the rubbery modulus and the glassy modulus, $\mu_0 = \mu_\infty + \mu_1 + \mu_2$. The fitted coefficients are shown in Appendix C. Both the relaxation modulus values (μ_o, μ_∞) for PC remained unaltered until T=140ºC (860MPa, 200MPa) and beyond that it decreased sharply to a very low value of (0.01MPa, 0.005MPa) at T=180ºC.

In FBO/PC laminates, similar behaviour to FBO/PP laminates was seen where wrinkling was observed on samples that approached 135°C. Wrinkles seen on samples between 135-150°C, though visible do not completely cover the FBO film surface. At this range the sample is viscoelastic in nature. Samples taken to temperatures beyond 150°C, showed more prominent wrinkles with softening of PP segment in the base layer of FBO film.

Thus from observing both FBO/PP and FBO/PC laminates, it could be concluded that the onset of wrinkling was more dependent on the softening of PE segment in the base layer of the FBO film with more prominent wrinkles and surface coverage seen when softening of PP segment of base layer occurred in addition to possible contributions due to softening of the PP substrate or PC substrate. However, the compliancy and conformation of the substrates to FBO wrinkle patterns are dependent on the stiffness of the respective substrate and interestingly follow different modes of deformation. This will be discussed in detail in the following sections.

4.3. Wrinkle Evolution for FBO/PP Laminates

4.3.1. Influence of Temperature and Heating rate

FBO/PP laminated samples were heated from an initial room temperature (23ºC) to elevated temperatures in the range of 130ºC to 180ºC (with runs differing by 10ºC intervals) at varying apparent heating rates of 45 - 85ºC/min. Irrespective of the heating rate, wrinkling was observed on the film surface but only when the sample temperature

exceeded 135ºC; this onset temperature was similarly noted in a previous work whereby the same decorative film was applied to a metal substrate [80], indicating the film itself determined this value. The low magnification surface images of the wrinkled FBO/PP laminates heated to temperatures between 135ºC and 180ºC are shown in Figure 4-3. The wavelength (λ) increased from 460 μm to 850 μm and the amplitude (A) increased from 7.2 μm to 24 μm for the wrinkled pattern as the sample temperature increased from 135ºC to 180ºC, respectively.

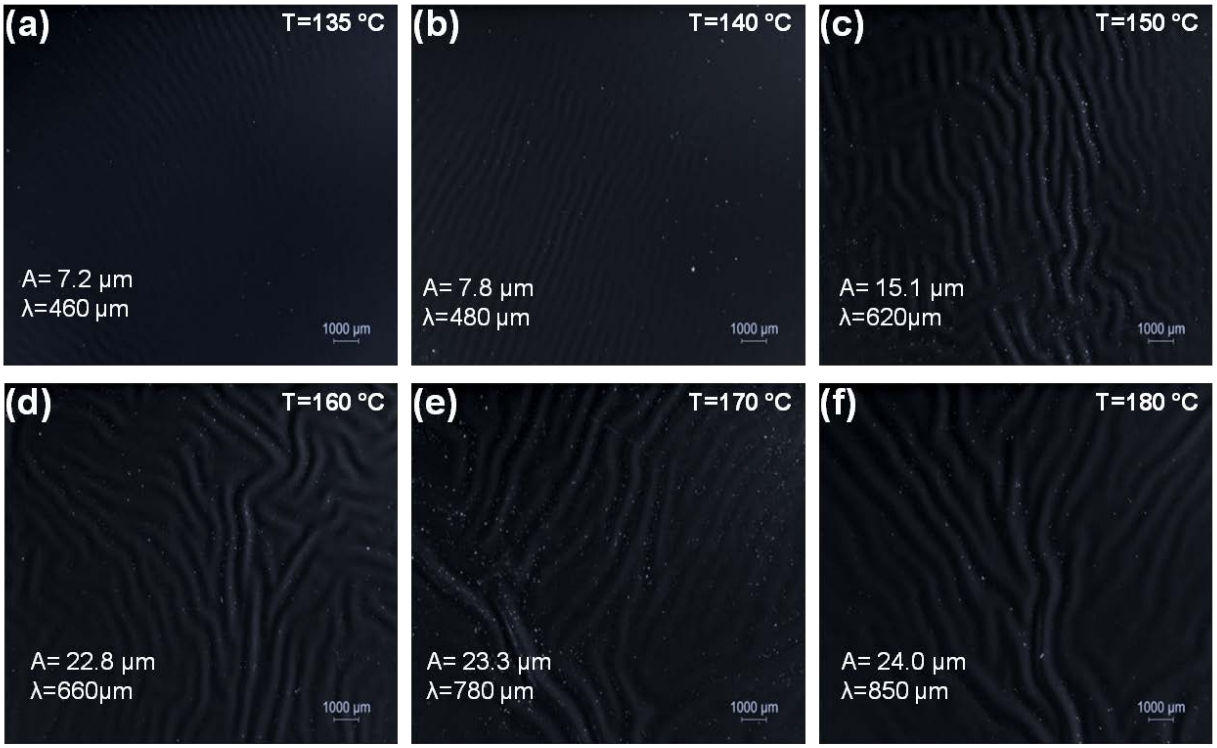

Figure 4-3: Optical images of the wrinkled FBO/PP laminates with increasing temperature (T= 135 - 180ºC) at a heating rate of 70ºC/min

The orientation of the wrinkles at lower temperatures, 135-150ºC, was more unidirectional in nature but as the temperature increased further (160-180ºC), discrete

regions of complex wrinkling pattern with random orientations were noticed. Complex wrinkling pattern appeared as the modulus of the substrate approached that of the film or further decreased lower than the film. The discrete regions grew larger in dimension with increasing temperature. At these higher temperatures, the component layers became ever more viscous and thus, random orientation and converging of wrinkles could be seen. Also, it could be seen for this temperature range between 135-150°C that wrinkles only partial covered the film surface. Above 150°C, the wrinkles were more evenly distributed on the surface as well as more prominent with complex random orientations.

With the heating rate increasing from 45 - 85ºC/min, micrographs of the film surface, in Figure 4-4 showed that the wrinkle wavelength increased from λ= 500μm to 680μm and the amplitude increased from A=8.8μm to 23.6μm, respectively. It is evident that both values of λ and A were influenced by both changing temperature and heating rate in the study.

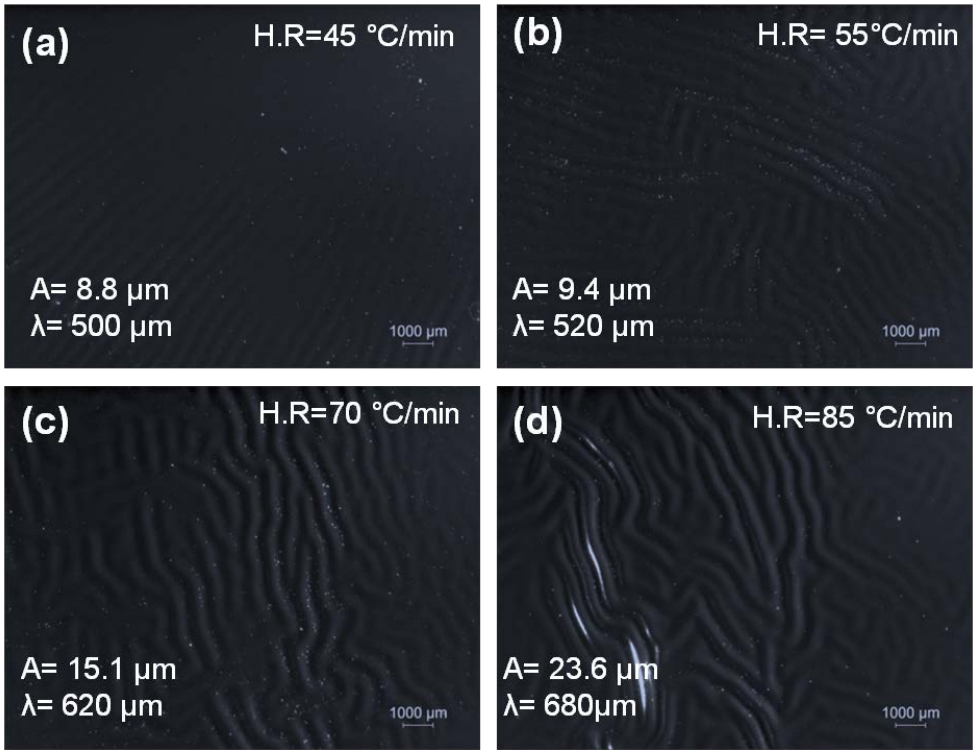

Figure 4-4:Optical images of the wrinkled FBO/PP laminates with increasing heating rate from 45-85ºC/min at T=150ºC

The experimental amplitude values (*A*) were plotted with respect to temperature (*T*) for different heating rates in Figure 4-5. The progression in the amplitude growth with increasing temperature for different heating rates, was found to be sigmoidal in nature (lines are sigmoidal fittings, Figure 4-5), with a steeper growth region in the mid-range of temperatures, along with a lower and an upper asymptote value at the extremes. The temperature range spanning the growth region narrowed as the heating rate increased.

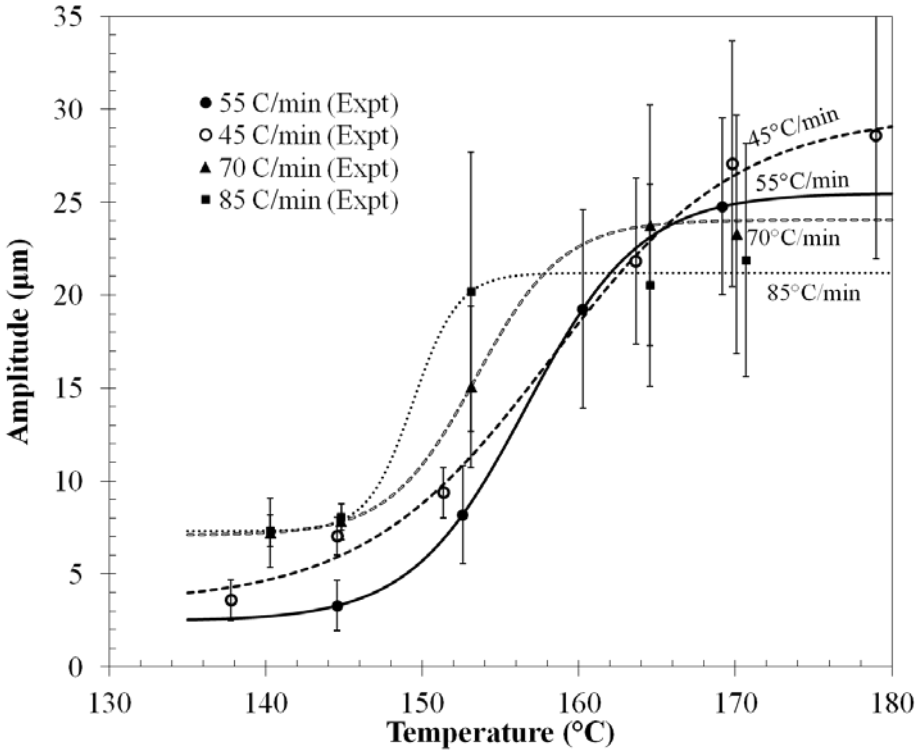

Figure 4-5:Amplitude growth with increasing temperature (T) for different heating rates for the FBO/PP system. Lines included to clarity of the trend.

In Figure 4-5, the lower asymptote of the sigmoidal curves (130-145°C) exhibited lower amplitude values with lower heating rates. Conversely, an opposite observation was seen at temperatures greater than 155°C where the upper asymptote of the sigmoidal curves showed smaller amplitudes values for higher heating rates. As a result, in that the range wrinkle amplitude levelled-off with increasing heating rate. It is fair to state that the film exhibited severe distortions, deviating far from a desired Class-A surface for temperatures above 150^{o}C when affixed to the PP substrate.

A similar analysis of the experimental amplitude (*A*) values was done with respect to heating time (*t*). The plot again showed sigmoidal growth, as seen in Figure 4-6. This

sigmoidal behavior was analyzed by fitting the data to the model expression given in Eqn (4-4):

$$A = c + \frac{d - c}{1 + \exp(-a(t - b))} \tag{4-4}$$

where the factors a represents the growth rate in s^{-1}, b is the inflection point, c is the lower asymptote and d is the upper asymptote. The growth rate (a) increased exponentially with the heating rate from a value of $0.067s^{-1}$ at 45ºC/min to a value of $0.95s^{-1}$ at 85ºC/min. This indicated that the growth rate for wrinkle amplitude was strongly influenced by the heating rate of the process. It needs a special mention here that the reported studies on wrinkling in the literature were primarily limited to elastic film/substrate material systems, they only considered the wrinkling phenomenon to be temperature dependent and the heating rate dependency has never been reported. The viscoelastic-viscoelastic film-substrate system in this study is showing different dependency than elastic systems.

It was interesting to note that the initial amplitude observed at time t=0 (i.e., lower asymptote) increased with the heating rate and the final amplitude present at time $t=\infty$ (i.e., upper asymptote) decreased with the heating rate. Although, the heating rate facilitated the formation of larger amplitudes in the initial period of time, it suppressed the formation of larger amplitudes at infinite time. This could be strongly influenced by the heat absorption rate of the material under the applied heating rate. In other words, the rate of absorption of heat by the sample was much lower than the applied heating rate,

especially at higher heating rates. Hence when the heat energy supplied at a faster rate, the system would be able to only partially utilize the energy for the growth of the amplitude, corresponding to the energy absorption rate at the temperature. As a result of which the amplitude growth reaches a stable equilibrium value at a much lower temperature.

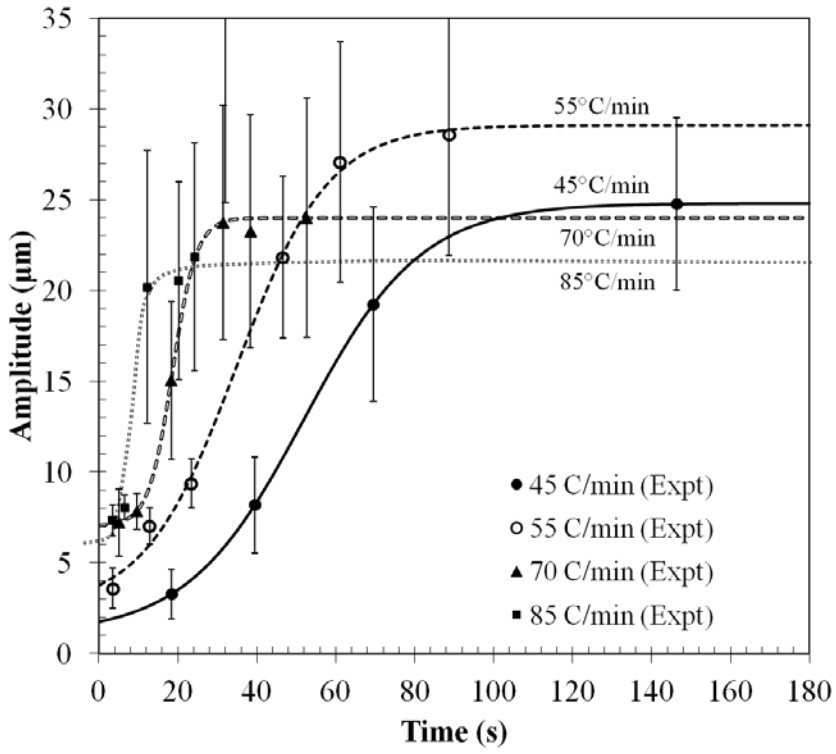

Figure 4-6: Amplitude growth over time (t) for different heating rates for the FBO/PP system. Time normalized to t=0 at 135°C (onset of wrinkling) Lines correspond to the fitted model in Eqn (4-4).

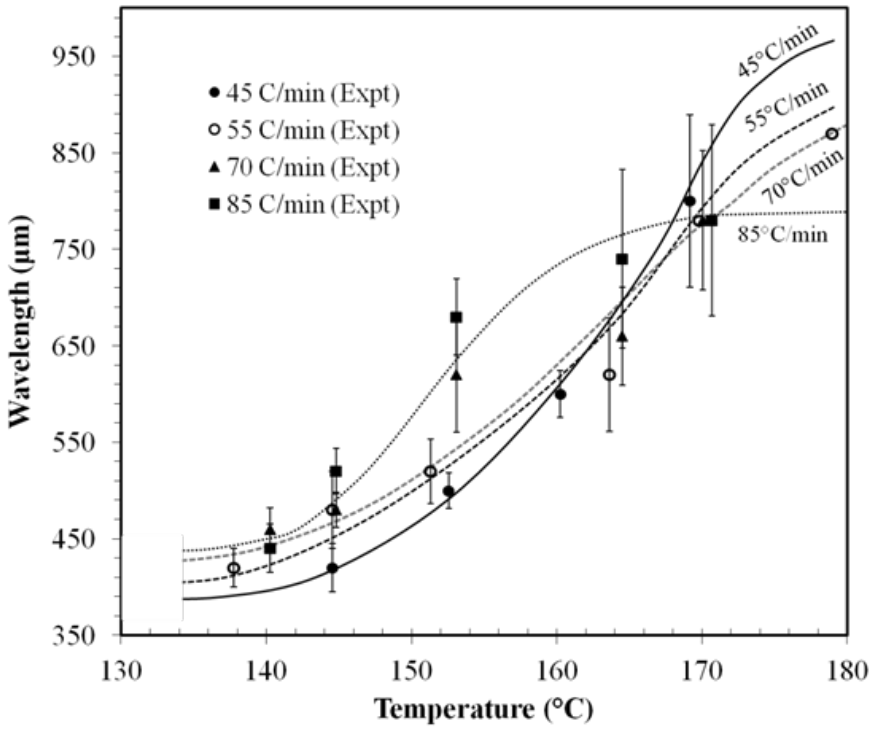

Figure 4-7: Wavelength vs. temperature (T) for different heating rates for the FBO/PP system. Lines shown to clarify the trend.

The measured wavelength (λ) also increased in a sigmoidal manner with increasing temperature (T) and time (t) at the heating rates employed for the study, as shown in Figure 4-7 & Figure 4-8 respectively. From the sigmoidal curves of λ vs. t, Figure 4-8, the growth rate values were estimated for the corresponding heating rates using the same expression of Eqn (4-4). Again, there was an exponential increase in the growth rate factor from a value of $0.07s^{-1}$ at 135ºC to $0.22s^{-1}$ at 180ºC showing heating rate to be a significant influence on wrinkle wavelength. The lower asymptote values of the wavelength were found to be larger for the higher heating rates, whereas the higher asymptotes values were found to be smaller for the lower heating rates. Hence the

variation of the wavelength with temperature and time are identical in nature to the variation of the amplitude.

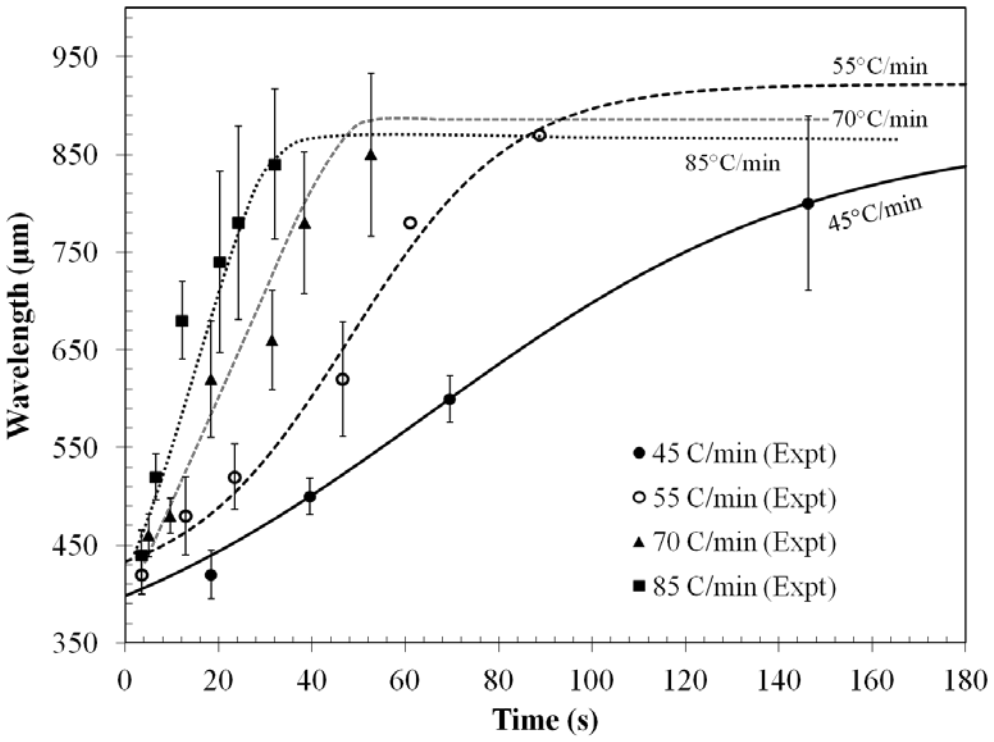

Figure 4-8: Wavelength vs. time (t) for different heating rates for the FBO/PP system. Lines correspond to best fit models of Eqn (4-4).

4.3.2. Influence of Substrate Compliancy

The final wrinkled state of the laminate is considered in the literature to be a function of the relative level of compliancy of the substrate to the film. Considering that the FBO film was more elastic and yet thinner than the substrate, three different wrinkled states were possible, as included in Figure 4-9. The state-I represents the non-compliancy of the substrate to the wrinkles whereas state-II and III represents varying levels of compliancy by the substrate to the wrinkling film. In state-I, the winkles are formed only

on the film surface and substrate is completely resistant to wrinkles; debonding frequently occurs for such a state. In state-II, only the surface of the substrate is complaint to wrinkles formed in the film whereas the whole bulk phase of the substrate is complaint to wrinkles in the film for state-III; there are many practical examples of state-III wrinkling but the models in the wrinkle literature do not consider this complex behavior. All three states occurred over the temperature range of this study and they will be identified after the compliancy data has been reported. There is also another possible wrinkle state-IV, where both the substrate and film wrinkle independently in opposite direction perpendicular to their interfacial plane [29] though such a system is beyond the scope of this work.

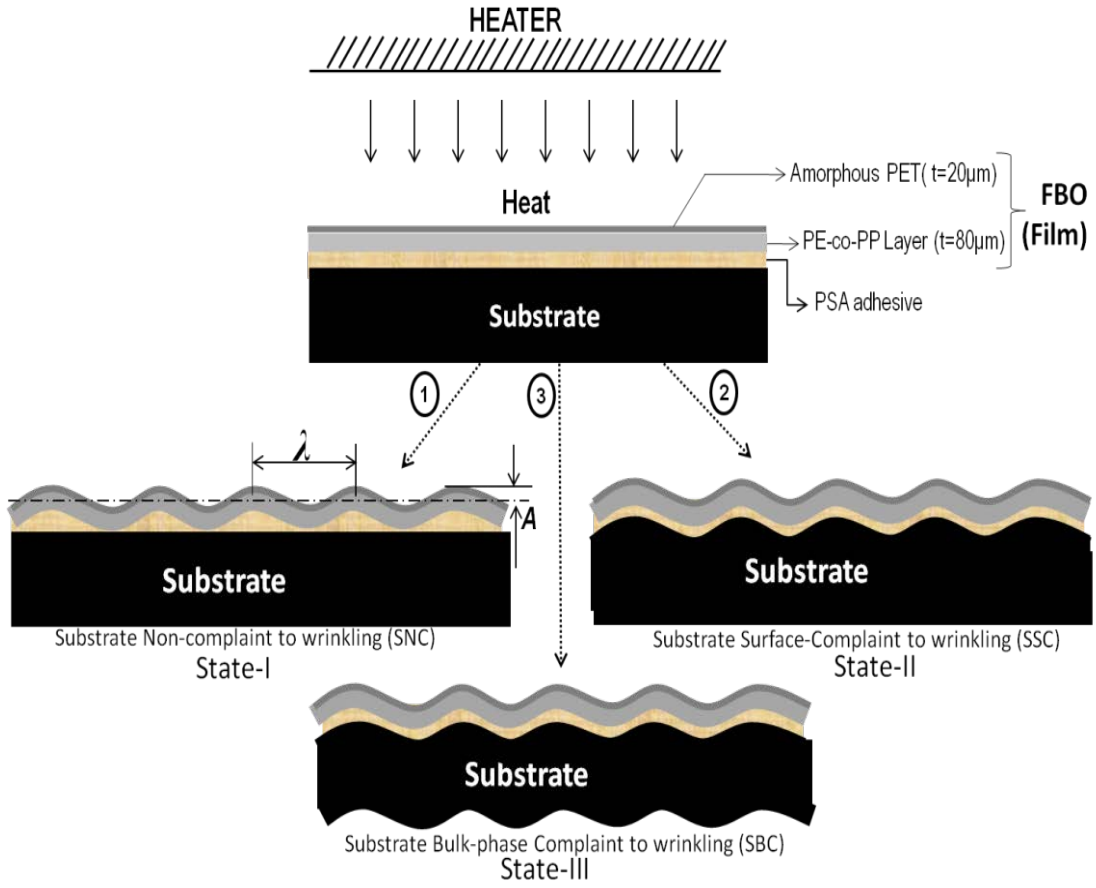

Figure 4-9: Film/substrate construction in the laminate structure and proposed different possible wrinkled states

The changing relative compliancy between the film and substrate can be strongly tied to the buckling distortions formed. In the temperature range of 130ºC to 180ºC employed for the study, the relative modulus of PP substrate to the FBO film (E_s/E_f) decreased from a value of approximately 7.5 to 0.1. In the presence of thermal stresses this decreasing relative compliancy influenced the wrinkle growth process as well as the final wrinkle morphology generated. Plots of amplitude and wavelength corresponding to the varying relative modulus (E_s/E_f) for the FBO/PP system, with respect to different heating rates are shown in Figure 4-10 & Figure 4-11; note that the axis for relative

modulus is labelled in reverse order so that the progression of time is still left to right in the plots, matching Figure 4-6 & Figure 4-8.

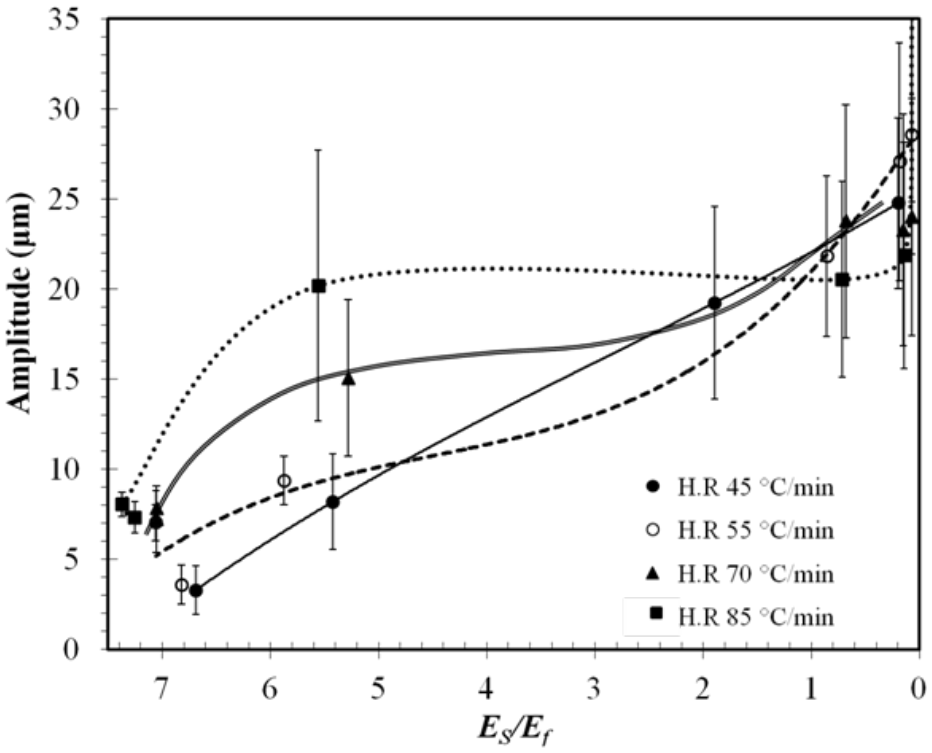

Figure 4-10: Growth of amplitude with varying relative modulus (E_s/E_f) at different heating rates for the FBO/PP system. Lines included to clarify trend.

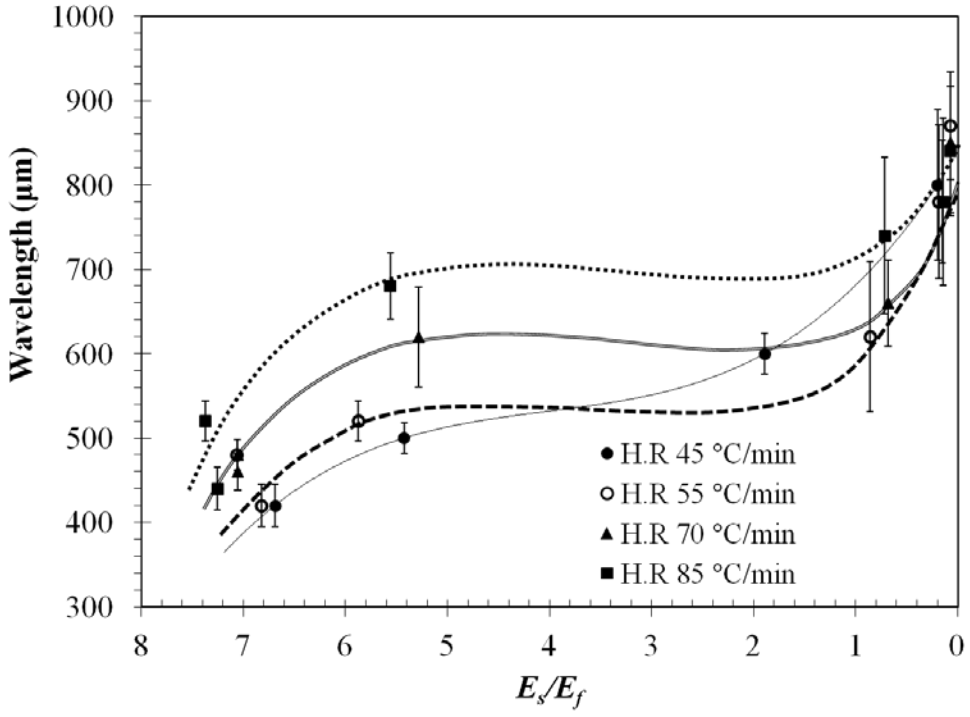

Figure 4-11: Wavelength growth with varying relative modulus (Es/Ef) at different heating rates for the FBO/PP system. Lines included to clarify trend.

The wavelength showed an inverse-sigmoidal growth relationship (i.e., inverse s-shaped curves, (Figure 4-11) with the decreasing E_s/E_f value, exhibiting three distinct growth regions: (i) an initial gradual growth region ($E_s/E_f \geq 5$), followed by a plateau region where there was almost no further growth ($5 \leq E_s/E_f \leq 1$), and which was again followed by a steeper growth region ($1 \leq E_s/E_f \leq 0$). As the E_s/E_f value dropped below 1, wrinkles with higher order wavelength were common since now the substrate was increasingly viscous in nature and incapable of storing the elastic energy acting on it. Thus, faster wrinkle growth was promoted. Similar behaviour was observed for all heating rates, and the values of λ were found to be higher at higher heating rates for the same corresponding E_s/E_f ratio, as seen in Figure 4-11.

The amplitude growth with decreasing E_s/E_f displayed a transition from a linear growth trend at the lowest heating rate (45ºC/min) to an inverse sigmoidal growth for higher heating rates (55-85ºC/min), as seen in Figure 4-10. At higher heating rates, amplitude growth showed three distinctive growth stages like the growth process observed with the wavelength for decreasing E_s/E_f ratio. The active growth regime was observed only when the E_s/E_f was above 5 and below 1, whereas almost no growth was observed in the region where $E_s/E_f \approx 1$ to 5. Higher amplitude values were recorded when E_s/E_f was below 1, indicated that the viscous nature of substrate can promote wrinkle growth. It should also be noted that these A, λ values were recorded during the initial period (time, $t = 0^+$) of the wrinkle growth process at a given temperature. These values do not represent the equilibrium amplitude (A_e) and wavelength (λ_e) values mentioned in other literatures [28][59][55][27][73]. For a given temperature, these large wrinkle perturbations, corresponding to A_e and λ_e, are achieved after a considerable period of time and are dictated by viscous dissipation and thermodynamic equilibrium that are prominent at temperatures where E_s/E_f is below 1.

Physically, as the E_s/E_f value decreased below 1 the substrate, being more viscous, complied and increasingly participated in wrinkling whereas for higher ratio values, wrinkling occurred entirely within the layers of the FBO. Optical image showing the top view of wrinkled laminates are presented in Figure 4-12 where the film layer was partly peeled off to expose the contacting surface of the substrate.

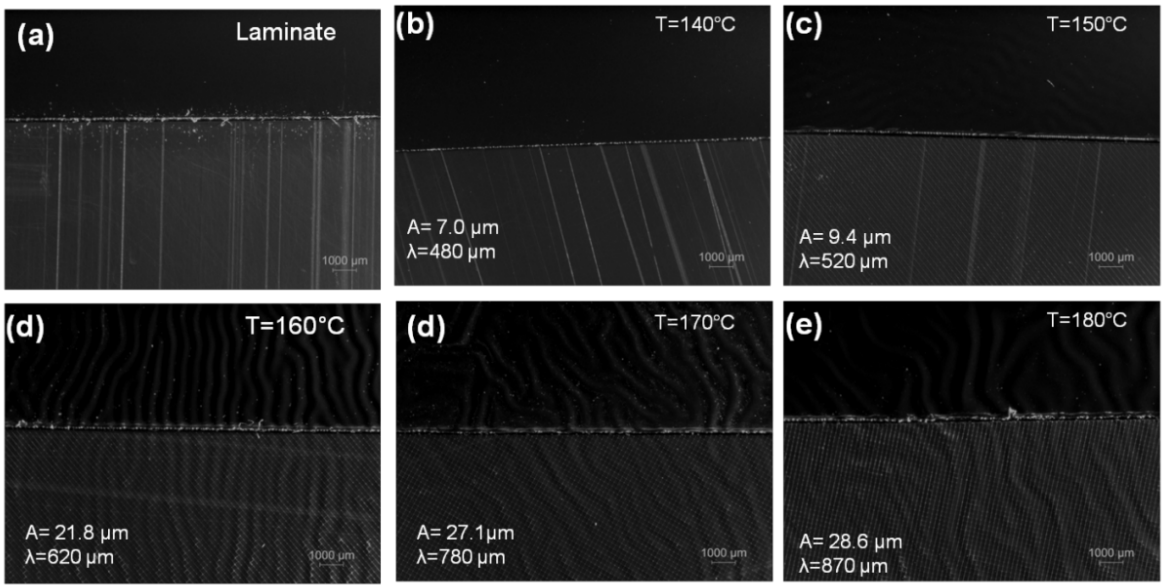

Figure 4-12: Optical images showing the impression of wrinkle pattern transferred to the PP substrate (visible in the exposed PP substrate shown in the lower half of each image where the film was peeled away)

Comparing Figure 4-9 and Figure 4-12, the following observations and the state of compliancy were assigned over the tested temperature range:

i. From 135°C to 150°C: **(E_s/E_f>5)-State I**- where the base layer and possibly the adhesive layer complied under the compressive stress generated in the top PET layer. This state is predominantly observed when stiff polymer films (elastic) are adhered to metal substrate (rigid) [2]. Substrate is considered an infinitely thick plate in this case.

ii. From 150°C to 160°C: **(5>E_s/E_f>1)- State I to State II** where the wrinkles formed in the FBO film created impressions of the undulated wrinkle pattern in the PP substrate surface. Predominantly seen in viscoelastic systems. Substrate is considered a semi-infinite plate in this case.

iii. From 160°C to 180°C: **(E_s/E_f<1)- State II to State III** where wrinkles formed in the FBO film not only created impressions of the undulated wrinkle pattern on the PP substrate surface, but transferred the localized buckling pattern through the entire thickness of the substrate. Substrate is considered a finite plate in this case.

Further evidence to these transitions can be seen in Figure 4-13. The transition from State II to State III indicates that the out-of-plane displacement of the film was compensated by the concurrent out-of-plane displacement of substrate.

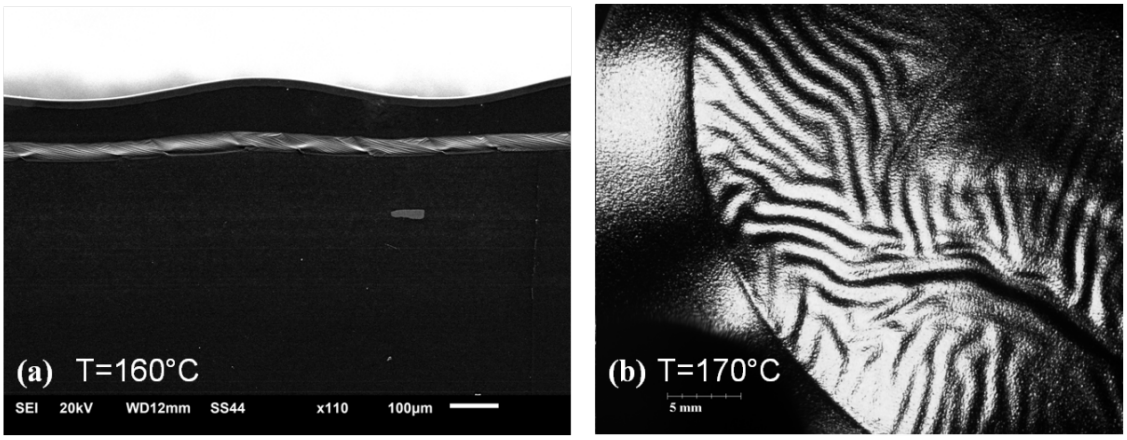

Figure 4-13: (a) SEM cross section image of FBO/PP laminate showing the compliancy of substrate to film surface wrinkle similar to State II (b) Optical image of FBO/PP laminate photographed from its bottom surface (i.e. PP substrate) showing its full compliance, corresponding to State III

4.3.3. Theoretical Estimates of Wrinkle Parameters

The descriptive wrinkling parameters (A and λ) were compared against selected theoretical models by Allen, Eqn (4-7, 4-8); Groenewold Eqn (4-9, 4-10); and Huang, Eqn (4-13 to 4-16) for a system with a compliant substrate in an elastic, viscoelastic or

viscous state. For convenience, the applicable equations and related conditions are summarized in Table 4-1. Their estimated values were compared with the experimental values for the FBO/PP system to determine the model best describing the polymer film-polymer substrate system in this study.

Table 4-1: Critical conditions for wrinkling for typical film/substrate combination and wrinkle scaling parameters prediction by theoretical models summarized from works of Allen[29][55], Groenewold [59], and Huang [27]

Film/substrate system with Critical parameters & conditions	**Theoretical wavelength & Amplitude**
Elastic/elastic system Spontaneous unstable wrinkling $\frac{\sigma_0^C}{\overline{E_f}} = \frac{1}{4}\left(\frac{3\overline{E_s}}{\overline{E_f}}\right)^{1/3}$ ..... (4-5) $\varepsilon_c = -\frac{1}{4}\left(\frac{3\overline{E_s}}{\overline{E_f}}\right)^{2/3}$ ..... (4-6) **Critical condition** If $\sigma_o > \sigma_o^c$ then wrinkling occurs spontaneously	**Allen's Model** $\lambda = 2\pi h\left(\frac{3\overline{E_f}}{\overline{E_s}}\right)^{1/3}$ .....(4-7) $A = h\left(\frac{\sigma_0}{\sigma_0^c} - 1\right)^{1/2}$ .....(4-8) **Groenewold's Model** $\lambda = 2\pi h\left(\frac{E_f}{E_s}\frac{(1+\upsilon_s)(3-4\upsilon_s)}{12(1-\upsilon_s)(1-\upsilon_f^2)}\right)^{\Psi}$, $\Psi = 1/3$.....(4-9) $A = \sqrt{\varepsilon_0}\left(\frac{2}{k}\right)$ where $k = 2\pi/\lambda$ .....(4-10)
Elastic/viscous system Kinetic wrinkling process Glassy and rubbery state $\sigma_{Co} = \left[\frac{2hE_f\mu_o(1-\upsilon_s)}{3H(1-\upsilon_f^2)(1-2\upsilon_s)}\right]^{1/2}$ .....(4-11) $\sigma_{C\infty} = \left[\frac{2hE_f\mu_\infty(1-\upsilon_s)}{3H(1-\upsilon_f^2)(1-2\upsilon_s)}\right]^{1/2}$ .....(4-12) where the relaxation modulus $\mu(t) = \mu_\infty + \mu_i\sum_i \exp(-p_i t)$ and $\mu_0 = \mu_\infty + \mu_{i=1-n}$	**Huang's Model (**for thin substrates, i.e. H/h->1**)** $A_{eo} = \frac{2\sqrt{6(1-\upsilon_f^2)}}{3k}\left[-\frac{\sigma_0}{E_f} - \frac{(kh)^2}{12(1-\upsilon_f^2)} - \frac{2}{\gamma_{22}}\frac{\mu_o}{E_f}\frac{1}{kh}\right]^{1/2}$ .....(4-13) $A_{e\infty} = \frac{2\sqrt{6(1-\upsilon_f^2)}}{3k}\left[-\frac{\sigma_0}{E_f} - \frac{(kh)^2}{12(1-\upsilon_f^2)} - \frac{2}{\gamma_{22}}\frac{\mu_\infty}{E_f}\frac{1}{kh}\right]^{1/2}$ .....(4-14) where $\gamma_{22} = \frac{1+\kappa}{4}\frac{\kappa\sinh(2kH) - 2kH}{k\cosh^2(kH) + (kH)^2 + ((1-\kappa)/2)^2}$ & $\kappa = 3 - 4\upsilon_s$ $\lambda_0 = \pi h\left[\frac{2E_f H(1-2\upsilon_s)}{3h\mu_0(1-\upsilon_f^2)(1-\upsilon_s)}\right]^{1/4}$ (glassy state) .....(4-15)

Critical conditions	
i. If $\lvert\sigma_0\rvert < \lvert\sigma_{c\infty}\rvert$, the film is stable at both glassy and rubbery states ii. If $\lvert\sigma_0\rvert < \lvert\sigma_{c0}\rvert$, the film wrinkles immediately at the glassy state iii. If $\lvert\sigma_{C\infty}\rvert < \lvert\sigma_0\rvert < \lvert\sigma_{c0}\rvert$ the film is stable at the glassy state but unstable at the rubbery state	$\lambda_\infty = \pi h\left[\frac{2E_f H(1-2\upsilon_s)}{3h\mu_\infty(1-\upsilon_f^2)(1-\upsilon_s)}\right]^{1/4}$ (rubbery state).....(4-16)

Plots of the theoretical estimates for λ and A along with the experimental values for the FBO/PP system for increasing temperature at different heating rates are shown in Figure 4-14 & Figure 4-15. It should be noted that the theoretical values of λ and A calculated using the models of Allen and Groenewold were based on the assumption that the substrate was elastic and infinitely thick when compared to the film. On the other hand, the λ and A values evaluated using model of Huang were based on the assumption that the substrate was viscoelastic in nature with glassy and rubbery phases contributing to wrinkling and their response to the compressive stress defined the limits of the values at equilibrium condition. The model of Huang was derived for a laminate system in which the elastic film/visco-elastic substrate system was affixed to a rigid support underneath the substrate (See Chapter 2). Thus, comparing with Figure 4-9 on proposed wrinkling states, the models proposed by Allen, Groenewold, and Huang models assume State II where the substrate surface is compliant to wrinkling and not a bulk-phase compliancy as seen in State III. It should be noted that most literature papers consider a

compliant substrate which is typically State II. However, in this study, transition to state III was also observed.

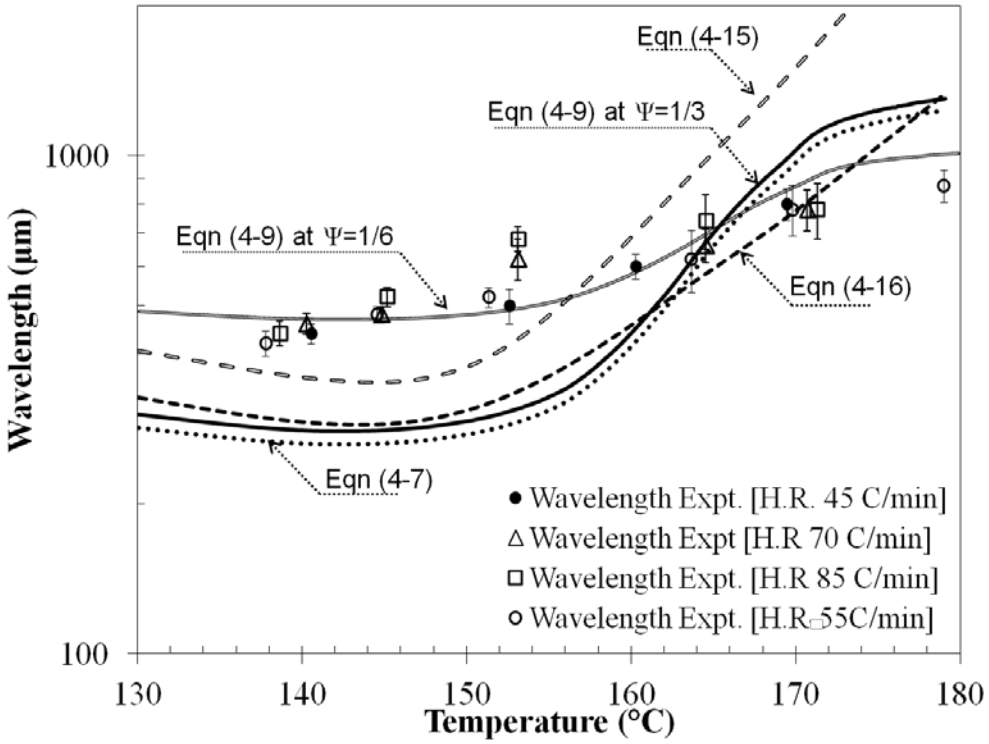

Figure 4-14: Comparison of experimental and theoretically predicted values of wavelength for the FBO/PP system. Theoretical equations listed in Table 4-1

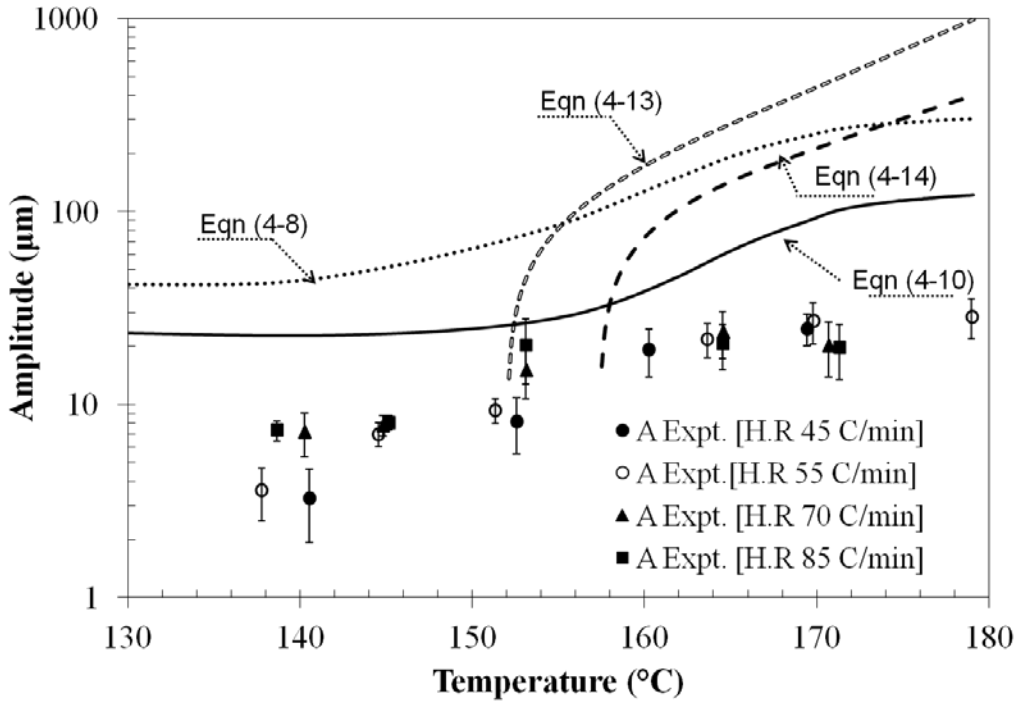

Figure 4-15: Comparison of experimental and theoretically predicted values of amplitude for the FBO/PP system. Theoretical equations listed in Table 4-1

In Figure 4-14, the experimental wavelength values of λ were shown to be higher than the theoretical predictions of any stated model for increasing temperature until T=162ºC, and then beyond that the experimental values were lower than the predicted. This was interesting as the temperature of 162ºC corresponded to the condition where the modulus, E_s dropped below the value of E_f, shown in Figure 4-1. Although there was considerable deviation in the predicted λ values when compared to the experimental values, it was worth noticing that the growth trend of wavelength predicted by Allen, Eqn (4-7) and Groenewold model, Eqn (4-9) was similar to the actual experimental growth trend. It was found that the system obeyed Groenewold wavelength prediction, if the amplification factor, Ψ in Eqn (4-9) was replaced by 1/6 instead of 1/3. Similar prediction

of $1/6^{th}$ power dependency of wavelength on the modulus ratio E_s/E_f was noticed in wrinkling of thin elastic sheet on a thick elastic substrate by Cerda et al.[28] for biological layered systems such as wrinkling of human skin-flesh and shriveled old apple skin-pulp.

Both the original Allen and Groenewold relations, Eqn (4-7) and Eqn (4-9) are considered applicable for a thin elastic film-infinitely thick elastic substrate laminate systems. The amplification factor Ψ *could* be a decreasing function of substrate thickness (H) implying that the value of it might be lower for system with finite substrate thickness ($H \rightarrow 0$) and higher for infinite thickness of substrate ($H \rightarrow \infty$); note the amplification factor Ψ of 1/3 in the original model was also an empirical parameter and not mechanistically determined, so there was already precedence given to consider this as an adjustable parameter. Even at temperatures above 162ºC, where the substrate was viscous, the predictions of Groenewold with Ψ=1/6 was obeyed by the system. This could be because, the experimental λ values were obtained at the initial time period (at $t=0^+$) where the elastic response would be more prevalent implying that the substrate even in its viscous state would have some melt elasticity. For the same reason, the predicted λ values by Huang's model were much higher than the experimental values beyond 162ºC, as they were estimates of the equilibrium values at infinite time, $t = \infty$. It was worth noting that the proposed amplification factor (Ψ=1/6) predicted wavelength for whole range of samples transitioning from State I to State III (Figure 4-9)where complete bulk compliancy of the substrate to wrinkling was observed.

Considering amplitude in the evaluation of a suitable model, the theoretical estimates based on the Allen, Groenewold and Huang relations using Eqn (4-8), Eqn (4-10) and Eqn (4-13, 4-14), respectively are shown in comparison to the experimental data in Figure 4-15. Each model overestimated the predicted amplitude; however, the Groenewold model, Eqn (4-10) represented the amplitude growth trend properly and the values were reasonably closer to the experimental data when compared to other models. The experimental amplitude values for the FBO/PP system were almost 10 times lower in magnitude than the model wavelength values across all temperatures. This suggested that the in-plane displacement causing wavelength growth may be higher in magnitude when compared to the out-of-plane displacement. This could be explained to a certain extent by considering the contribution of the film-substrate adhesive interface to wrinkle formation. As previously seen, with increasing temperature, the substrate transitions from elastic to viscoelastic to viscous medium and the resultant compliancy of the substrate to wrinkle could be observed as it transition from State I (substrate elastic) to State II (viscoelastic) to State III (viscous) as shown in Figure 4-12 & Figure 4-13. As the substrate became more compliant relative to the film, the energy which was otherwise to be utilized for growth in wrinkle amplitude was being partially utilized for the localized out-of-plane displacement of the substrate, creating an asymmetric wrinkle pattern. In addition, during these transitions, the adhesive interface was strong enough to prevent delamination. An evidence to this conclusion can be seen Figure 4-12 where the micro-pattern of the adhesive layer was distinctly visible in the exposed substrate surface after laminated samples were heated 150°C and higher. The micro-pattern had become imprinted into the

softened substrate as it conformed to wrinkles. The indentations revealed in the substrate left the impression that mechanical locking was occurring that prevent delamination of film from substrate surface. Therefore, the FBO/PP adhesive interface could be stronger in resisting the out-of-plane displacement than providing shear resistance to prevent in-plane displacement. Overall, the wavelength growth was favoured since the wrinkles were formed during thermal expansion process and not during contraction

4.4. Wrinkle Evolution for FBO/PC Laminates

4.4.1. Influence of Temperature and Heating Rate

To probe further the effect of substrate compliancy on wrinkling, a polycarbonate (PC) substrate of higher stiffness than PP was subsequently examined. In the experimental range of 130- 180°C, the elastic modulus of PC substrate varied from 1500 MPa- 6.5 MPa whereas, for PP substrate had varied from 53 MPa- 0.26 MPa. FBO/PC laminates were prepared using PC with two different sheet thicknesses, PC_t (h =132μm; H/h =1.32) and PC_T (h=525μm; H/h =5.25). Two distinctive heating rates of 170 ºC/min and 290 ºC/min were chosen for FBO/PC_t system and 80 ºC/min and 135 ºC/min for the FBO/PC_T to study the variation with the heating rates. As polycarbonate is more conductive than PP substrate, for a given setting of the heating source (HS) in thermoformer simulator, FBO/PC laminates would show higher heating rates than FBO/PP laminates, with the FBO/PC_t laminates showing even higher heating rates than the FBO/PC_T laminates. In this work, to mimic the practical thermoforming conditions,

the heating source setpoint was kept constant and the resultant apparent heating rates depended upon the type and overall thickness of laminate sample used.

Surface wrinkling of the FBO film affixed to either PC substrate (PC_t and PC_T) was visually observed to change with increasing temperature but showed only minimal dependency on heating rates, as demonstrated by the micrographs presented in Figure 4-16 to Figure 4-18**.**

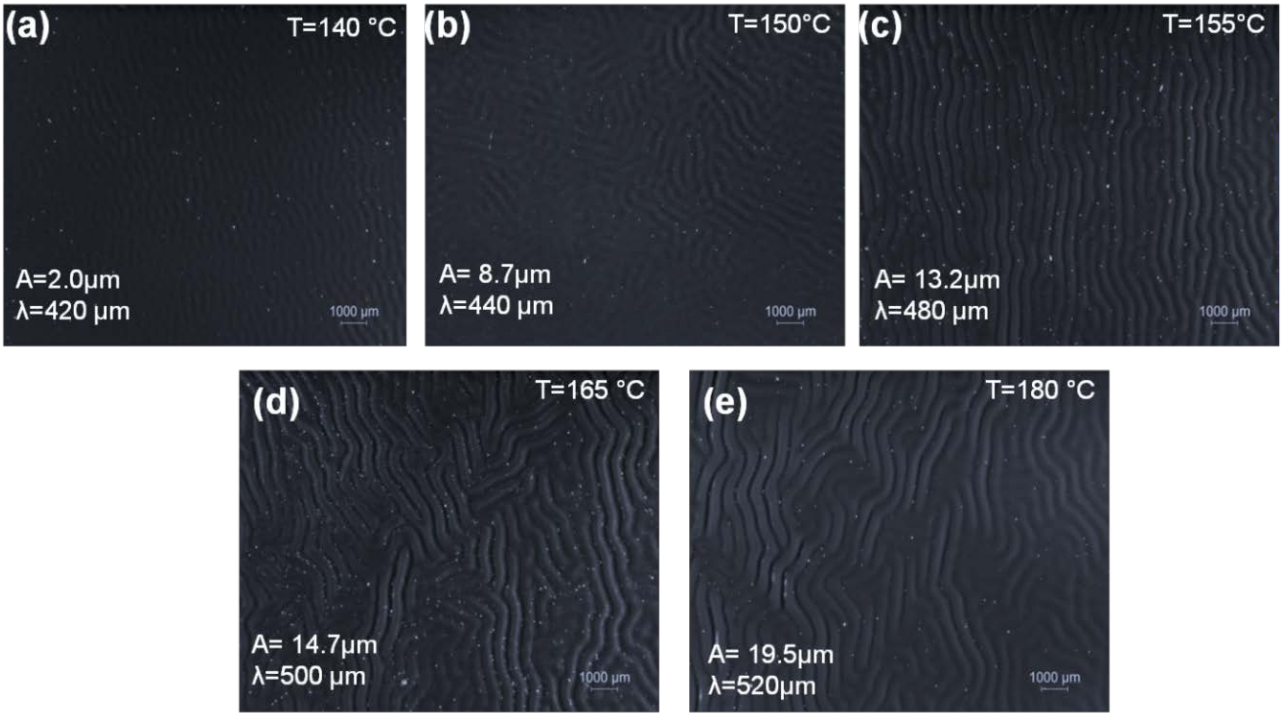

Figure 4-16: Optical images of the wrinkled FBO/PC_t laminates with increasing temperature (T= 140 - 180ºC) at a heating rate of 170ºC/min

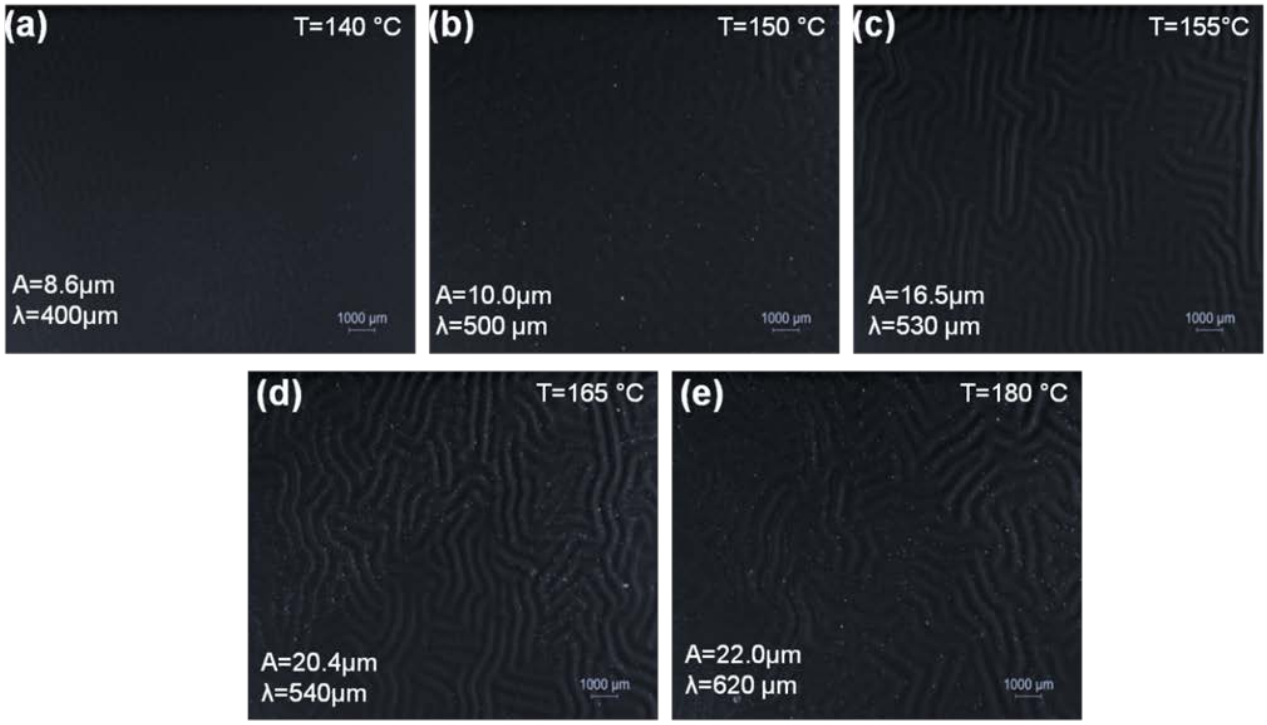

Figure 4-17: Optical images of the wrinkled FBO/PC_T laminates with increasing temperature (T= 140 - 180°C) at a heating rate of 135°C/min

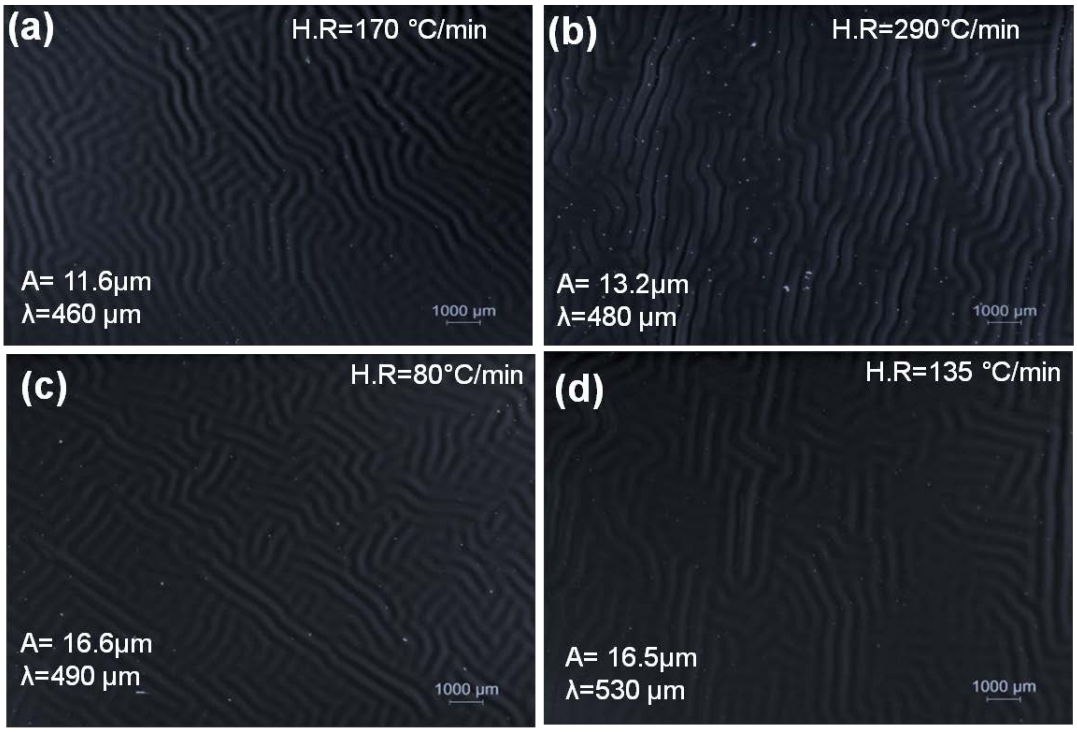

Figure 4-18: Optical images of the wrinkled FBO/PC_t laminates at (a) 170ºC/min (b) 290ºC/min and FBO/PC_T laminates at (c) 80ºC/min (d) 135ºC/min

As shown in Figure 4-16 & Figure 4-17 , prominent wrinkle patterns started appearing on the film surface when sample temperature exceeded 140ºC, first showing unidirectional distortions and later discrete regions of randomly oriented wrinkles were observed for higher temperatures (T>150ºC). For FBO/PC_t system shown visually in Figure 4-16, the wavelength λ and the amplitude A of the wrinkled patterns varied from 420-520µm and 2-19.5µm, respectively when temperature increased from 140ºC to 180ºC at 170 ºC/min. Comparably, the λ and the A values varied from 460-480µm and 11.6-13.2 µm, respectively, Figure 4-18 (a, b) when the heating rate increased from 170ºC/min to 290ºC/min. On the other hand, for the FBO/PC_T system, the wavelength λ and the amplitude A of the wrinkled patterns varied from 400-620µm and 8.6-22µm,

respectively as seen in Figure 4-17, when temperature increased from 140ºC to 180ºC. With increasing heating rate, the λ and the A values varied from 490-530μm and 16.6-16.5μm, respectively from 80ºC/min to 135ºC/min, shown in Figure 4-18 (c, d). It was interesting to note that considering minimal influence of heating rate to wrinkling for FBP/PC laminates, the increase in thickness of the PC substrate (132 to 525μm) resulted in only a slight increase in wrinkle amplitude and wavelength.

The influence of temperature and heating rate on the wavelength and amplitude for both the FBO/PC_t and FBO/PC_T are shown in Figure 4-19 to Figure 4-22, displaying sigmoidal trends similar to those observed with the FBO/PP laminate. There was a gradual increase in λ and A values with temperature and time, and these values were always found to be higher for PC_T (thicker substrate) than PC_t (thinner substrate) for identical temperature conditions.

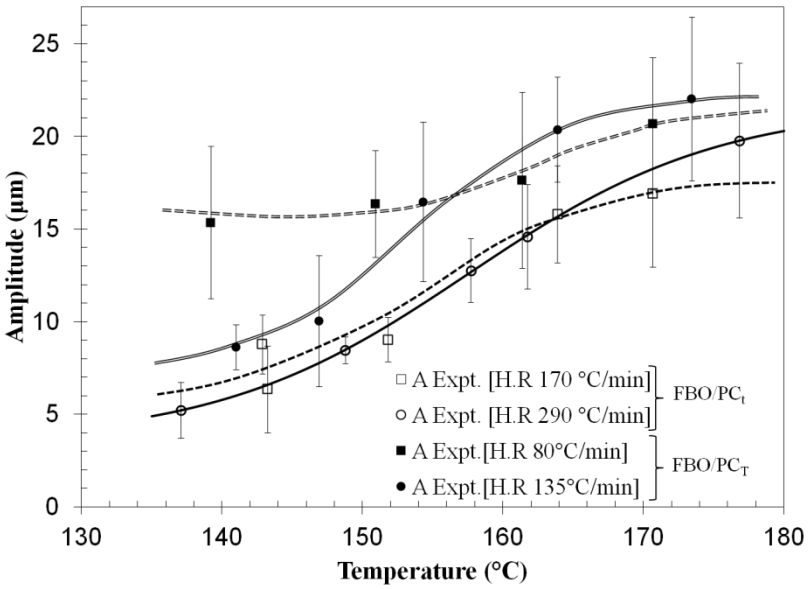

Figure 4-19: Amplitude growth with increasing temperature for the FBO/PC_t & FBO/PC_T systems at different heating rates. Lines included to clarify trends.

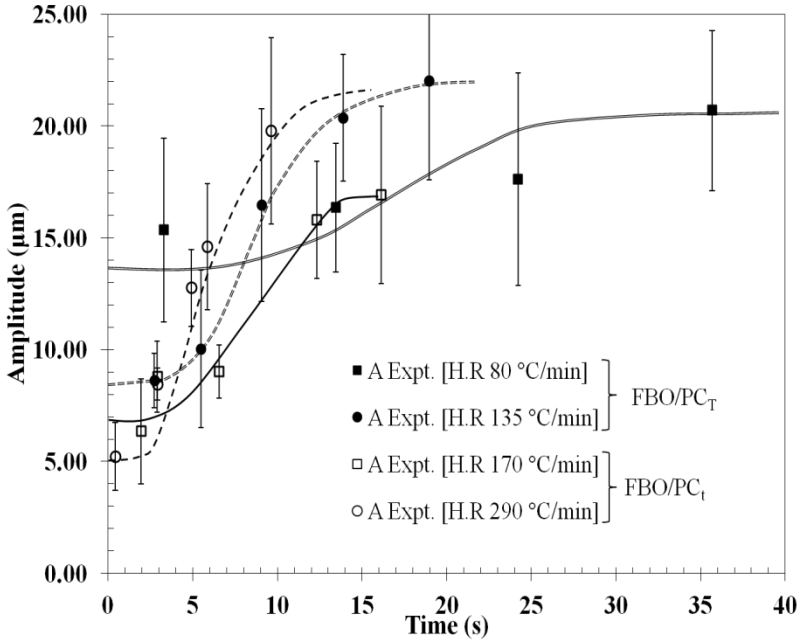

Figure 4-20: Amplitude vs. time for the FBO/PC_t & FBO/PC_T systems at different heating rate. Lines included to clarify trends.

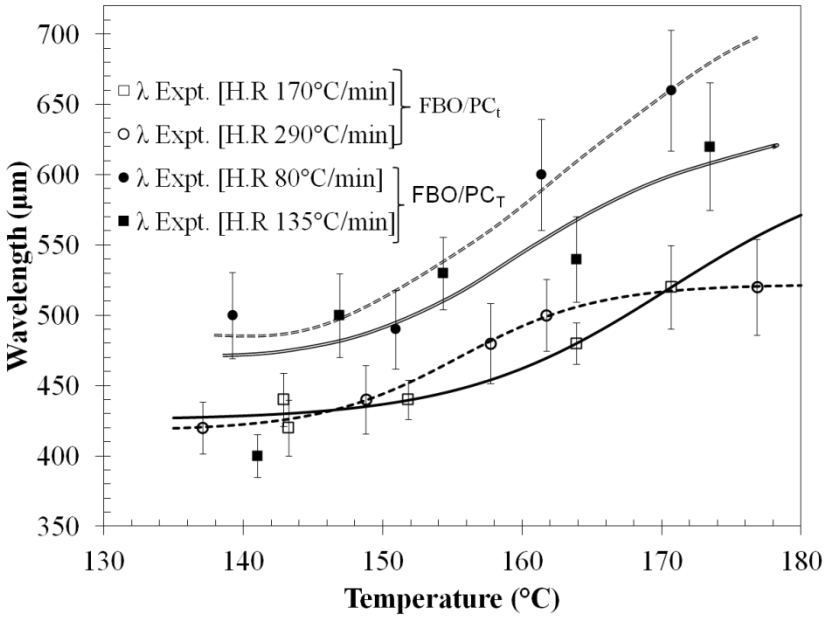

Figure 4-21: Wavelength with increasing temperature for the FBO/PC_t & FBO/PC_T systems at different heating rates. Lines included to clarify trends.

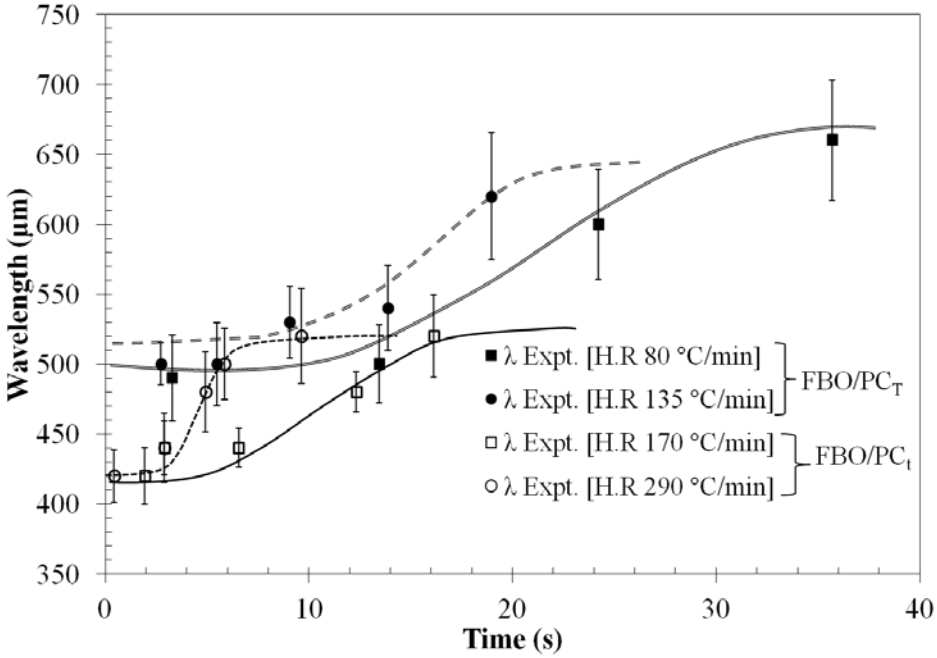

Figure 4-22: Wavelength vs. time for the FBO/PC_t & FBO/PC_T systems at different heating rates. Lines included to clarify trends.

Although both PC substrates were made of the same material, having the same modulus, their compliance (stiffness) changed in accordance with thickness. The stiffness (S) of a material is directly related to modulus (E) and thickness (t) by equation:

$$S = \frac{Et^3}{12} \tag{4-17}$$

Unlike the FBO/PP laminate, the heating rate for the PC laminates had a smaller influence on the growth rate of wrinkles. The growth rate range for the amplitude calculated from the growth function described by Eqn (4-4), was $0.61s^{-1}$ at 170ºC/min and 0.48 s^{-1} at 290ºC/min for FBO/PC_t compared to $0.15s^{-1}$ at 80ºC/min and 0.53 s^{-1} at 135ºC/min for FBO/PC_T. Similarly, the growth rate range for the wavelength varied from a value of $0.29s^{-1}$ to $0.88s^{-1}$, for the FBO/PC_t system, and $1.57s^{-1}$ to $0.57s^{-1}$ for the FBO/PC_T system in the two heating rates selected for the study. These smaller variations in growth rates over much broader ranges of heating rates showed the reduced influence seen with this parameter for PC versus PP substrate, while temperature remained strongly influential on wrinkling.

4.4.2. Influence of Substrate Compliancy

From previous sections on the FBO/PP laminate system, substrate compliancy (based on temperature) was observed to influence wrinkling and comparison was made to three possible wrinkle states (see Figure 4.10). Similarly, in this section, the influence of PC substrate on wrinkling of the FBO/PC laminates was examined to determine any peculiarities or similarities to the FBO/PP substrates.

The modulus ratio E_s/E_f plotted against the amplitude and wavelength for both FBO/ PC_t and FBO/PC_T systems is given in Figure 4-23 & Figure 4-24. E_s/E_f varied from a very high value of 400 at 130ºC to a value of 4 by 180ºC; however, the E_s/E_f values never reached 1 or below 1, as in the case of the FBO/PP laminate. Therefore, the PC substrate always exhibited dominant elastic characteristics as compared to the film throughout the temperature range studied and as witnessed in the trials, wrinkling did not involve compliancy of the substrate. Maintaining E_s/E_f above unity appeared sufficient to restrain wrinkling in state-I conditions, previously shown in Figure 4-9. The state persisted over the full range of temperatures studied because PC being an amorphous polymer underwent glass transition at around 150°C (See DSC curves, Figure 3-5) and did not undergo further transition to a completely viscous state even until 180°C. Hence the level of compliancy of PC substrate to the wrinkles formed on FBO film surface to reach State II or State III did not occur. Therefore, PC substrate when compared to FBO film was relatively rigid behaving more so like an elastic substrate (similar to polymer film-metal substrate system corresponding to State I)

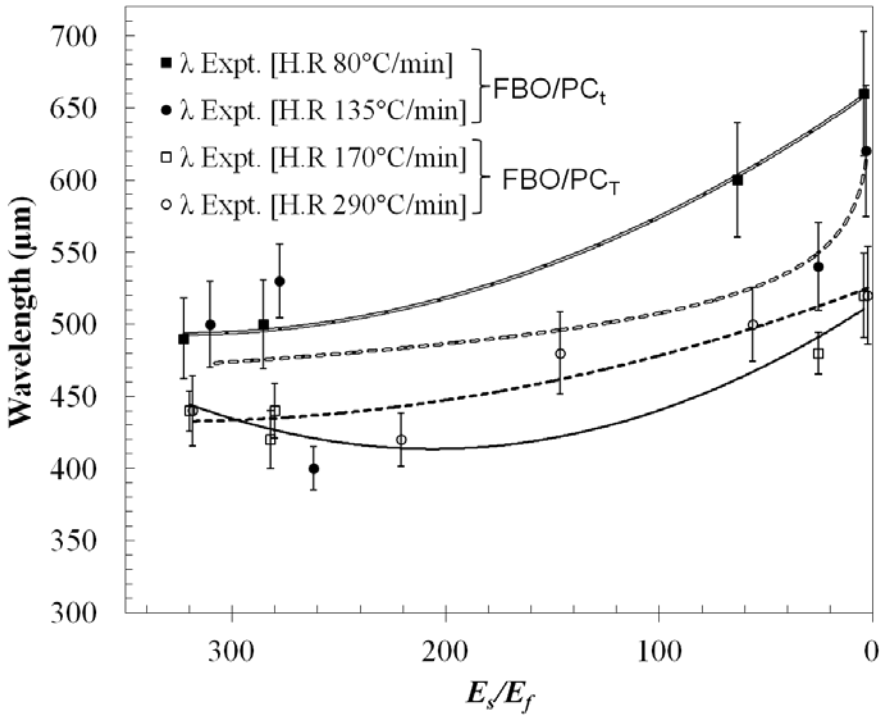

Figure 4-23: Wavelength growth with varying relative modulus (Es/Ef) at different heating rates for the FBO/PCt & FBO/PCT systems. Lines included to clarify trends.

Both the wavelength and amplitude gradually increased with decreasing E_s/E_f during heating. The values of λ were 40-140µm higher for the FBO/PC_T system when compared to the FBO/PC_t system for the corresponding temperatures in the range of the study, as shown in Figure 4-23. Similarly *A* values were 4-6 µm higher for the FBO/PC_T when compared to the FBO/PC_t system, as shown in Figure 4-24**.**

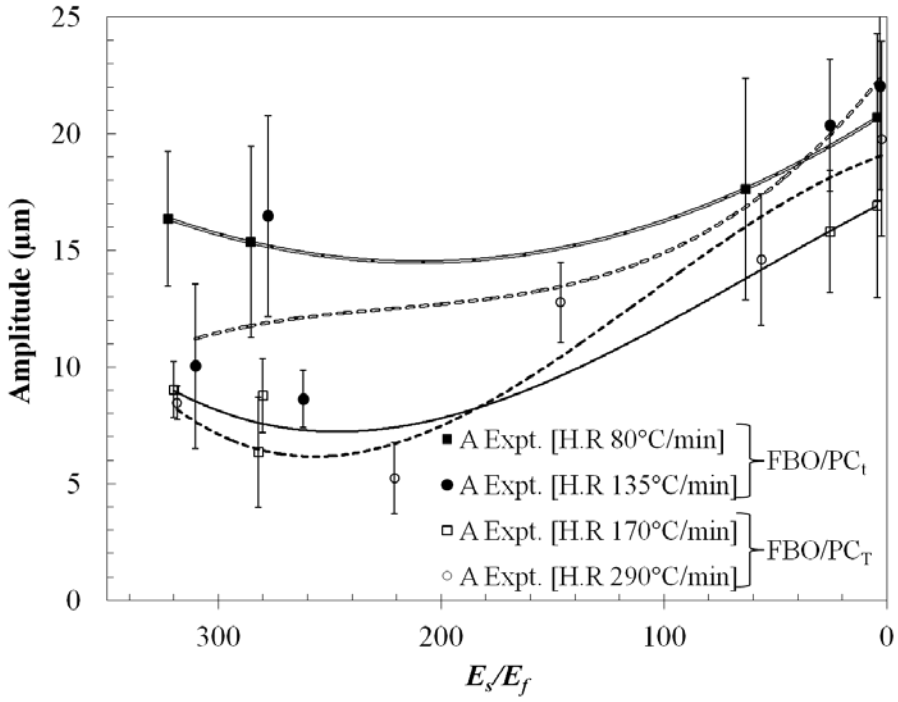

Figure 4-24: Amplitude growth with varying relative modulus (Es/Ef) at different heating rates for the FBO/PCt & FBO/PCT systems. Lines included to clarify trends.

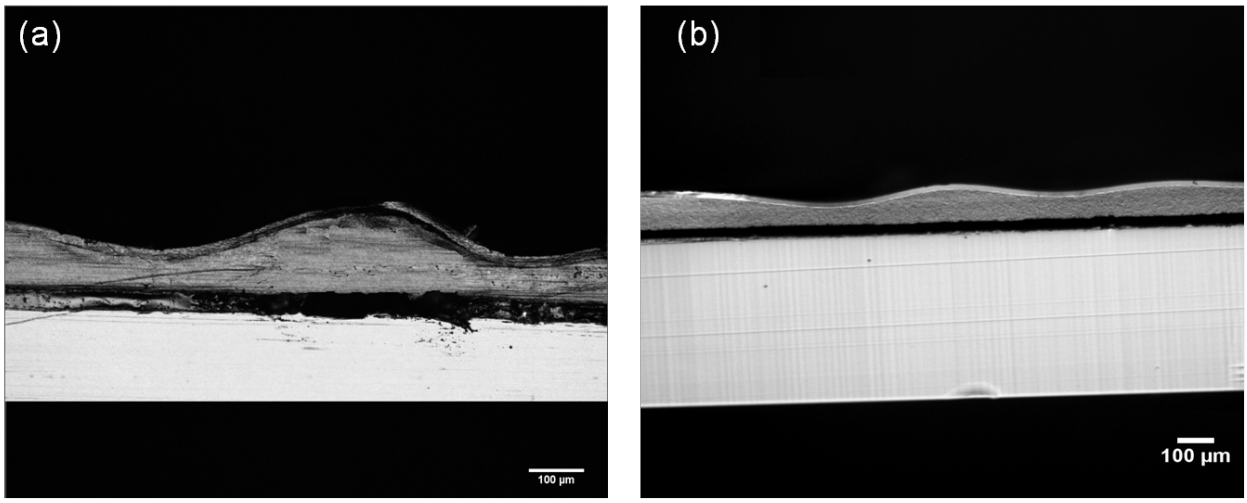

Figure 4-25: Optical Images with cross sectional view of wrinkled samples of FBO/PC system wrinkled at 170°C showing State I compliancy of PC susbtrate (a) FBO/PC$_t$ (b) FBO/PC$_T$ system

The overall comparison of wrinkling behaviour of FBO/PC substrates with the FBO/PP system indicated that the effects of heating rate on the wavelength and amplitude growth was much stronger on FBO/PP system (λ=440-850μm; A=3-36μm & H.R=45-85ºC/min) as compared to the FBO/PC system (λ=460-520μm; A=11-20μm; H.R=170-290ºC/min for FBO/PC_t and λ=400-620μm; A=11-20μm; H.R=80-135ºC/min for FBO/PC_t). This could be because of several reasons such as (i) PC substrate was non-compliant (State I) to wrinkles whereas the PP substrate was complaint (State I to State III), (ii) the substrate/film stiffness ratio larger for PC as compared to PP substrate system, (ii) the variation in the heat absorbance capability of PC versus PP, and iv) the PC being transparent whereas PP was opaque. The varying heat absorbance and the increasing thickness of the PC substrates may have caused a temperature gradient within the layer during transient heating.

4.4.3. Theoretical estimates of wrinkle parameters

Experimental values of FBO/PC laminates were compared with selected theoretical models to understand the model applicability and predictability. Figure 4-26 & Figure 4-27 compare the thermally induced compressive stresses on the film to the critical stresses calculated based on Huang and Allen's models (See Eqns 4-5, 4-11 & 4-12). Inputting the concerned material parameters to the equations, it was seen that the models neither predicted amplitude nor wavelength for temperature region where the thermally induced compressive stress was less than the critical stress. These temperatures correspond to 149°C for FBO/PC_T and 155°C for FBO/PC_t based on Huang's model (Eqn

4-11, 4-12) and 163°C for both FBO/PC_T & FBO/PC_t based on Allen's model (Eqn 4-5). Below the critical compressive stress, the models claim no wrinkling occurs. However, experimental evidence showed that at these temperatures prominent wrinkling would occur. The predicted values of wavelength and amplitude versus experimental data are shown in Figure 4-28 to Figure 4-31, respectively for the thin and thick PC substrate laminates at different heating rates. Theoretical estimates of wavelength for both PC thin and thick substrates based on the models of Allen and Groenewold under-predicted the experimental values in the entire temperature range. Huang's model under predicted the values only below 155ºC and 168 ºC for PC_t and PC_T respectively, and over estimated them above those temperatures. However, the models of Allen and Groenewold were reasonably descriptive of the measured trend, as they were exclusively derived for an elastic non-compliant substrate.

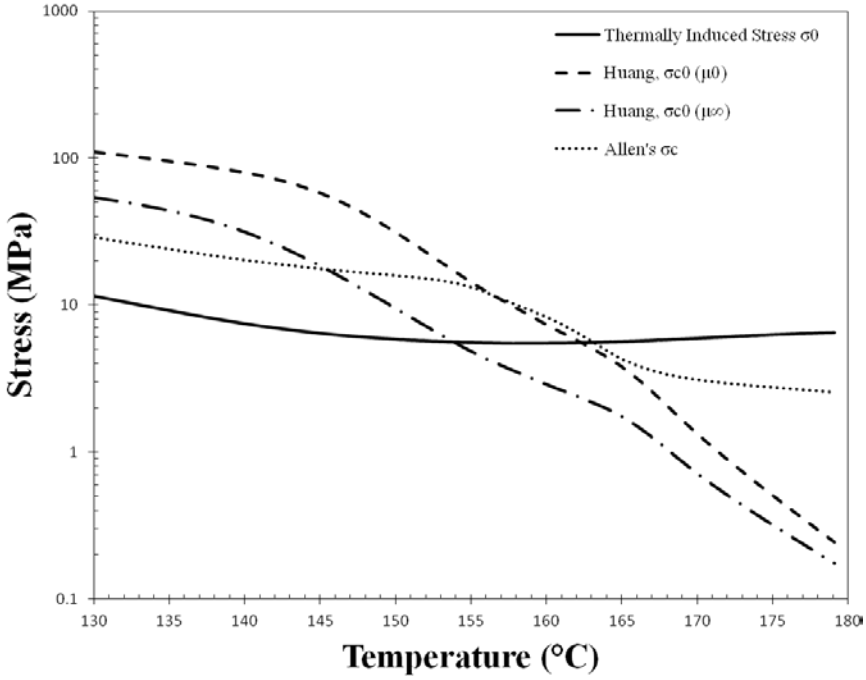

Figure 4-26: Comparison of thermally induced compressive stresses to theoretical stresses calculated based on Huang and Allen's models for FBO/PC_t. Theoretical equations listed in Table 4-1

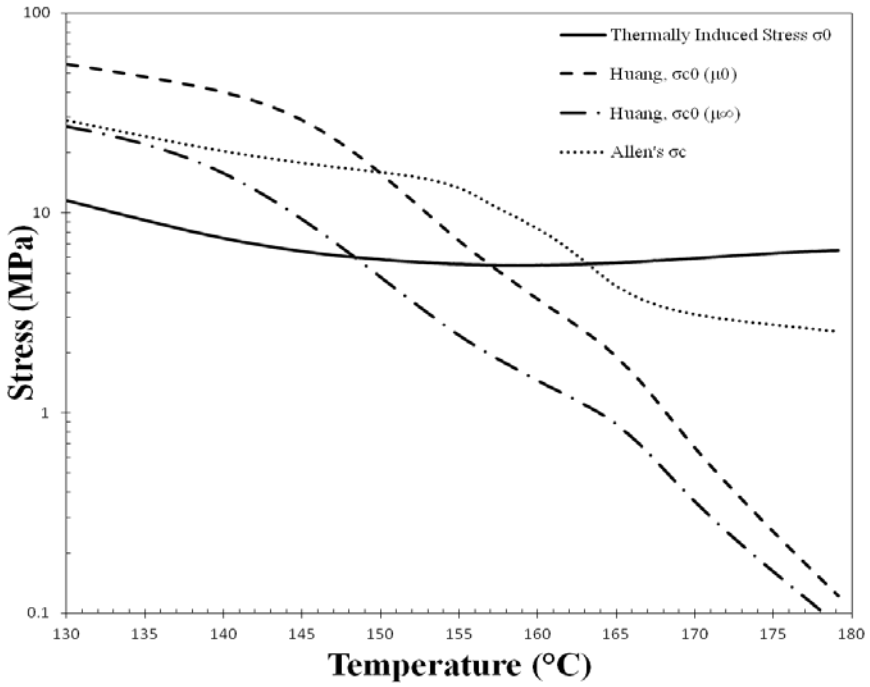

Figure 4-27: Comparison of thermally induced compressive stresses to theoretical stresses calculated based on Huang and Allen's models for FBO/PC_T Theoretical equations listed in Table 4-1

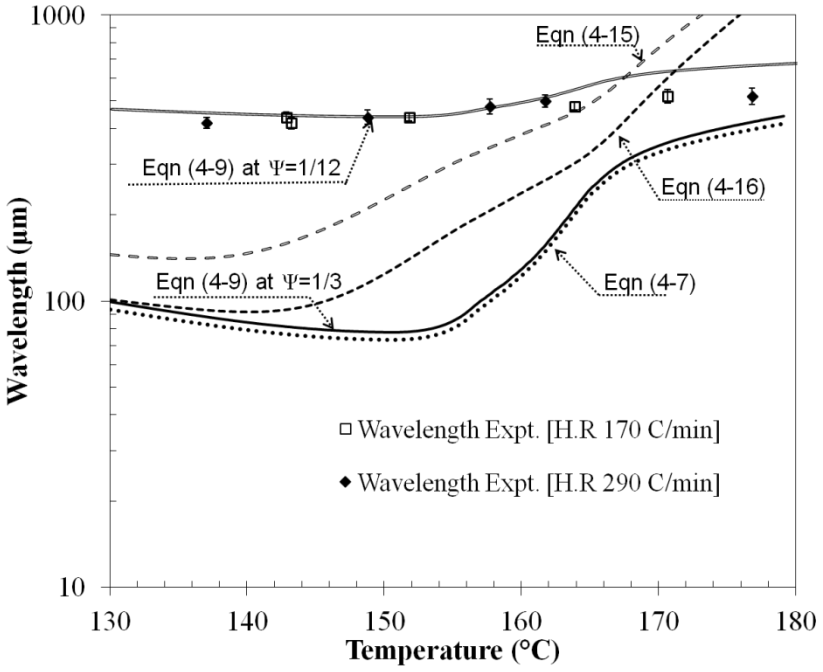

Figure 4-28: Comparison of experimental and theoretically predicted values of wavelength for FBO/PC_t. Lines correspond to the model of the stated equations listed in Table 4-1

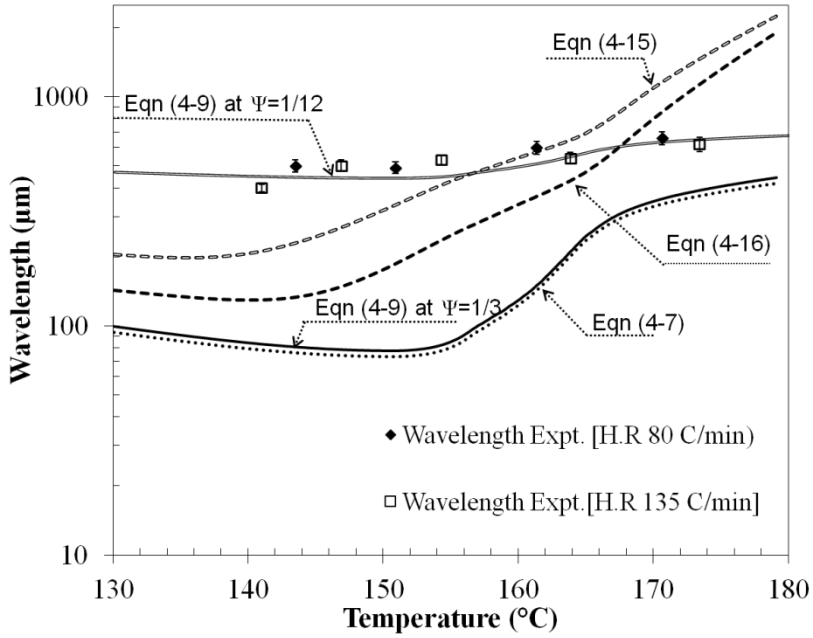

Figure 4-29: Comparison of experimental and theoretically predicted values of wavelength for FBO/PC_T. Lines correspond to the model of the stated equations listed in Table 4-1

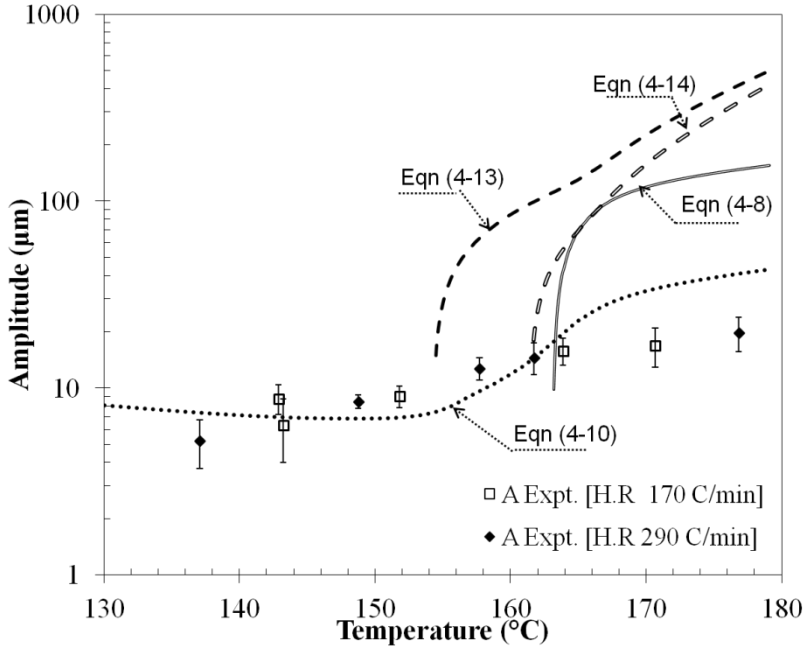

Figure 4-30: Comparison of experimental and theoretically predicted values of amplitude for FBO/PC$_t$. Lines correspond to the model of the stated equations listed in Table 4-1

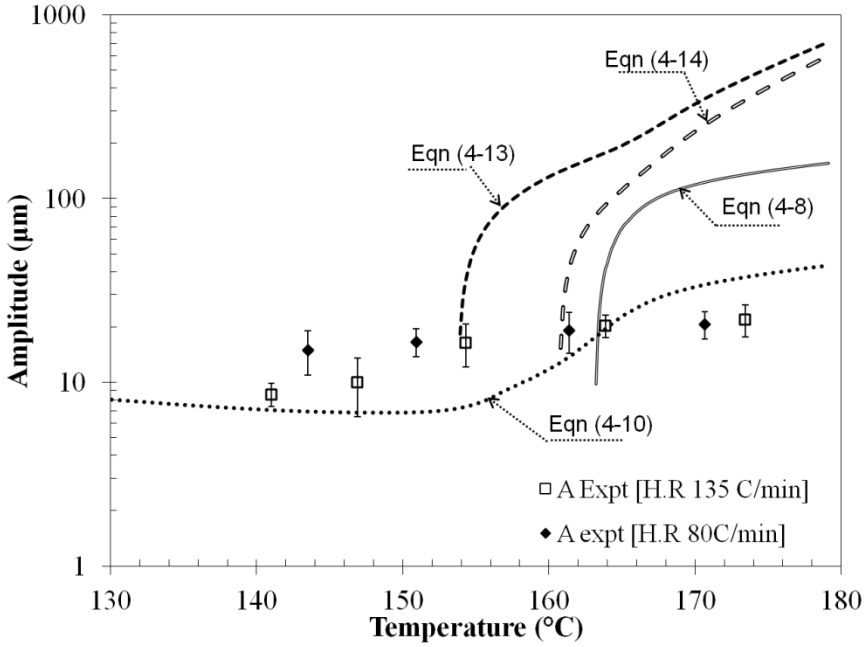

Figure 4-31: Comparison of experimental and theoretically predicted values of amplitude for FBO/PC$_T$. Lines correspond to the model of the stated equations listed in Table 4-1

As with the FBO/PP system, replacing the original amplification factor, $\Psi=1/3$ in the Groenewold model (Eqn 4-9) by substituting a new value, in this case 1/12, improved the predicted λ values for both FBO/PC_t and FBO/PC_T systems. It was interesting to note that the amplification factor remained the same for both thicknesses of PC substrate used in this study. In regards to predicting amplitude, the Groenewold relation, Eqn (4-10) was the only model to follow the trends found experimentally with both PC_t and PC_T substrate systems, and the magnitude of predicted values more closely match the experimental data unlike the FBO/PP system. Allen's model, despite being based on an elastic film/elastic substrate foundation like the Groenewold model, gave a very poor estimate of amplitude because it was only able to predict amplitudes for conditions were compressive stress was greater than critical compressive stress (Eqn 4-8).

As an overall conclusion, the wrinkling parameters estimated by the models such as Allen and Groenewold, for complaint substrates appear to describe the trend of their variation with increasing temperature. However, when the modulus ratio between the substrate and film varied considerably, the amplification factor (Ψ) in the wavelength relation, Eqn (4-9), must be changed according to the laminate system used and should not be considered a constant value. Similarly, the amplitude determined by the Allen and Groenewold can predict its variation with temperature, while the exact value might deviate depending upon whether the substrate was complaint or non-complaint to wrinkling. On the other hand, Huang's model, can estimate the final equilibrium values of λ and A only when the substrate was completely in the viscous state and its surface was complaint to wrinkling in State-II, but not when the bulk-phase was complaint to

wrinkling, i.e. State-III. All three states were visually observed in FBO/PP laminates, however only State-I was observed for FBO/PC laminates irrespective of the thickness of PC substrate used. The Groenewold and Huang model developed for elastic substrate on viscoelastic/viscous compliant substrate claimed to predict wrinkling typical of state-II; however, the predicted values were not a good estimation for experimental data for FBO/PP system when in a similar state. And the Allen model, which was more applicable to elastic film on an elastic substrate (State I), did not suitably work for the FBO/PC system which demonstrated such a wrinkling state. The Groenewold's equation which is a modification of Allen's equation predicts wavelength for both FBO/PP and FBO/PC systems only when the amplification factor (Ψ) was changed from (1/3) to (1/6) for FBO/PP and (1/12) for FBO/PC system.

4.5.Film Light Transmission Study

The polycarbonate substrates were not only used to study compliancy but also being optically transparent, they allowed detection of damage caused by wrinkling in the black colored FBO film, especially at higher temperatures. The damage was visibly apparent when a FBO/PC laminate was held up to the light but in order to convey this quantitatively, the variation in the amount of light transmitted through the unwrinkled laminate and wrinkled laminates at different temperatures was measured. The mean gray value was used to measure transmittance, which is plotted versus temperature for the FBO/PC_t and FBO/PC_T systems, in Figure 4-32; a higher grey value indicating more transmittance of light and hence more damage. Appendix D (Figure D-1, Figure D-2)

contains the optical images of wrinkled FBO/PC_t and FBO/PC_T laminates at varying temperatures for a given heating rate. The regions of damage is visibly seen here. It was found that at temperatures above T=155ºC the mean gray value increased with localized thinning and potentially yielding within the pigmented base layer of the film. The damaged areas of the film corresponded to the undulations of the formed wrinkles. The mean gray values were higher for the FBO/PC_T system as its higher resistance to wrinkling thus caused more damage to the film. It is our premise that such damage to the film is undesirable for long term stability in practical use, which is why later in this study methods were compared to remove wrinkles once formed versus avoid wrinkling altogether during heating.

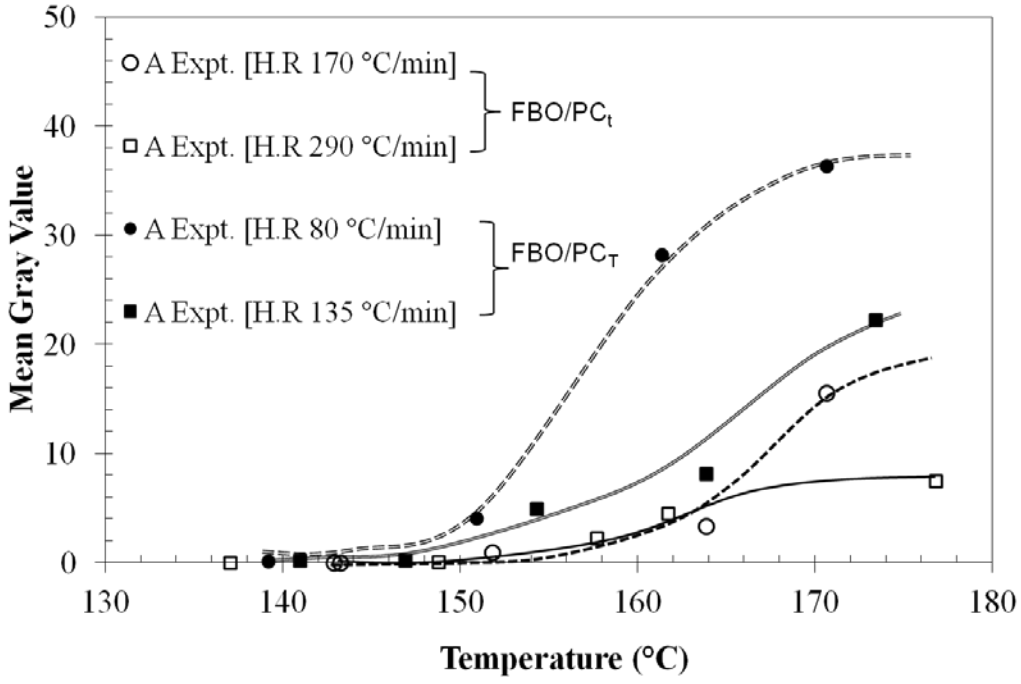

Figure 4-32:Mean grey value from the light transmission measurements for the FBO/PC substrates systems. Lines included to clarify trends.

4.6.Biaxial Stretching to Minimize Wrinkling

With well-established conditions for wrinkling given in the previous sections, the FBO/PP laminate was subsequently subjected to biaxial stretching by bulging to control this undesirable phenomenon. The laminates were heated to high temperature by one of two methods: (1) Isothermal bulge method where the sample was heated to a constant temperature followed by bulging under different pressures, and (2) Dynamic bulge method where the sample was continually strained at different pressures while being heated to temperature.

4.6.1. Isothermal Bulge Method (IBM)

For the isothermal bulge method (IBM), wrinkling was allowed to occur before bulging at different pressures (from 3.45 kPa to 17.24 kPa) to subsequently remove or diminish the appearance of such distortions. The estimated values of applied biaxial strain (using Equation 3-5) and thermally induced strain at different applied pressures (i.e. minimum and maximum values are indicated in the graph for each temperature) with increasing temperature are shown in Figure 4-33 for FBO/PP. The applied pressure (stress) window at higher temperatures becomes very narrow (indicated by the shaded area in Figure 4-33). Due to the thin compliant nature of the laminate and ever-changing gas volume required to maintain a constant applied stress, it was found to be very difficult to create strain levels below the thermal strain threshold; lower pressures did not result in sustained inflation during the experiment as the laminate had to yield prior to

inflating. The nominal applied biaxial strain in the pressure range employed was higher than the induced thermal strain up to T=165ºC. However, at T > 165ºC the laminate samples ruptured with application of even the very lowest pressure, indicating that the system was now too viscous for thermoforming above this temperature.

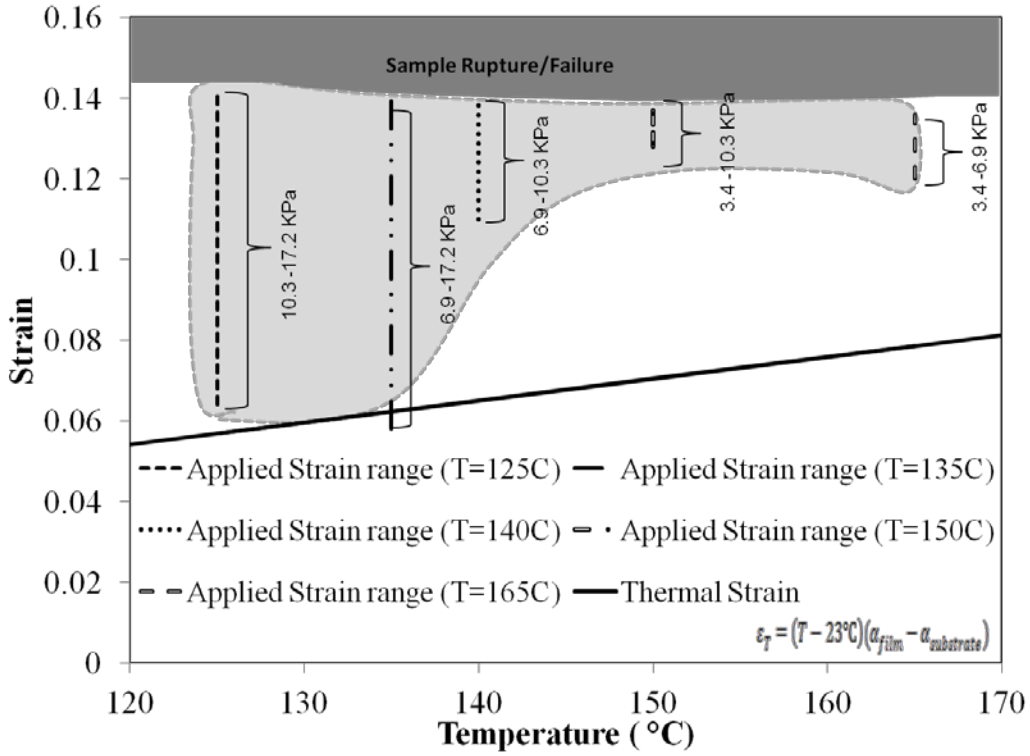

Figure 4-33: Biaxial stretching window and thermal strain induced at different temperatures using Isothermal Bulge Method. Thermal strain (ε_T) equation shown in legend.

By bulging at temperatures where the film and substrate were compliant, the increase in transient pressure would increase the biaxial strain in the sample gradually. The applied biaxial strain was intended to oppose the thermally-induced compressive strain and subsequent out-of-plane deformation that resulted from wrinkling, causing the distortions to disappear gradually. In principle, once the applied biaxial strain exceeded a critical limit, the wrinkles should disappear. However, simply matching the critical

compressive strain that initiated the wrinkles may result in relaxing the distortion so that the sample appears to have taken on its original shape, but there will be a reoccurrence of wrinkling once the applied biaxial strain is removed; this relapse in distortions was observed from time to time as the study's methodology was being setup but since the corresponding pressures were too low to reliably reproduce, their data was not included. Hence, for IBM to succeed in removing wrinkles a biaxial strain higher than the total induced thermal strain must be applied rather than only exceeding the critical limit value. It was also noted that the highest applied strain in this study could lead to creep in the samples (noted by a continuously increasing bulge height), particularly when the temperature was very high. At higher temperatures, the modulus of the laminate was considered too low and bulging led to rupture/failure of the sample.

4.6.2. Dynamic Bulge Method (DBM)

In dynamic bulge method (DBM) the clamped FBO/PP laminates were simultaneously heated and bulged to prevent wrinkle formation in the sample. Bulging while heating the laminate led to a constantly varying biaxial strain in the sample, as the modulus of the constituent layers decreased with increasing temperature. The biaxial strain was increased by varying the set-point pressure from 6.89 to 17.23kPa till a final strain of 10% at the dome peak was reached. To study the feasibility of this technique for practical thermoforming conditions where minimizing the heating and forming time is essential, four different heating rates were selected in the range of 20°C/min to 70°C/min, accomplished by changing the setpoint temperature of the heating source. The change in

strain rate depended on both heating rate and applied pressure and could be altered by changing either. For a given heating rate, strain rate increased by increasing the pressure as more force was applied to induce deformation. Conversely, for a given applied pressure with increasing heating rate, an increased strain rate would be seen as the material lost its stiffness faster.

It was hypothesized that as long as the applied biaxial strain always remained just higher than the critical strain for wrinkling at any particular temperature, then wrinkles would not appear during the forming processes. The variation in the applied strain and the critical strain for wrinkling with increasing temperature is shown in Figure 4-34. The applied strain was found to be well above the critical limit over the full range of bulge pressures (6.89 to 17.23kPa) as well as the full range of heating rates used, as shown in Figure 4-34. No wrinkles formed during the bulging process and hence this method was found to be very effective in preventing the formation of the wrinkles during heating

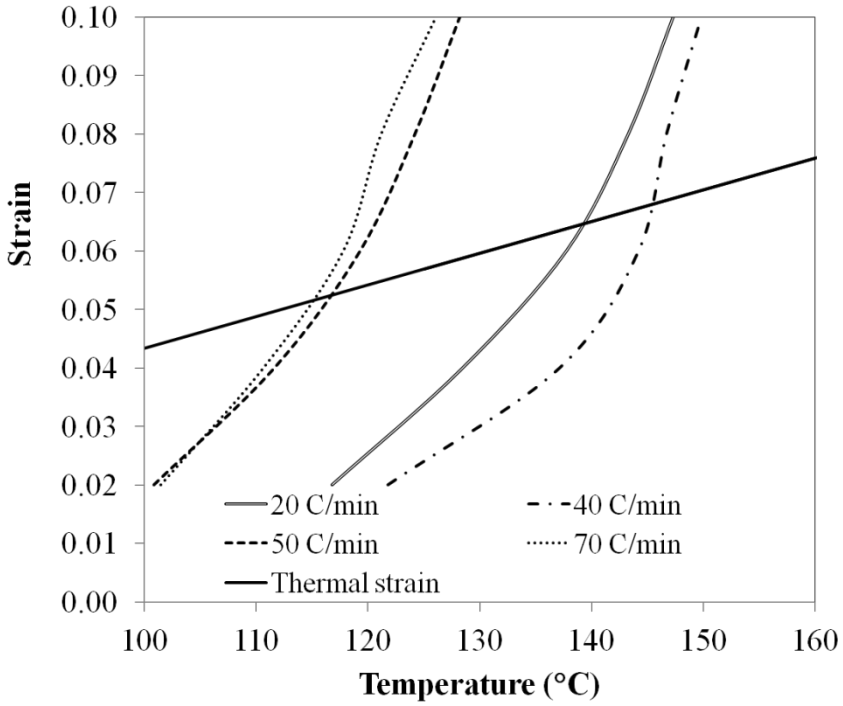

Figure 4-34: Dynamic strain applied and thermal strain induced at different temperatures by Dynamic Bulge method

4.7.Thermoforming

4.7.1. Stretch-assisted thermoforming (STF) for wrinkled laminates

Practical demonstration of the DBM versus IBM was done in a standard vacuum thermoformer to confirm that wrinkles in finished products could be minimized or avoided under real-world conditions. For simplicity of reference, both methods are considered to be examples of a technique now being referred to as 'stretch-assisted thermoforming' (STF). The mould shape in the study was chosen so that some regions of the laminate sheet experienced deep drawing whereas for other regions, practically no strain occurred. The mold design in shown in Appendix A.

The finished products from both proposed methodology was compared for differences in color, gloss, and surface finish (i.e. roughness). Also, changes in the adhesive interface were briefly studied by conducting a limited number of 180° peel tests.

4.7.2. Surface Topography Analysis of the Thermoformed Samples

The optical images of samples produced by conventional thermoforming (without stretching) and the samples produced by adapting both IBM and DBM using STF, are shown in Figure 4-35, Figure 4-36, & Figure 4-37. The finished products shown in these figures were all formed at the pre-set heating source temperature (300°C) which corresponded to a maximum sample temperature (isothermal condition) of 160°C. For

Dynamic STF and Isothermal STF, the specimens were bulged to a predestined height that corresponded to a strain at its pole of 8% which was sufficient to remove wrinkles.

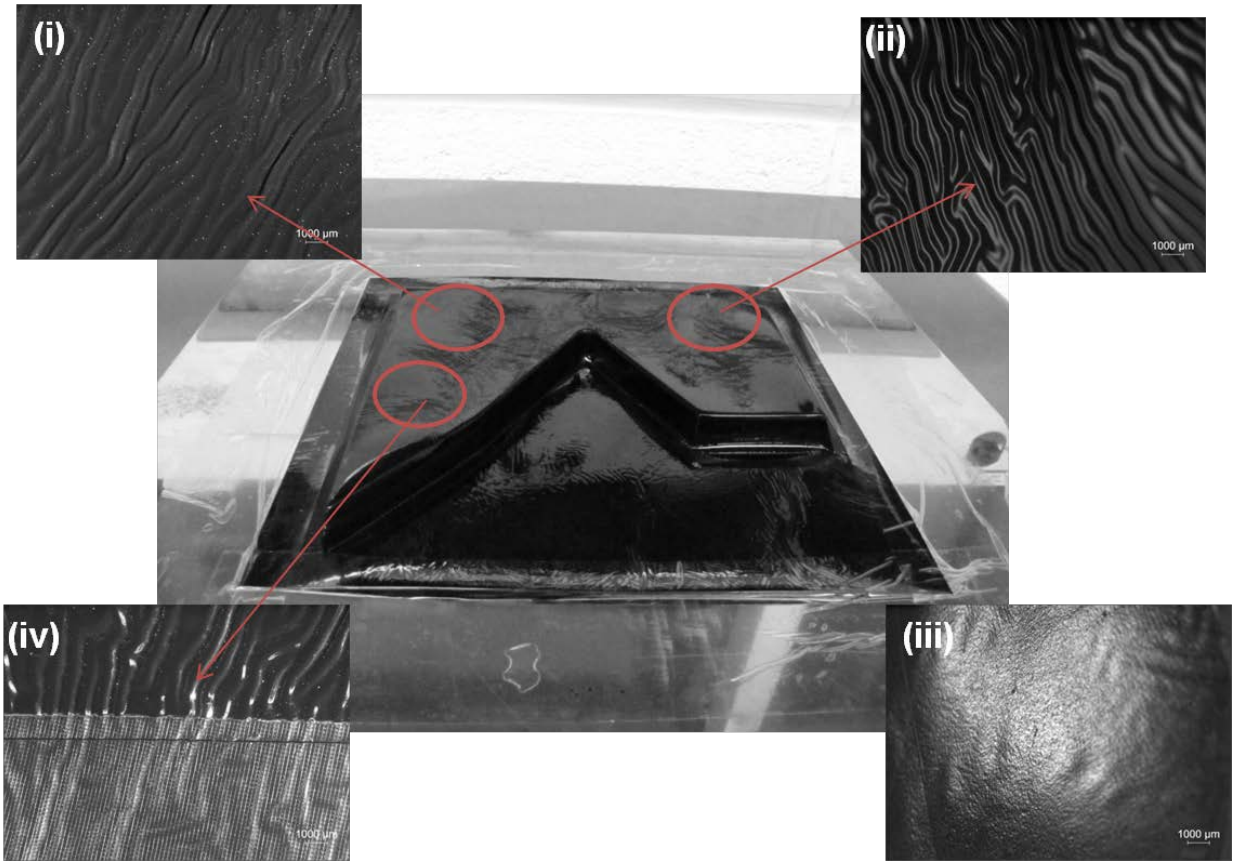

Figure 4-35: Conventional formed thermoformed sample of FBO/PP laminates with inserts showing (i) top sample surface (ii) Top surface at 35° degree inclination (iii) back-side/reverse (iv) visible portion of the PP substrate where the film was partly peeled away.

Figure 4-35 shows a FBO/PP specimen formed by conventional method of thermoforming where sample was initially heated to 160°C and subsequently formed by pulling vacuum (snap back procedure). Wrinkles are prominently observed on all surfaces of the finished product. State III wrinkling was observed where the substrate conformed to wrinkles in the film.

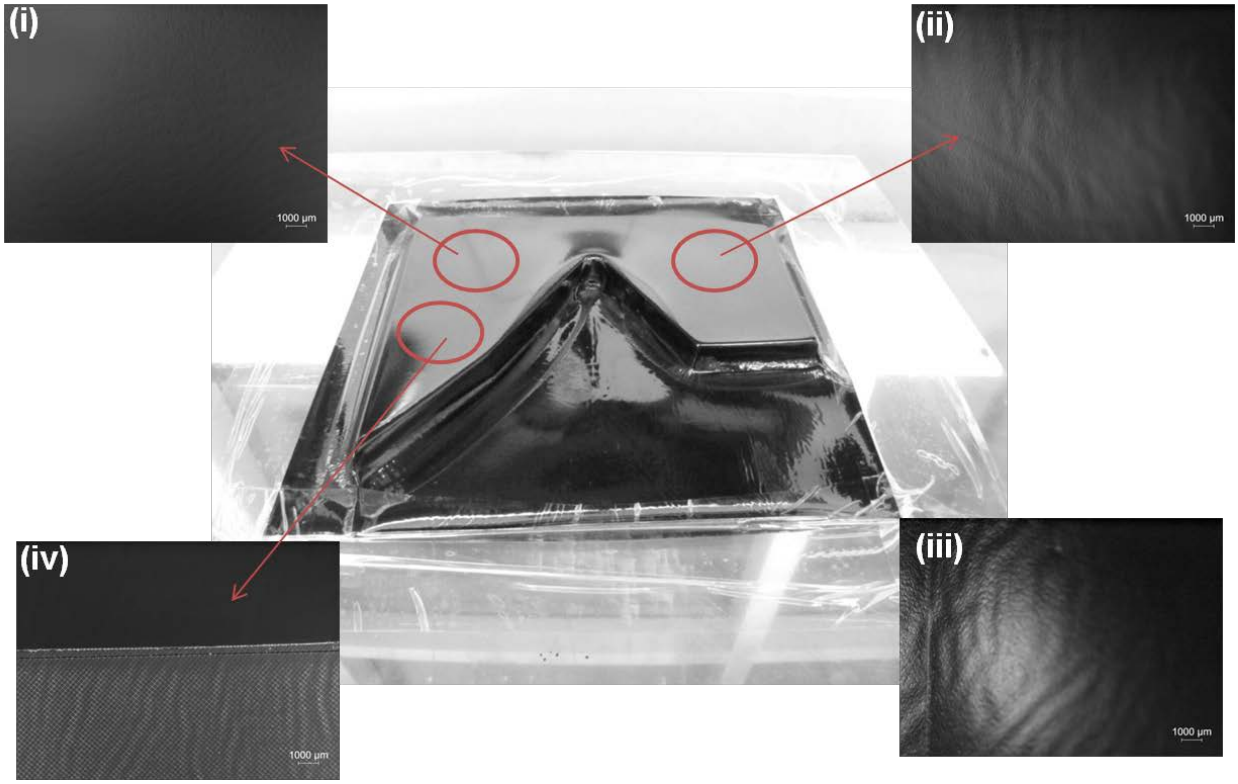

Figure 4-36: Isothermally formed thermoformed sample of FBO/PP laminates with inserts showing (i)Top sample surface (ii) Top surface at 35° degree inclination (iii) back-side/reverse (iv) visible portion of the PP substrate surface where the film was partly peeled away.

Figure 4-36 shows a FBO/PP specimen formed by Isothermal STF. Figure 4-36(ii) & (iii) are the optical images at normal and 35° to the top surface of the formed specimen. Even though the specimen was bulged to 8% strain before pulling vacuum to drape over the mold, some remnant wrinkle undulations were still visible when the light struck at the correct angle but otherwise these distortions were difficult to see. The top surface does show a relatively smooth finish (smooth PET clearcoat surface); however, when tilted to an angle, the surface show wrinkle undulations. This could be the underlying base layer that though stretched still recovered the "wrinkle-like" features. This was further affirmed from Figure 4-36(iv) where the exposed substrate surface also

showed wrinkles. There are several plausible causes where any combination could explain this observation, namely (a) wrinkle formed when pressure was relieved and vacuum was pulled and sample cooled, (b) pigmented base layer of FBO film underwent permanent damage (dislocation of the black pigments) when sample wrinkled during heating (as proven in earlier sections - see the light transmission study) and even though the subsequent bulging removed wrinkles, the original state was not achieved, or (c) adhesive layer holding the base layer of FBO film and PP substrate prevented in-plane-displacement thereby preventing complete removal of wrinkles.

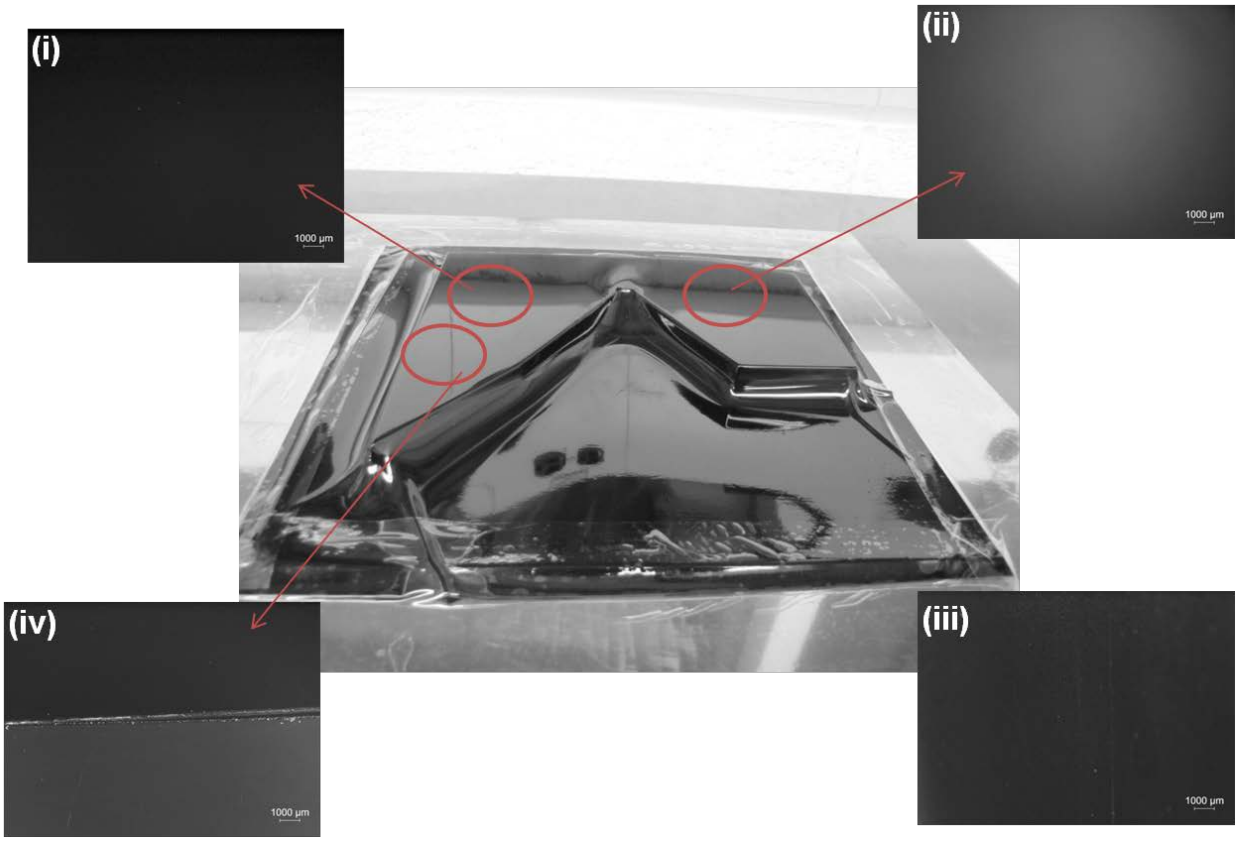

Figure 4-37: Dynamic formed thermoformed sample of FBO/PP laminates with inserts showing (i) top sample surface (ii) Top surface at 35° degree inclination (iii) back-side/reverse (iv) visible portion of the PP substrate surface where the film was partly peeled away.

Figure 4-37 shows the FBO/PP specimen formed by Dynamic STF. The specimen showed a smooth Class A finished surface with no surface deformations. It was interesting to note that imprinting of adhesive to substrate surface did not happen, unlike that of the Isothermal STF specimen or conventionally thermoformed specimen.

4.7.3. Color and Gloss Measurements

FBO/PP specimens formed by Isothermal and Dynamic STF were compared with pristine laminate samples for color and gloss readings. As these multilayer laminates are used decorative applications in the different fascias of automobiles, color and gloss becomes important criteria as evidence of molded part suitability. The color & gloss measurements were compared to the pristine FBO/PP sample so as to evaluate the drop in color and gloss of the formed specimens. Figure 4-38 & Figure 4-39 show the color and gloss measurements respectively for Isothermal STF and Dynamic STF specimens. The color and gloss measurements were taken at top flat surface of formed specimen.

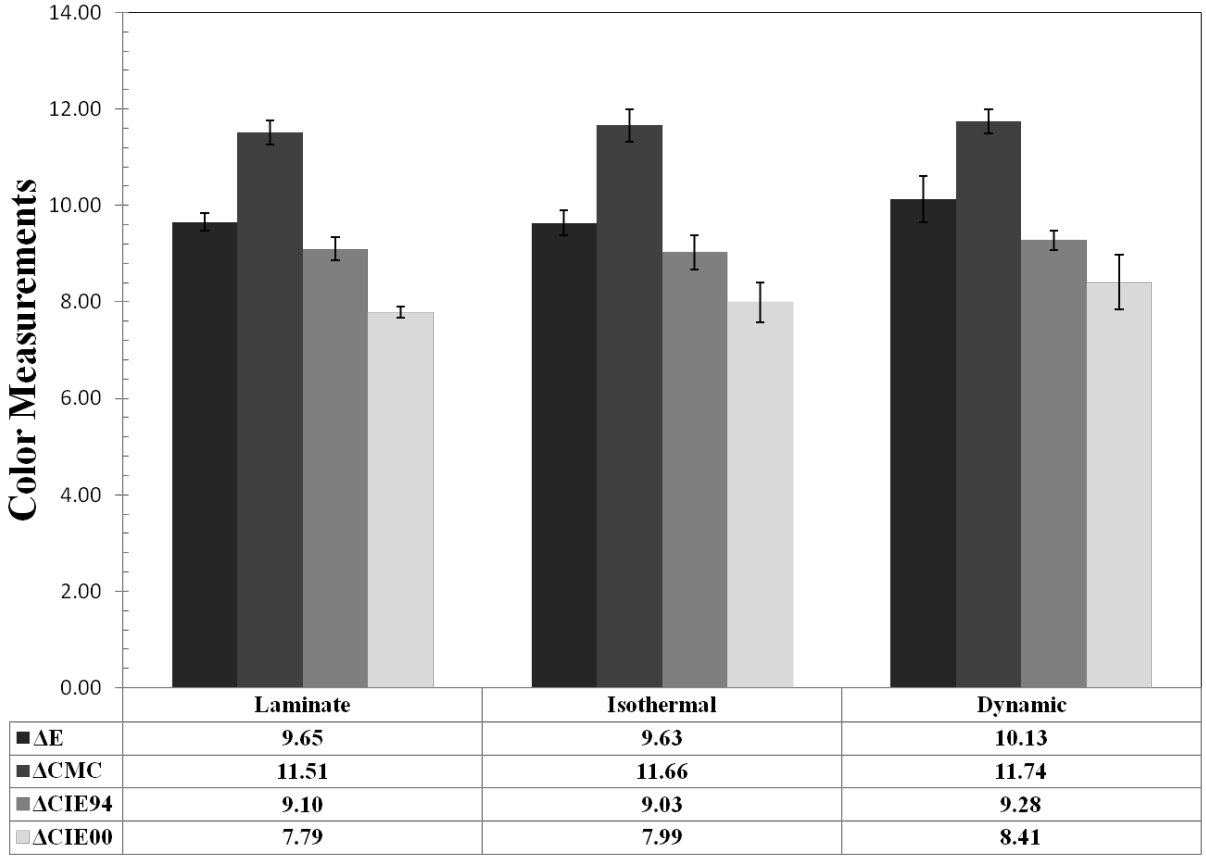

	Laminate	Isothermal	Dynamic
ΔE	9.65	9.63	10.13
ΔCMC	11.51	11.66	11.74
ΔCIE94	9.10	9.03	9.28
ΔCIE00	7.79	7.99	8.41

Figure 4-38: Comparison of color measurements for FBO/PP specimens formed by Dynamic STF and Isothermal STF to neat FBO/PP laminate

The color measurements did not significantly differ between the dynamic and isothermal STF methods in comparison to the never-heated pristine FBO/PP sample. As the substrate and film were both black pigmented, any damage due to wrinkling was masked and hence damage could not be picked up by color measurement. The gloss measurements showed marked difference between the three samples. For high gloss decorative applications, a gloss value of minimum 60 units is required at an incidence angle of 20^{o} and 60^{o}[4]. The drop in gloss was significantly large in Isothermal STF specimen due to mentioned presence of remnant wrinkle undulations on its surface. The

gloss value dropped below the set minimum for automotive decorative applications. However for dynamic STF specimen, a very minor drop in gloss was observed when compared to the original FBO/PP sample and retained most of its gloss to be applicable for use in automotive decorative parts.

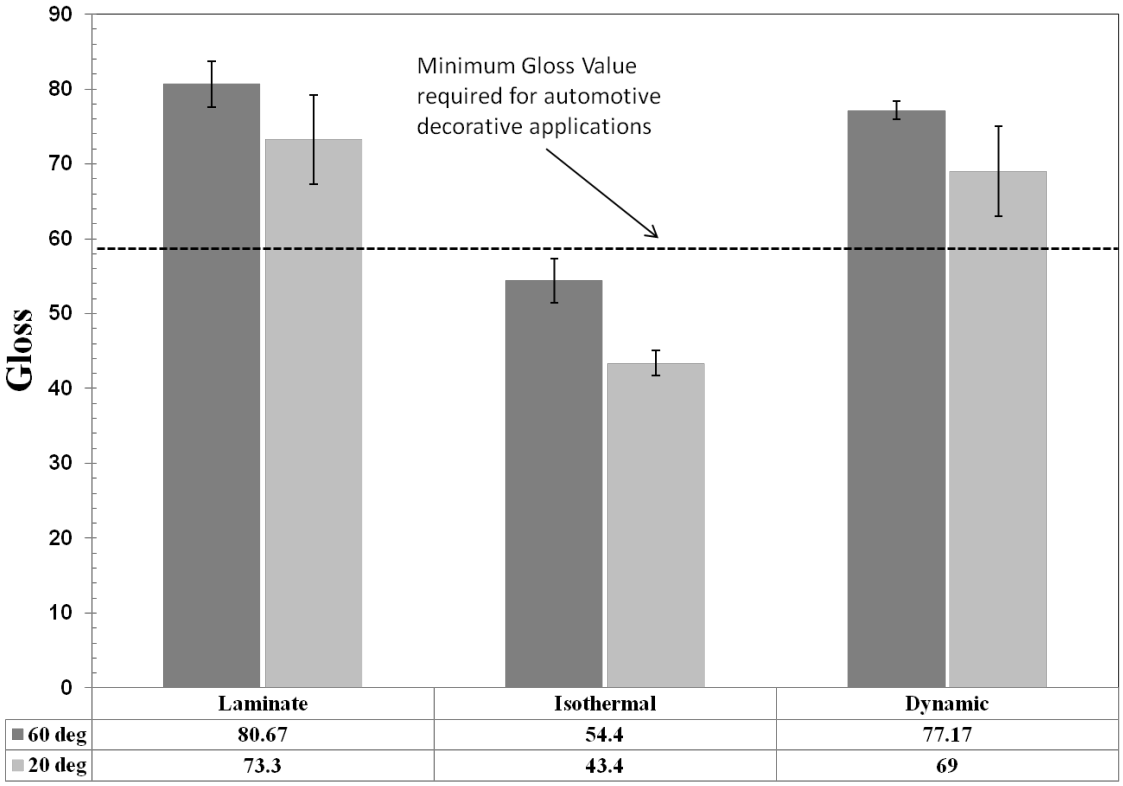

Figure 4-39: Comparison of gloss measurements for FBO/PP specimens formed by Dynamic STF and Isothermal STF to neat FBO/PP laminate. Dotted line represents the minimum gloss value for automotive decorative film application [4]

4.7.4. Study of Adhesive Interface by 180° Peel Test

From previously stated observations in this chapter, imprinting of the adhesive micro-pattern into substrate surface for wrinkled FBO/PP samples has been noticed at elevated temperatures (>150°C). This imprinting phenomenon was influenced by

wrinkling morphology and thus understanding the influence of the adhesive interface could be an important factor in developing wrinkle free multilayer laminates. Here, changes in adhesive interface were observed before and after forming. Comparison between the peel behaviour of Isothermal and Dynamic STF specimens to that of a pristine laminate is given to better appreciate the influence of wrinkling on forming. The 180° peel test were conducted using the procedure described in ASTM D903-98. The peel rate was maintained at constant 1 mm/min. The experimental setup, methodology and additional information is similar to work done in [81]. In this work, the influence of micro-patterning in formability of polymer film/polymer substrate laminates were explored in detail. For the peel test, the sample strips were cut out from the top flat surface of the formed specimens. Figure 4-40 shows the peel curves for Isothermal STF, Dynamic STF and a new laminate of FBO/PP system.

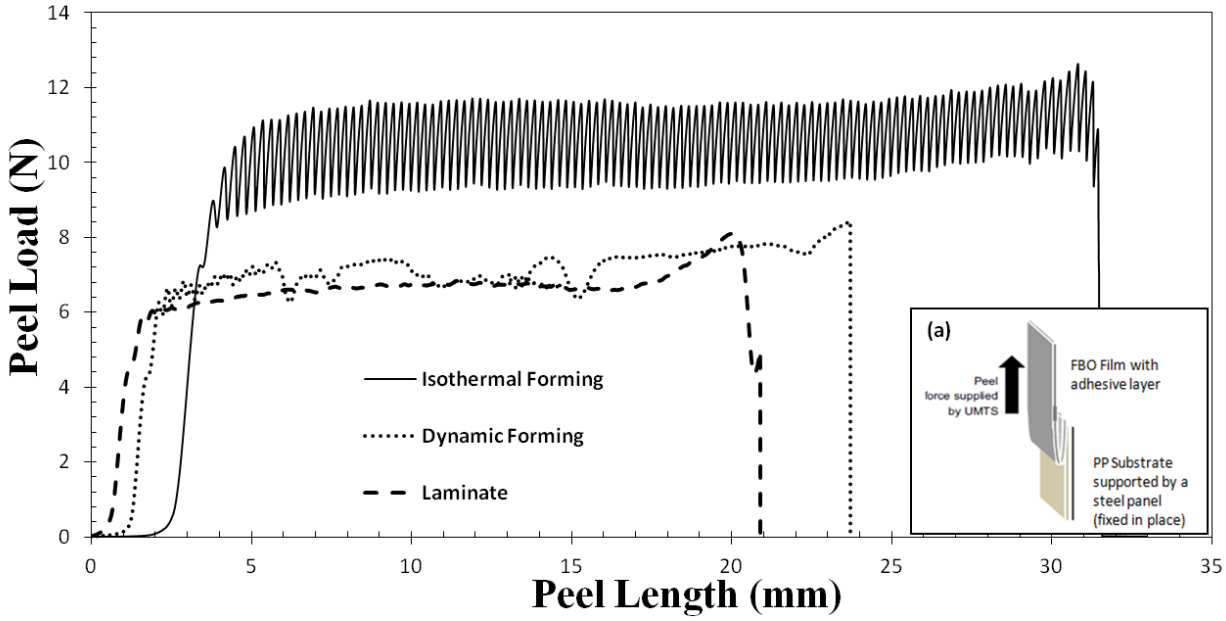

Figure 4-40: Comparison of peel behaviour of FBO/PP systems for Dynamic STF, Isothermal STF and neat laminate. Insert (a) Schematic representation of 180° peel test

In Figure 4-40, Isothermal STF showed a higher peel load than dynamic STF specimen and neat laminate. It was interesting to note that the isothermal STF peel curve had a consistent cyclic peel load fluctuation with progressing peel length. The distance between two adjacent minima/maxima was found to be exactly the same (260μm) which corresponds to the distance between grid lines in the micro-patterned adhesive. It was previously observed that adhesive micro-pattern grid was imprinted onto the substrate surface in Isothermal STF specimen along with the wrinkle macro-pattern. Thus the optical evidence and peel load data suggests that mechanical bonding was created when the sample was allowed to wrinkle, which resulted in a higher peel strength than original or dynamic STF specimens. The increased adhesive bonding created during wrinkling could be cause for remnant wrinkles seen after bulging and forming in Isothermal STF

specimens. Conversely, the peel curves for Dynamic STF and neat sample were quite similar in shape and magnitude, which showed that no alterations to the interface occurred for these samples.

CHAPTER 5 CONCLUSIONS

Although the use of polymeric decorative films as a potential substitute for paint in automotive parts can be an economical and environment friendly option, there is a need to address certain problems encountered during forming/thermoforming operations. The usage of multiple layers with distinctly different physical and chemical properties is inevitable in order to produce a long-standing film with the appearance and longevity rivaling paint. However, the variance in thermal expansion behaviour by each constituent layer in such a structure makes parts created with them susceptible to wrinkling due to the resulting strain mismatch while being heated. For the automotive decorative film studied being affixed to either polymer substrates (PP or PC), wrinkling was observed when heated to a forming temperature between 130°C - 180°C; the temperature dependency shown for wrinkling was specific to the film rather than the substrate.

The wrinkling phenomenon was investigated by varying both temperature and heating rate. A previous study on the same multilayer film (FBO) on a rigid substrate (metal) had shown a correlation between wrinkle growth to both heating rate and temperature. In this study, more compliant polymeric substrates (PP & PC) were used instead of metal. Wrinkle growth and growth rate characterized by the pattern's amplitude and wavelength were once again seen to be strongly dependent on the temperature and heating rate of the process. The onset of wrinkling for the FBO film was first noticed at a temperature of 135°C which corresponded to the softening of PE segments within the base layer. Above 135°C, the building compressive stresses within the film due to thermally-induced strain mismatch between the layers, were sufficient to cause wrinkle growth. The wavelength

and amplitude of these wrinkles changed in a sigmoidal manner with increasing temperature; the sigmoidal curve characterized by a lower and upper asymptote. Beyond a threshold temperature, the wrinkle growth was observed to increase and reach an equilibrium value beyond which no significant changes in amplitude or wavelength was observed. The upper equilibrium value for either wavelength or amplitude occurred at a lower temperature as the heating rate increased, which could be related to the characteristic absorption and emission rate of the laminate to the applied radiant heat at that temperature. At higher temperatures, wrinkling is a compromise between elastic energy as a driving force and the viscous flow as a kinetic process. The wrinkles have infinitely many unstable equilibrium configurations and these unstable wrinkles are kinetically constrained. The compliancy of the substrates to wrinkle perturbations similarly increased with increasing temperature due to diminishing stiffness relative to the film, particularly its transparent top coat layer. This added a very interesting element to analyze since the wrinkling literature does not consider the substrate to participate in wrinkling to the extent observed in this study and so there are no reports on the phenomenon. Comparison of two polymer substrates with very different thermo-mechanical properties, it was observed that the E_s/E_f ratio dictated the compliancy of the wrinkle and conformation of the substrate to wrinkle undulations. In FBO/PP laminates, with increasing temperatures, wrinkles in the defined states of I, II, III were observed. Whereas, in FBO/PC laminates, irrespective of the thickness of the substrate used, wrinkles in only state I (i.e. a rigid substrate, like the previous work on metal) was observed in the temperature range of study.

The influence of heating rate was observed to be very different on FBO/PP laminates when compared to FBO/PC laminates. The heating rate was observed to influence wrinkle amplitude and wavelength in a manner corresponding to the rate of heat absorption as well as thermal conductivity through the layers of the film-substrate laminate. The influence of heating rate was more pronounced for the substrate with lower thermal conductivity (i.e. PP), which affected the ability of the multilayer laminate to absorb the energy at faster rates. At high heating rates, temperature gradient through the component layers could have also arisen resulting in compressive stresses acting at varying rates on the film; this is only a hypothesis but it is difficult to assess such gradients in practice due to the slow, low resolution methods to detect temperature which are presently available in such thin structures. Damage was noted to the film due to wrinkling which was visibly apparent in the FBO/PC laminates as the substrate was optically transparent. Light transmission studies conducted on these samples concluded that for temperatures above 155°C, the damage was more severe with possible localized thinning and/or yielding within the pigmented base layer of the FBO film.

The prediction of wavelength and amplitude using theoretical elastic models of Allen and Groenewold explained the trend of variation during heating but could never reasonably match the experimental values in terms of order of magnitude. However, the Groenewold equation could be adjusted to being quite predictive when the amplification factor for the modulus ratio in the relation was changed. The most complex Huang models did not agree well with the experimentally determined values as they were more applicable to thick viscous substrate or thin viscous substrate held in place by a rigid

backing. Since none of these models consider a compliant substrate or properly represent a viscoelastic substrate in the calculations, it was quite surprising how well any of the models performed in this analysis.

The induced mismatch compressive stresses that caused wrinkling during heating were notably relieved by stretching the laminate biaxially, which was achieved in this work by modifying a conventional thermoformer. The level of biaxial stretching needed in opposition to wrinkle formation was dictated by the modulus of the constituent layers at the temperature of the process. Controlled bulging of the laminate sample at appropriate temperature settings resulted in producing an unwrinkled laminate; however, applying just the minimum amount of stress necessary to avoid wrinkling proved almost impossible as the value was too low for practical control. Biaxially stretching (bulging) the sample after it reaches the wrinkling temperature range (isothermal STF) was not recommended, since it was found to be the more difficult case to inflate without rupturing the softened laminate and as noted above, the local distortions in the base layer induced by wrinkling may leave it susceptible to environmental damage once aging in an exterior automotive application. However, isothermal STF was found to increase the adhesive bond with a substrate, caused in this case by a mechanical interlock as the compliant substrate conformed with the wrinkles of the film. Alternative, biaxial stretching of the sample during heating (dynamic STF) was considered to be the more recommended approach to preparing wrinkle-free thermoformed parts with the FBO. The specimens by dynamic STF most closely resembled the pristine appearance of the original film based on color & gloss measurements, surface finish, and peel strength. Overall, Dynamic STF

technique was found to be very effective in retaining the Class-A finished surface in the finished product.

REFERENCE

[1] D. Weill, L. Besland, G. Klink and G. Rouilloux, "ATKearney," Ideas and Insights, 06 2012. [Online]. Available: http://www.atkearney.com/issue-papers-perspectives. [Accessed February 2013].

[2] L. M. Sherman, "Where the Action Is: Decorating with Formable Films," *Plastics Technology,* 2004.

[3] W. J. Buehne, H. H. ,. Enlow, J. R. Johnson, K. L. Truog and F. Young, "Exterior automotive laminate with pressure sensitive adhesive". USA Patent US5518786 A, 21 May 1996.

[4] J. Fan, J. Patton and Q. Song, "Decorative paint film laminate". USA Patent US7854985 B2, 21 December 2010.

[5] M. Naitove, "Automotive Innovation Trend-Setting Technologies Garner SPE Awards," *Plastics Technology,* 2002.

[6] "Stainless-Steel Film Can Replace the Real Thing," *Plastics Technology,* July 2012.

[7] S. Wagner, S. P. Lacour, J. Jones, P.-h. I. Hsu, J. C. Sturm, T. Li and Z. Suo, "Electronic skin: architecture and components," *Physica E,* vol. 25, pp. 326-334, 28 July 2004.

[8] W. N. Malek, "Gravel-resistant selfadhesive decorative film". Hamburg, Germany Patent US4550052 A, 29 October 1985.

[9] M. F. Weber, T. J. Nevitt, A. J. Ouderkirk, J. A. Wheatley, J. M. Jonza, Y. Q. Liu, A. T. Ruff and J. A. Boettcher, "Multilayer optical films having one or more reflection bands". USA Patent US7851054 B2, 14 December 2010.

[10] W. J. Schrenk, J. A. Wheatley and D. M. Wisniewski, "Multilayer polymeric reflective bodies for decorative and security applications". USA Patent US5234729 A, 10 August 1993.

[11] L. Poole, "Decorative Film Laminates," Chicago, IL, 2007.

[12] K. L. Thunhorst and J. F. Pitzen, "Laminate from which decorative films can be applied to a substrate". USA Patent US6984429 B2, 10 January 2006.

[13] R. R. Niazy, "Decorative films and laminated formable sheets with dual protective film layers". Michigan, USA Patent US5919537 A, 6 July 1999.

[14] W. J. Schrenk, "All-polymeric ultraviolet light reflecting film". USA Patent US5540978 A, 30 July 1996.

[15] W. Grimes and R. A. Lombardi, "Method of forming a Metallized decorative film laminate". USA Patent US4330352, 18 May 1982.

[16] F. T. Sher, L. A. Meixner, F. V. Loncar and C. D. Calhoun, "Adhesives having a microreplicated topography and methods of making and using same". USA Patent US6197397 B1, 6 March 1996.

[17] R. D. Leaversuch, "Thermoforming Goes Paint-Free, Too," *Plastics Technology,* January 2004.

[18] Evco Plastics, "Custom Plastic In-Mold Decorating (IMD) & In-Mold Labelling (IML)," Evco Plastics, 2013. [Online]. Available: http://www.evcoplastics.com/in-mold-decorating-labeling. [Accessed 26 06 2013].

[19] J. Avery, Injection Molding Alternatives: A guide for Designers and Product Engineers, Hanser Verlag, 1998.

[20] T. A. Osswald, L.-S. Turng and P. Gramann, Injection Molding Handbook, Hanser Gardner Publications Inc., 2008.

[21] M. P. Sepe, "Dimensional Stability After Molding: Part 1, Part 2, Part 3," *Plastics Technology,* January 2013.

[22] S. H. Im and R. Huang, "Ratcheting-induced wrinkling of an elastic film on a metal layer under cyclic temperatures," *Acta Materialia,* vol. 52, no. 12, pp. 3707-3719, 2004.

[23] S. Goyal, K. Srinivasan, G. Subbarayan and T. Siegmund, "On Instability-Induced

Debond Initiation in Thin Film Systems," *Engineering Fracture Mechanics,* vol. 77, pp. 1298-1313, 2010.

[24] Y. Cao and J. Hutchinson, "From wrinkles to creases in elastomres: the instability and imperfection-sensitivity of wrinkling," *Proceeding of the Royal Society,* vol. 468, pp. 94-115, 2012.

[25] J. E. Roys and L. S. Coons, "High gloss laminates for decorative automotive parts". USA Patent WO2007081915 A1, 19 July 2007.

[26] J. Hutchinson and Z. Suo, "Mixed Mode Cracking in Layered Materials," *Advances in Applied Mechanics,* vol. 29, pp. 63-191, 1992.

[27] R. Huang, "Kinetic wrinkling of an elastic film on a viscoelastic substrate," *Journal of Mechanics and Physics of Solids,* vol. 53, pp. 63-89, 2005.

[28] E. Cerda and L. Mahadevan, "Geometry and Physics of Wrinkling," *Physical Review Letters,* vol. 90, no. 7, pp. 74302:1-4, 2003.

[29] H. G. Allen, Analysis and Design of Structural Sandwich Panels, Pergamon Press, 1969.

[30] D. Williams, D. M. A. Leggett and H. G. Hopkins, "Flat sandwich panels under compressive end loads (ARC Technical Report)," H.M. Stationery Office, 1941.

[31] M. A. Biot, "Folding instability of a layered viscoelastic medium under compression," *Proceedings of the Royal Society of London, Ser. A,* vol. 242, pp. 444-454, 1957.

[32] M. A. Biot, Mechanics of Incremental Deformation, Wiley, 1965.

[33] N. Bowden, W. Huck, K. E. Paul and G. Whitesides, "The controlled formation of ordered, sinusoidal structures by plasma oxidation of an elastomeric polymer," *Applied Physics Letters,* vol. 75, p. 2558, 1999.

[34] N. Bowden, S. Brittain, A. G. Evans, J. W. Hutchinson and G. M. Whitesides, "Spontaneous formation of ordered structures in thin films of metals supported on an elastomeric polymer," *Nature,* vol. 393, pp. 146-149, 14 May 1998.

[35] T. Tanaka, S. Sun, Y. Hirokawa, S. Katayama, J. Kucera, Y. Hirose and T. Amiya, "Mechanical instability of gels at the phase transition," *Nature,* vol. 325, pp. 796-798, 1987.

[36] B. Grzybowski, K. J. M. Bishop, C. J. Campbell, M. Fialkowski and S. K. Smoukov, "Micro- and nanotechnology via reaction–diffusion," *Soft Matter,* vol. 1, pp. 114-128, 2005.

[37] C. Jiang, M. McConney, S. Singamaneni, E. Merrick, Y. Chen, J. Zhao, L. Zhang and V. V. Tsukruk, "Thermo-optical arrays of flexible Nanoscale nanomembranes freely suspended over microfabricated cavities as IR microimagers," *Chemistry of*

Materials, vol. 18, no. 11, pp. 2632-2634, 2006.

[38] Y. Zhang, E. A. Matsumoto, A. Pete, P.-C. Lin, R. D. Kamien and S. Yang, "One-Step Nanoscale Assembly of Complex Structures via Harnessing of an Elastic Instability," *Nano Letters,* vol. 8, no. 4, pp. 1192-1196, 2008.

[39] Y. Klein, E. Efrati and E. Sharon, "Shaping of Elastic Sheets by Prescription of Non-Euclidean Metrics," *Science,* vol. 315, no. 5815, pp. 1116-1120, 2007.

[40] S. Wagner, S. P. Lacour, J. Jones, P.-h. I. Hsu, J. C. Sturm, T. Li and Z. Suo, "Electronic skin: architecture and components," *Physica E,* vol. 25, no. 2, pp. 326-334, 2004.

[41] D. Y. Khang, H. Jiang, Q., Y. Huang and J. A. Rogers, "A Stretchable form of single-crystal silicon for high performance electronics on rubber substrate.," *Science,* vol. 311, pp. 208-212, 2006.

[42] E. P. Chan and A. J. Crosby, "Fabricating Microlens Arrays by Surface Wrinkling," *Advanced Materials,* vol. 18, pp. 3238-3242, 2006.

[43] D. Chandra, P. Lin and S. Yang, "Strain responsive concave and convex microlens arrays," *Applied Physics Letters,* vol. 91, p. 251912, 2007.

[44] J. Chung, J. P. Youngblood and C. M. Stafford, "Anisotropic wetting on tunable micro-wrinkled surfaces," *Soft Matter,* vol. 3, pp. 1163-1169, 2007.

[45] P. Lin, S. Vajpayee, A. Jagota, C. Y. Hui and S. Yang, "Mechanically tunable dry adhesive from wrinkled elastomers," *Soft Matter,* vol. 4, no. 9, pp. 1830-1835, 2008.

[46] P. Lin and S. Yang, "Mechanically switchable wetting on wrinkled elastomers with dual-scale roughness," *Soft Matter,* vol. 5, no. 5, pp. 1011-1018, 2009.

[47] X. Zhu, Y. Zhang, D. Chandra, S. Cheng, J. Kikkawa and S. Yang, "Two-dimensional photonic crystals with anisotropic unit cells imprinted from poly (dimethylsiloxane) membranes under elastic deformation," *Applied Physics Letters,* vol. 93, p. 161911, 2008.

[48] J. Jang, C. Y. Koh, K. Bertoldi, M. C. Boyce and E. L. Thomas, "Combining Pattern Instability and Shape-Memory Hysteresis for Phononic Switching," *Nano Letters,* vol. 9, pp. 2113-2119, 2009.

[49] C. M. Stafford, C. Harrison, K. L. Beers, A. Karim, E. J. Amis, M. R. VanLandingham, H. ,. Kim, W. Volksen, R. D. Miller and E. E. Simonyi, "A buckling-based metrology for measuring the elastic moduli of polymeric thin films," *Nature Materials,* vol. 3, no. 8, pp. 545-550, 2004.

[50] M.-W. Moon, K. R. Lee, K. Oh and J. Hutchinson, "Buckle delamination on patterned substrates," *Acta Materialia,* vol. 52, no. 10, pp. 3151-3159, 2004.

[51] M. Moona, H. Jensenb, J. Hutchinson, K. Oh and A. Evans, "The characterization of telephone cord buckling of compressed thin films on substrates," *Journal of the*

Mechanics and Physics of Solids, vol. 50, pp. 2355-2377, 2002.

[52] E. Chan, E. J. Smith, R. C. Hayward and A. J. Crosby, "Surface wrinkles for smart adhesion," *Advanced Materials,* vol. 20, pp. 711-716, 2008.

[53] M.-W. Moon, S. Lee, J. Sun, K. Oh, A. Vaziri and J. Hutchinson, "Wrinkled hard skins on polymers created by focused ion beam," *Proceedings of the National Academy of Sciences of the USA,* vol. 104, no. 4, pp. 1130-1133, 2006.

[54] H. Jiang, D.-Y. Khang, J. Song, Y. Sun, Y. Huang and J. A. Rogers, "Finite deformation mechanics in buckled thin films on compliant supports," *Proceedings of the National Academy of Siences USA,* vol. 104, no. 40, pp. 15607-15612, 2007.

[55] X. Chen and J. W. Hutchinson, "Herringbone Buckling Patterns of Compressed Thin Films on Compliant Substrates," *Journal of Applied Mechanics,* vol. 71, p. 597, 2004.

[56] R. Huang, "Kinetic wrinkling of an elastic film on a viscoelastic substrate," *Journal of Mechanics & Physics of solids,* vol. 53, pp. 63-89, 2005.

[57] R. Huang and Z. Suo, "Wrinkling of an elastic film on a viscous layer," *Journal of Applied Physics,* vol. 91, pp. 1135-1142, 2002.

[58] J. Liang, R. Huang, H. Yin, J. Sturm, K. Hobart and Z. Suo, "Relaxation of compressed elastic islands on a viscous layer.," *Acta Materialia,* vol. 50, no. 11, pp.

2933-2944, 2002.

[59] J. Groenewold, "Wrinkling of plates coupled with soft elastic media," *Physica A,* vol. 298, pp. 32-45, 2001.

[60] N. J. Hoff and S. E. Mautner, "Buckling of sandwich-type panels," *Journal of the Aeronautical Sciences,* vol. 12, no. 3, pp. 285-297, 1945.

[61] G. Gough, C. F. Elam and N. D. De Bruyne, "The stabilization of a thin sheet by a continuous supporting medium," *Journal of Royal Aeronautical Society,* vol. 44, no. 349, pp. 12-43, 1940.

[62] S. Yang, K. Khare and P. Lin, "Harnessing Surface Wrinkle Patterns in Soft Matter," *Advanced Functional Materials,* vol. 20, pp. 2550-2564, 2010.

[63] D.-Y. Khang, J. A. Rogers and H. H. Lee, "Mechanical Buckling: Mechanics, Metrology, and Stretchable Electronics," *Advanced Functional Materials,* vol. 18, pp. 1-11, 2008.

[64] S. K. Basu, A. V. McCormick and L. ,. Scriven, "Stress Generation by Solvent Absorption and Wrinkling of a Cross-Linked Coating atop a Viscous or Elastic Base," *Langmuir,* vol. 22, pp. 5916-5924, 2006.

[65] R. K. Maharajan, *Investigation of the effect of swelling and shrinkage on the wrinkling response of locally wetted papers subjected to tension with application to*

Web-Fed Ink Jet printing, 2007.

[66] H. Wagner, "Ebene Blechwandtrager mit sehr dunnem stegblech," *Z. Flugtechn Motorluftschiffahrt,* vol. 20, pp. 8-12, 1929.

[67] D. J. Steigmann, "Tension-field theory," *Proceedings of the Royal Society A: Mathematical, Physical & Engineering Science,* vol. 429, no. 1876, pp. 141-173, 1990.

[68] C. Coman, "On the applicability of tension field theory to a wrinkling instability problem.," *Acta Mechanica,* vol. 190, pp. 57-72, 2007.

[69] S. Im and R. Huang, "Evolution of Wrinkles in Elastic-Viscoelastic Bilayer thing films," *Journal of Applied Mechanics,* vol. 72, pp. 955-961, 2005.

[70] P. J. Yoo and H. H. Lee, "Morphological Diagram for Metal/Polymer Bilayer Wrinkling: Influence of Thermomechanical Properties of Polymer Layer," *Macromolecules,* vol. 28, pp. 2820-2831, 2005.

[71] K. D. Hobart, F. J. Kub, M. Fatemi, M. E. Twigg, P. E. Thompson, T. S. Kuan and C. K. Inoki, "Compliant substrates: A comparative study of the relaxation mechanisms of strained films bonded to high and low viscosity oxides," *Journal of Electronic Materials,* vol. 29, no. 7, pp. 897-900, 2000.

[72] N. Sridhar, D. J. Srolovitz and Z. Suo, "Kinetics of buckling of a compressed film on

a viscous substrate," *Applied Physics Letters,* vol. 78, no. 17, pp. 2482-2484, 2001.

[73] R. Huang and Z. Suo, "Wrinkling of a compressed elastic film on a viscous layer," *Journal of Applied Physics,* vol. 91, no. 3, pp. 1135-1142, 2002.

[74] O. Reynolds, "On the Theory of Lubrication and its Application to Mr. Beauchamp Tower's Experiments, including an Experimental determination of the viscosity of Olive Oil," *Philosophical Transactions of the Royal Society of London,* pp. 157-235, 1886.

[75] G. Gutscher, H.-C. Wu, G. Ngaile and T. Altan, "Determination of flow stress for sheet metal forming using the viscous pressure bulge (VPB) test," *Journal of Materials Processing Technology,* vol. 146, pp. 1-7, 2004.

[76] J. Liu, M. Ahmetoglu and T. Altan, "Evaluation of sheet metalformability, viscous pressure forming (VPF) dome test," *Journal of Matereial Process Technology,* vol. 98, pp. 1-6, 2000.

[77] J. Slota, E. Spisak and F. Stachowicz, "Investigation of biaxial stress-strain relationship of steel sheet metal," *Applied Mechanics and Engineering,* vol. 9, no. 1, pp. 161-168, 2004.

[78] P. Bing, X. Hui-min, H. Tao and A. Asundi, "Measurement of coefficient of thermal expansion of films using digital image correlation method," *Polymer Testing ,* vol.

28, no. 1, pp. 75-83, 2009.

[79] B. Pan, K. Qian, H. Xie and A. Asundi, "Two-dimensional digital image correlation for in-plane displacement and strain measurement: a review," *Measurment science and technology,* vol. 20, no. 6, p. 062001, 2009.

[80] M. M. Malayery, *Thermally Induced wrinkling behaviour of automotive decorative films,* Hamilton, ON: McMaster University (Open Access Dissertations and Theses), 2010.

[81] P. G. Balamurugan, R. Pukadyil, K. E. Nielsen and F. Brandys, "Role of a micro-patterned adhesive interface on the performance of thermoformable multi-layered decorative polymeric film laminates," *International Journal of Adhesion & Adhesives,* vol. 44, pp. 78-90, 2013.

[82] S. H. Im and R. Huang, "Ratcheting-induced wrinkling of an elastic film on a metal layer under cylic temperatures," *Acta Materialia,* vol. 52, pp. 3707-3719, 2004.

[83] C. Harrison, C. M. Stafford, W. Zhang and A. Karim, "Sinusoidal phase grating created by a tunably buckled surface," *Applied Physics Letters,* vol. 85, pp. 4016-4018, 2004.

APPENDICES

Appendix A. Thermoforming Mold Diagram

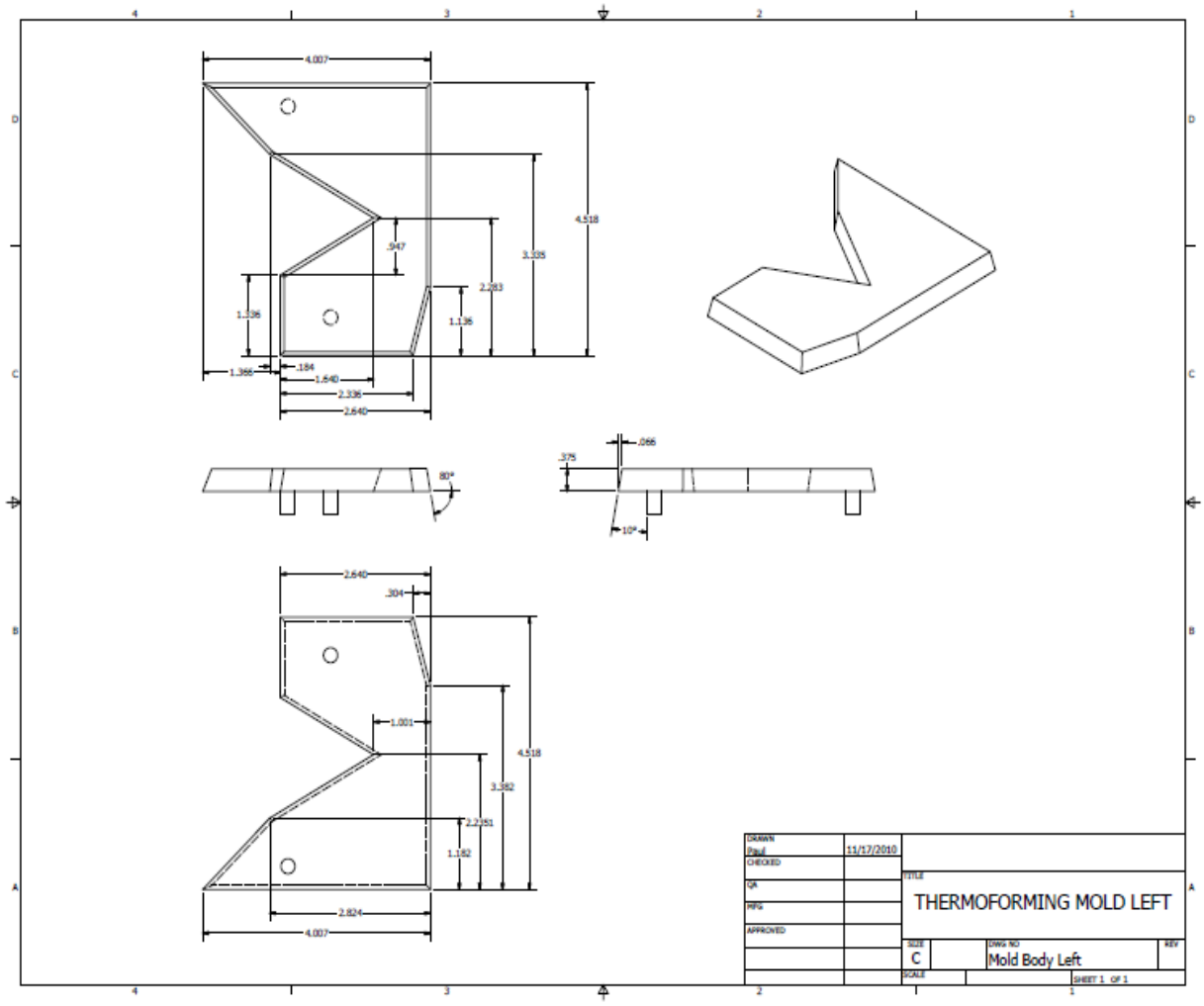

Appendix B. Relaxation Behaviour of PP Substrate

Relaxation Moduli estimated based on mechanical model fitting (Analysis done using JMP statistical software)

$$\mu(t) = \mu_\infty + \mu_i \sum\nolimits_i \exp(-p_i t) \quad \text{and} \quad \mu_0 = \mu_\infty + \mu_{i=1-n}$$

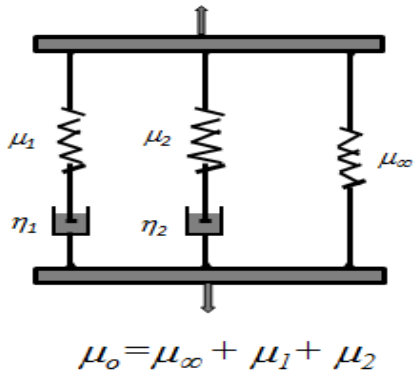

Figure B-1: Schematic of the Mechanical Model describing the relaxation behaviour of PP Substrate

Predicting equation

$$\mu(t) = \mu_\infty + \mu_1 \exp(-p_1 t) + \mu_2 \exp(-p_2 t)$$

Temperature	μ_∞	μ_1	p_1	μ_2	p_2	μ_0	R^2
130	4.284	10.647	0.008	10.439	0.153	25.370	0.998
135	10.747	6.664	0.007	9.309	0.132	26.721	0.997
140	11.548	5.734	0.007	8.107	0.126	25.389	0.999
145	9.865	4.473	0.007	6.764	0.134	21.102	0.996
150	6.511	5.178	0.146	3.299	0.008	14.988	0.996
155	2.483	4.032	0.214	1.535	0.009	8.049	0.995
160	0.391	0.645	0.177	0.362	0.007	1.399	0.992

Appendix C. Relaxation Behaviour of PC Substrate

Relaxation Moduli estimated based on mechanical model fitting (Analysis done using JMP statistical software)

$$\mu(t) = \mu_\infty + \mu_i \sum\nolimits_i \exp(-p_i t) \quad \textbf{\textit{and}} \quad \mu_0 = \mu_\infty + \mu_{i=1-n}$$

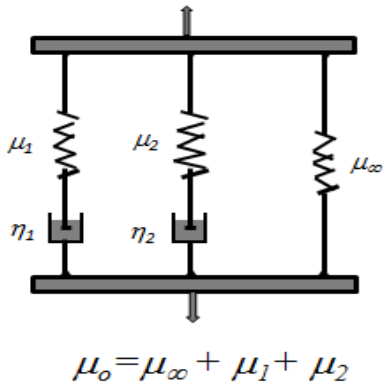

Figure C-1: Schematic of the Mechanical Model describing the relaxation behaviour of PC Substrate

Predicting equation:-

$$\mu(t) = \mu_\infty + \mu_1 \exp(-p_1 t) + \mu_2 \exp(-p_2 t)$$

Temperature	μ_∞	μ_1	p_1	μ_2	p_2	μ_0	R^2
130	167.120	328.404	0.005	148.789	0.055	644.314	0.999
140	76.521	438.561	0.008	334.351	0.066	849.434	0.999
150	13.032	7.331	0.018	157.299	0.233	177.663	0.997
160*	1.268	4.768	-0.015			6.035	0.849
170	0.049	2.542	0.053	2.122	0.039	4.713	0.999
180*	-0.768	-0.584	-0.060			-1.353	0.927

Note: for temperature 160 and 180, the data fitted for model to give value for only first two terms of the prediction equation

Appendix D. Light Transmission Study

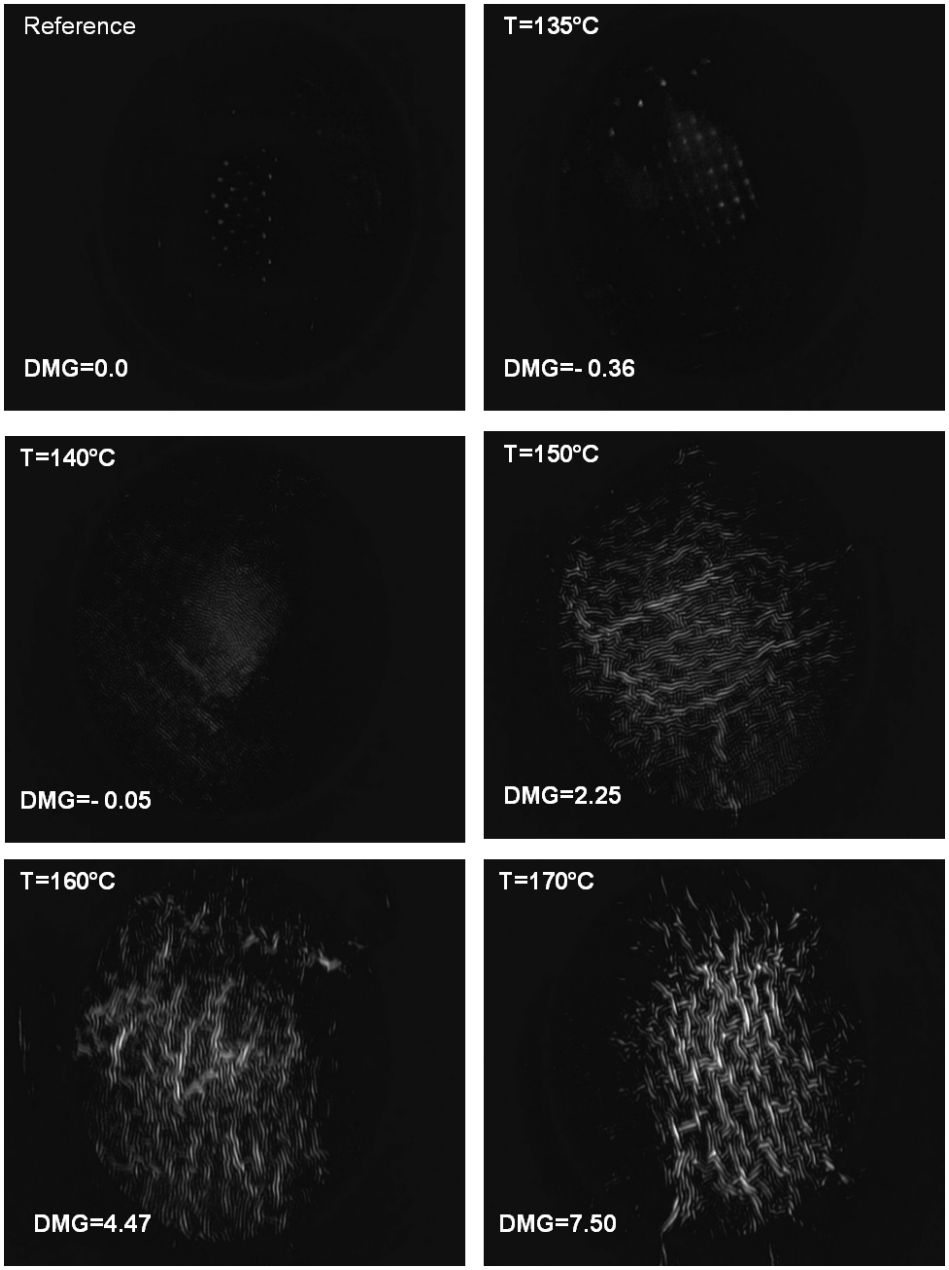

Figure D-1: Optical images of light transmission study conducted for FBO/PC_t laminates samples wrinkled at temperatures of 130-170°C. DMG- Difference in Mean Grey value

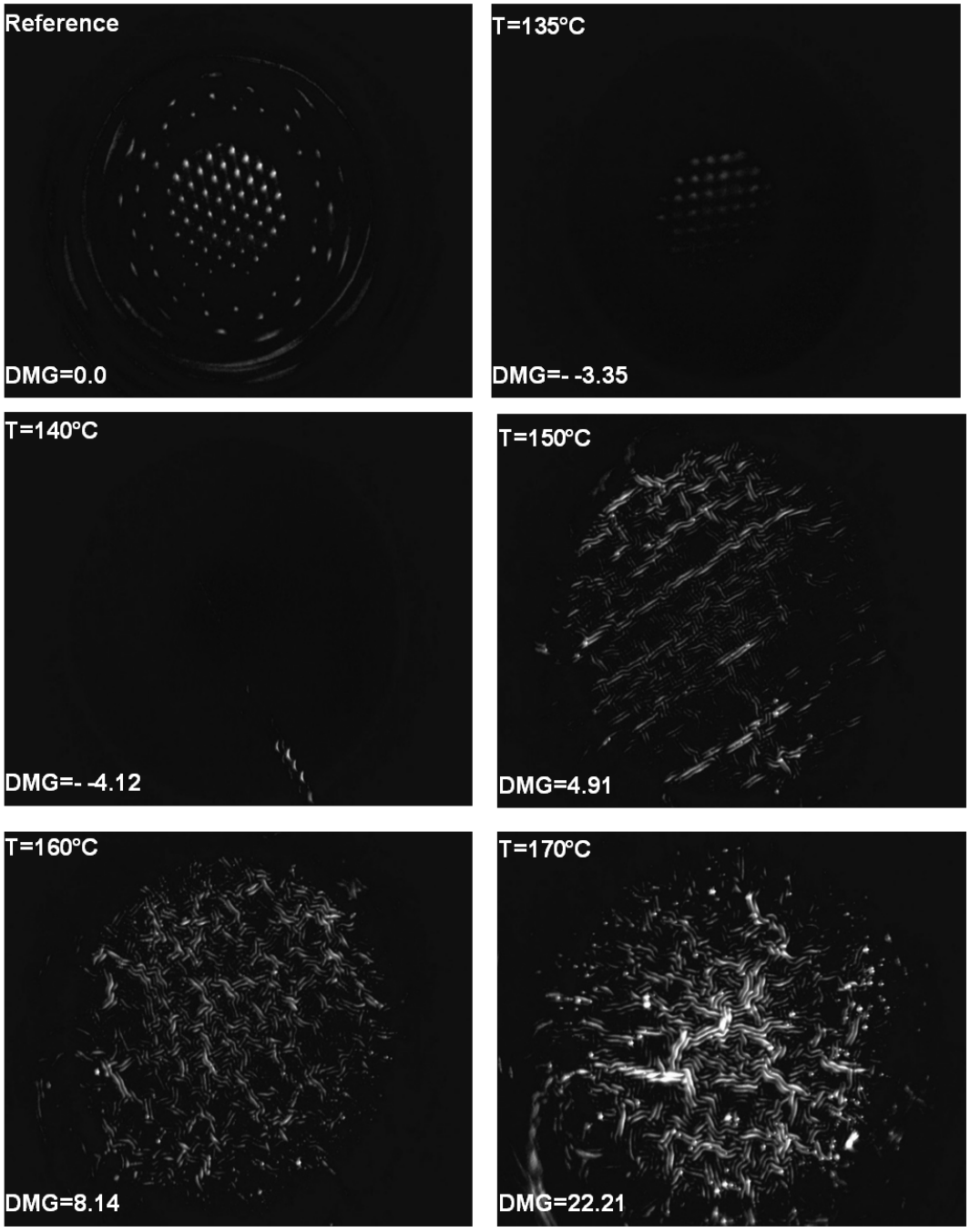

Figure D-2: Optical images of light transmission study conducted for FBO/PC_T laminates samples wrinkled at temperatures of 130-170°C. DMG - Difference in Mean Grey value

Appendix E. Stretched Assisted Thermoformer

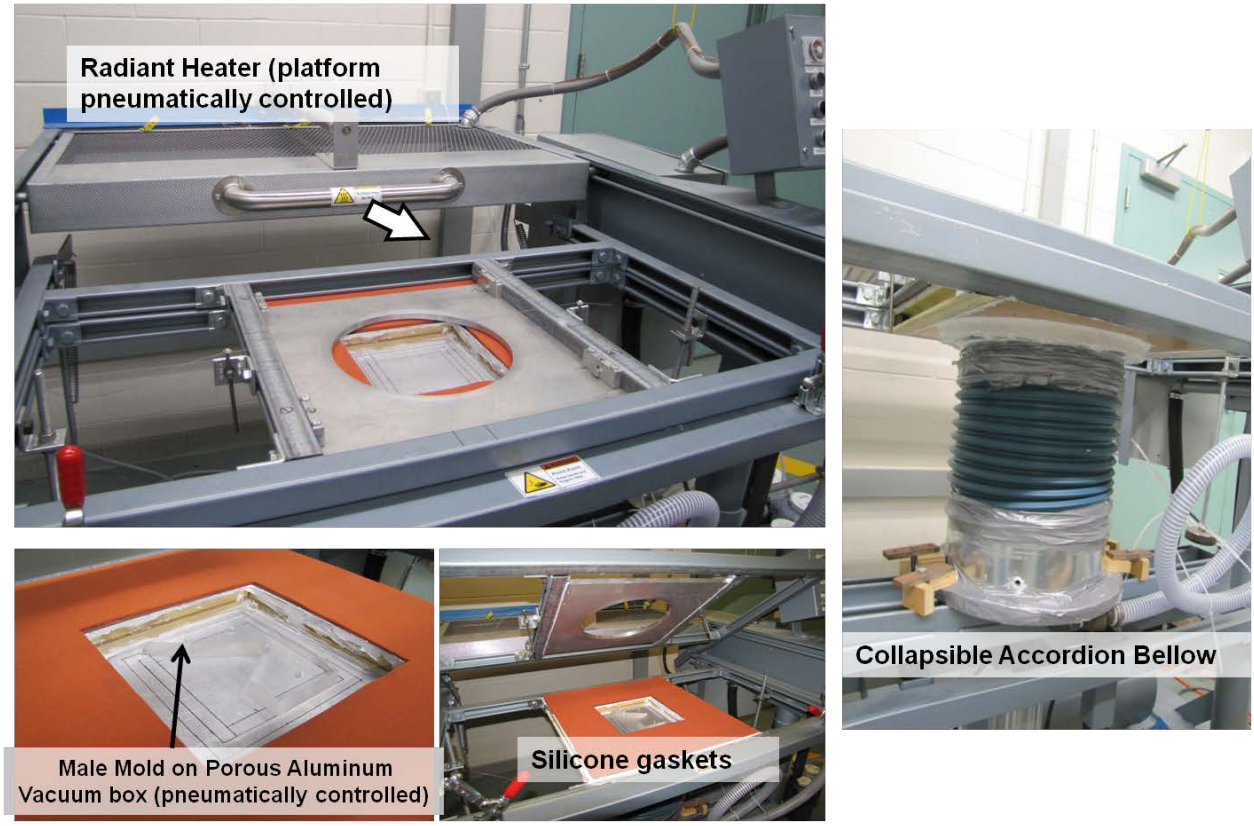

Figure E-1: Optical Images of Stretch assisted Thermoformer